Stralsund University of Applied Sciences

Department of Electrical Engineering and Computer Science

Zur Schwedenschanze 15, 18435, Stralsund, Germany

OPTIMIZATION OF AN HTS STATOR WINDING FOR WECS

A

<u>Master Thesis report</u>

Submitted in fulfilment of the requirements for the degree of Master of Engineering (M. Eng.)

in Renewable Energy and E-mobility at Hochschule Stralsund

Fraunhofer IEE, Kassel

Power System Stability and Converter Technology Division

By

Srikar Boddukuri

Matriculation number - 18200

Date: 25/07/2022

First Supervisor

Prof. Dr. –Ing. Michael Bierhoff

Vice Dean, Faculty of Electrical

Engineering and Computer Science

Hochschule Stralsund

Second Supervisor

Sebastian Lengsfeld, M. Sc.

Power System Stability and Converter

Technology Division

Fraunhofer IEE, Kassel

Acknowledgement

I am very grateful to my supervisor, Mr. Sebastian Lengsfeld, M. Sc., Department of Power System Stability and Converter Technology, Fraunhofer IEE, Kassel, for giving me the opportunity to write my master thesis at the most prestigious and leading research institute in Europe. I would like to thank you for your supervision, extensive patience, and providing the freedom to use all facilities available during the project work and writing of the master's thesis. I have to add that nothing would have been possible without your unwavering support.

I would like to express my sincere gratitude to my supervisor at university, Prof. Dr.-Ing. Michael Bierhoff, Vice Dean, Faculty of Electrical Engineering and Computer Science, Hochschule Stralsund, for the timely suggestions and motivation during the course of the thesis.

During the master thesis, I would like to express my gratitude to my entire Electrical Machines team at Fraunhofer IEE, Kassel, for their unwavering support and helpful recommendations.

I appreciate my parents and friends moral support throughout the master's thesis. Finally, I would like to convey my heartfelt gratitude to the other persons who, either directly or indirectly, contributed to the development and success of this master's thesis work at the correct moment.

Declaration of Authorship

I hereby declare that the master thesis work titled "Optimization of an HTS Stator Winding for WECS" where the investigations and results presented in this report are purely based on my own work. All the information used from external sources is properly cited in this report and cross-referenced where exactly the references are used in this thesis report.

Date and Place,

25/07/2022, Kassel

Srikar Boddukuri

Abstract

Superconducting generators can possibly give a compact and lightweight drive train at high torques and low rotational speeds since high magnetic fields can be created [8]. Among these superconducting generators, fully superconducting machines are more advantageous than others because of their high power density and efficiency.

In this thesis, a major focus is on optimizing the stator winding for a 10 MW fully superconducting offshore wind turbine synchronous generator (FSWTG), with High-Temperature Superconductors (HTS) used in both the stator and rotor winding. This study is part of the SuperGenSys project at Fraunhofer IEE, Kassel, which aims to design, optimize, and evaluate the 10 MW fully HTS generator. Due to the relationship between the critical current and the flux density, the performance of machines with HTS armature and field windings can be more sensitive to design parameters than conventional electrical machines. The effect of stator geometry on the machine with HTS armature windings is explored in this work [22].

In a fully superconducting generator, defining the armature winding entails making a key design decision. Therefore, an investigation is performed for the 10 MW FSWTG with four different armature windings (one and two-layer concentrated winding, air-gap winding, and one-layer distributed winding). To analyze the behavior of the 10 MW FSWTG at different ampere loading and operating temperatures, a detailed design and analysis has been carried out in this study to select the suitable winding concept using the FEM software called FEMAG-DC.

Table of Contents

I List of Figures

II List of Tables

III Abbreviations

HTS	High-Temperature Superconductor
LTS	Low-Temperature Superconductor
AC	Alternating Current
MW	Mega Watt
FEM	Finite Element Method
IWES	Institute for Wind Energy and Energy System Technology
ETH	Eidgenössische Technische Hochschule
1G	1 Generation
2G	2 Generation
MRI	Magnetic Resonance Imaging
NMR	Nuclear Magnetic Resonance
BSCCO	Bismuth Strontium Calcium Copper Oxide
YBCO	Yttrium Barium Copper Oxide
REBCO	Rare-Earth Barium Copper Oxide
2D	2 Dimensional
1ZW	Single Layer Concentrated Winding
2ZW	Double Layer Concentrated Winding
LSW	Air-gap winding
1VW	Single Layer Distributed Winding
SC	Superconductor
EMF	Electro Motive Force
FSWTG	Fully Superconducting Offshore Wind Turbine Synchronous Generator
DC	Direct Current
3D	3 Dimensional

IV List of Symbols

T_C	Critical temperature
I_C	Critical current
J_C	Critical current density
A	Area of cross-section of superconductor
L	Lift factor
P_{AC}	AC losses
B_{avg}	Flux density of the average tangential magnetic field
f	Frequency
d	Width of the HTS tape
l_{HTS}	Length of the HTS tape
n	Rotational speed of the machine
p	Number of pole pairs
θ_{slot}	Slot linkage
τ_{slot}	Slot pitch
W_{RT}	Number of turns
q	Number of slots per pole per phase
Z_1	Number of stator slots
A_1	Stator Ampere loading
m	Number of phases
D_i	Inner diameter
l_i	Active length
m_{fe}	Iron mass
P_{fe}	Iron losses
P_v	Total losses
η	Efficiency of the generator
C_t	Total cost of the generator
P_N	Rated output power
I_{SP}	Coil current
P_D	Power density
h_M	Height of permanent magnet

B_r Remanence induction

μ_r Relative permeability

h_M   Width of permanent magnet

Chapter 1   Introduction

1.1. Background

Wind energy conversion systems are considered one of the key technologies for future energy production. Existing wind energy technologies include on-shore and offshore wind energy. On-shore wind energy refers to wind turbines, which are installed on dry ground. The major drawback of on-shore wind turbines is that this type of wind energy technology generates less power because of the low wind speed due to high-rise buildings and hills. Offshore wind energy is known for generating more power by collecting wind energy since it is installed near places with strong wind speeds like large water bodies (oceans). Offshore wind energy becomes expensive due to its grid connection difficulties and extensive maintenance. The offshore wind turbine of the 10 MW class is currently being developed to build larger turbines, where installation becomes difficult and expensive [2]. For wind turbines in the multi-MW class, direct-drive turbines are best suited to generating high torque at low speeds. Removing the gearbox, which has been a tough component in a good deal of offshore wind farm projects, and replacing it with a much simpler mechanical system, will avoid misalignment or alterations in shaft torque, which enhances reliability and efficiency. Offshore turbines require a high level of reliability because access is difficult and expensive, and weather conditions frequently preclude access [17]. As a result, the prospect of using High-Temperature Superconductor (HTS) in wind turbine generators to build high power density, compact, and lightweight generators has come into the limelight.

There are two possibilities for designing High-Temperature Superconductor (HTS) electrical machines, which are partially superconducting and fully superconducting. In partially superconducting generators, the field winding is employed with superconducting material and the armature winding is employed with conventional copper winding. In fully superconducting generators, both armature and field windings are superconducting. Extensive research has been going on the fully superconducting generators for their advantages over the partially superconducting generators.

1.2. Scope of the Thesis

The main goal of this thesis is to optimize the stator winding of a fully HTS generator for wind energy conversion systems. The major challenge of this HTS is to reduce the AC losses in the armature winding. Therefore, one of the most important things to consider when designing is the stator winding.

For different ampere loading and operating temperatures, detailed design and analysis has been carried out to select the optimum. The analysis has been done for the following winding concepts:

1. Single Layer Concentrated Winding,
2. Double Layer Concentrated Winding,
3. Double Layer Distributed Air-gap Winding, and
4. Single Layer Distributed Winding

The simulations for the different winding concepts are done using the FEM simulation tool named FEMAG-DC. A lightweight and compact generator will be designed by analyzing and selecting the armature winding type and operating temperature.

1.3. Structure of the Thesis

This thesis report addresses the process to optimize the stator winding for a fully HTS generator by considering the ampere loading and operating temperature as design variables. The structure of this study is organized as shown in the below picture.
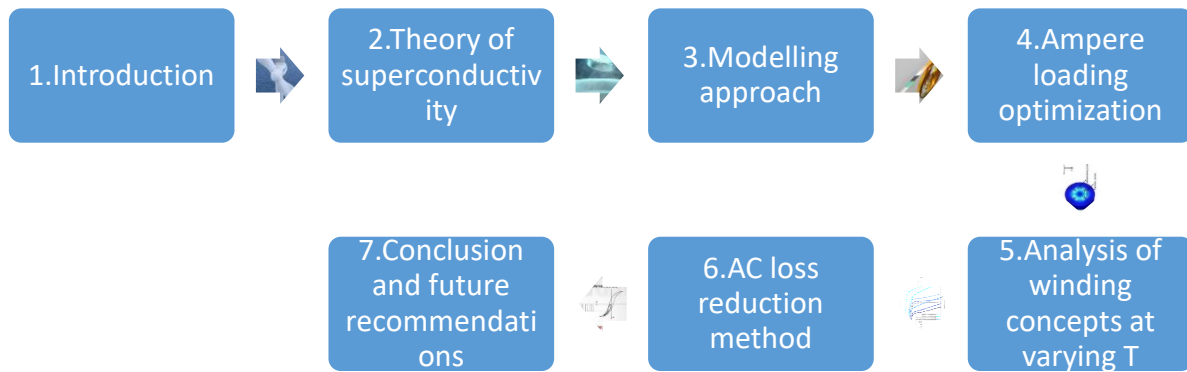
Figure 1 Schematic of the structure of the thesis

- Chapter 1 discusses the short history of the importance and use of superconducting generators for wind turbines, the important projects on fully superconducting generators, and the software used in this study

- Chapter 2 describes the basics of superconductivity and a preliminary approach to calculate AC losses

- Chapter 3 gives the detailed approach to optimize the stator winding by performing ampere loading simulations using FEMAG-DC

- Chapter 4 explains the behaviour of selected machine parameters for different winding concepts and comparison to select the suitable winding concept for the 10 MW machine design

- Chapter 5 analyses the influence of operating temperature on 10 MW machine design parameters by comparing the winding concepts at each selected temperature level

- Chapter 6 discusses the one technique to reduce AC losses in the generator and compares the results of this study with the research paper

- Chapter 7 draws out a final conclusion of this thesis and mentions some future recommendations.

1.4. Research Projects on Superconducting Generators

An enormous amount of research has been going on the HTS technology the type of superconducting material to be used, the operating temperature level where the HTS generator is to be operated, and some other factors. The following research projects are important to point out among all the other projects related to HTS technology.

1.4.1. The EcoSwing Project

The project EcoSwing (March 2015 – April 2019) is the first one of its kind to prove that the superconducting technology can be used in MW class Wind turbine applications funded by the Horizon 2020 framework. The EcoSwing generator used in this project is partially superconducting, with conventional armature winding and superconducting field winding. The EcoSwing project is partnered with nine companies as named below [21].

Table 1 EcoSwing Project partner companies and their contribution [21]

Partner company	Contribution
Envision Energy Aps, Denmark	Provided the wind turbine prototype on which the EcoSwing generator installed
ECO 5 GmbH	Supported in the design of superconducting rotor
Jeumont Electric SAS	Supported in the design of conventional Stator
Delta Energy Systems GmbH	Supported in the designing and building process of the Power converter and data acquisition
THEVA Dünnschichttechnik GmbH	Supported in building the superconducting rotor poles
Sumitomo Cryogenics of Europe Ltd.,	Supported with the Cryogenic cooling system
Fraunhofer Institute for Wind Energy and Energy System Technology (IWES)	Provided the ground based test bench to test the EcoSwing generator

Partner company	Contribution
The University of Twente	Supported with the testing of materials and rotor construction
DNV GL Renewables	Provided certification guidelines for the superconducting EcoSwing wind turbine generator

In March 2019, the EcoSwing generator was put to the test at Fraunhofer Institute for Wind Energy and Energy System Technology (IWES) in Bremerhaven and installed in Thyborøn, Denmark reached the electrical output of 3 MW. The superconducting coils are cooled down to -240 degree Celsius proving that they are durable and dependable in real world settings [7].

The basic specifications of the EcoSwing generator are.

Table 2 EcoSwing generator specifications [7]

Parameter	Value	Units
Power output	3.0	MW
Diameter	4.0	m
Speed	15	rpm
Number of coils	40	-
Coil length	1.4	m
Coil width	0.2	m
Length of superconducting wire	Approx. 25	km

1.4.2. The INNWIND Project

The INNWIND project (November 2012 – December 2017) was the research project funded by the European Union's Seventh Framework Programme with the budget of approx. 20 million € to focus on the conceptual design of 10-20 MW class offshore wind turbines. During the time of this project some key decisions were made regarding the 10-20 MW offshore wind turbines like the mechanical design of the rotor, the power density rating, the speed, the type of superconducting material to be used and the operational temperature of the superconducting material [6].
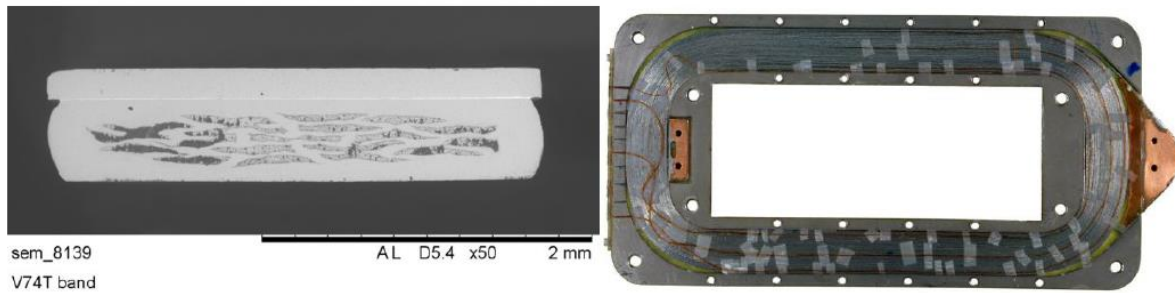
Figure 2 MgB2 superconducting wire dimensions with filaments and a racetrack coil [6]

One of the most important design decision among them is the type of superconducting material usage. The superconducting wire with magnesium diboride (MgB2) material was designed with the close cooperation of the superconducting wire manufacturers. The specifications of the wire like thickness and width of the wire are 0.7 mm and 3.0 mm respectively with the 19 filaments in the centre as shown in the above figure [6].

1.4.3. The SuperGenSys Project

The SuperGenSys project (May 2019 - Present) focuses on fully HTS generators where both stator and rotor windings are superconducting because of advantages over partially superconducting generators. This project is partnered by Karlsruhe Institute for Technology (KIT), Fraunhofer IEE, Siemens AG, Krämer Energietechnik GmbH. The project's overall goal is to design, optimize, and evaluate full-superconducting HTS generators for multi-MW wind turbines in order to improve performance and efficiency while lowering power specific weight in the drive train, as well as to limit nacelle mass expansion owing to size growth [3].

The use of High-Temperature Superconductors (HTS) in rotating electrical machines allows for:

- a significant reduction in size,
- a higher power and torque density,
- a significant increase in efficiency, and
- a significant reduction in AC losses.

The 10 MW generator size comparison between copper wound-coil with gearbox, permanent magnet, partially superconducting and fully superconducting generators has clearly shown in the below figure. Among all these four types of 10 MW class generators, fully HTS generator is the lightest one with just 70 Tons with huge reduction of 82.5% mass compared to conventional copper wound-coil generator with gearbox.
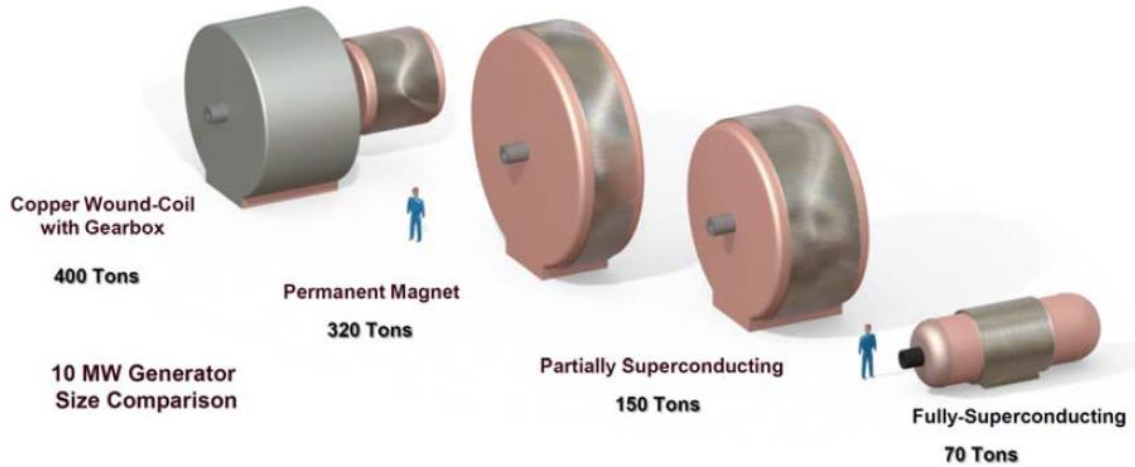
Figure 3 10MW Generator size comparison [5]

This thesis study is completely based on the SuperGenSys project to define the armature winding and operating temperature of the fully HTS generator of the SuperGenSys project.

1.5. FEM Simulation

1.5.1. FEMAG-DC

FEMAG is a finite element simulation tool for designing and analysing electrical machines was initially developed by Prof. Reichert in 1982 at the Institute for Electrical Machines, ETH Zurich, Switzerland and is regularly changed to meet the current needs. The FEMAG Software package is owned by ProFEMAG AG which was founded in July 2014 in Wettingen, Switzerland partnered by Semafor AG, Vetenco GmbH and the Institute for Drive Systems and Power Electronics (IAL) Leibniz University Hannover [10].

FEMAG is a software application system for the design of electrical machines that is quick, dependable, and cost-effective. FEMAG is an interactive programme to design the electrical machines with the help of Pre-defined / User-defined script files. FEMAG tools are divided into 5 categories as shown in the below figure. The FEMAG tool used in this master thesis is FEMAG – DC to calculate and analyse the induction, fluxes, torque, losses and many more by dividing the geometry of electrical machine into small finite elements called meshing using Finite Element Method (FEM).
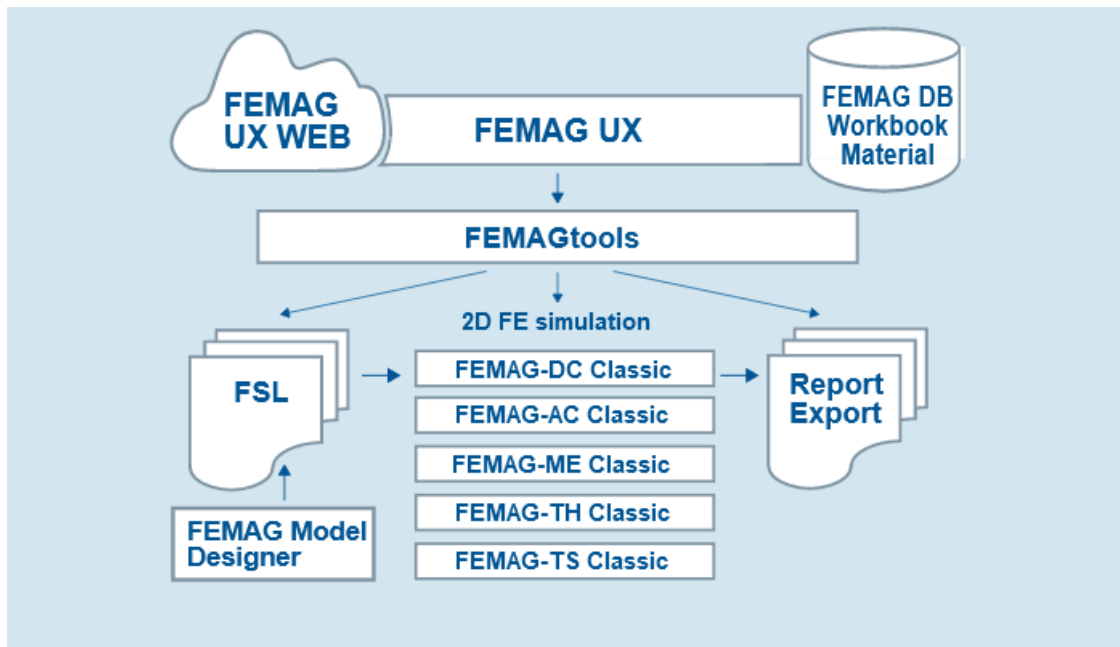
Figure 4 Different simulation modules available in FEMAG tool [11]

The FEMAG-DC software opens with two windows as shown in the below figures:

1. The window in white colour helps to navigate to different input fields and
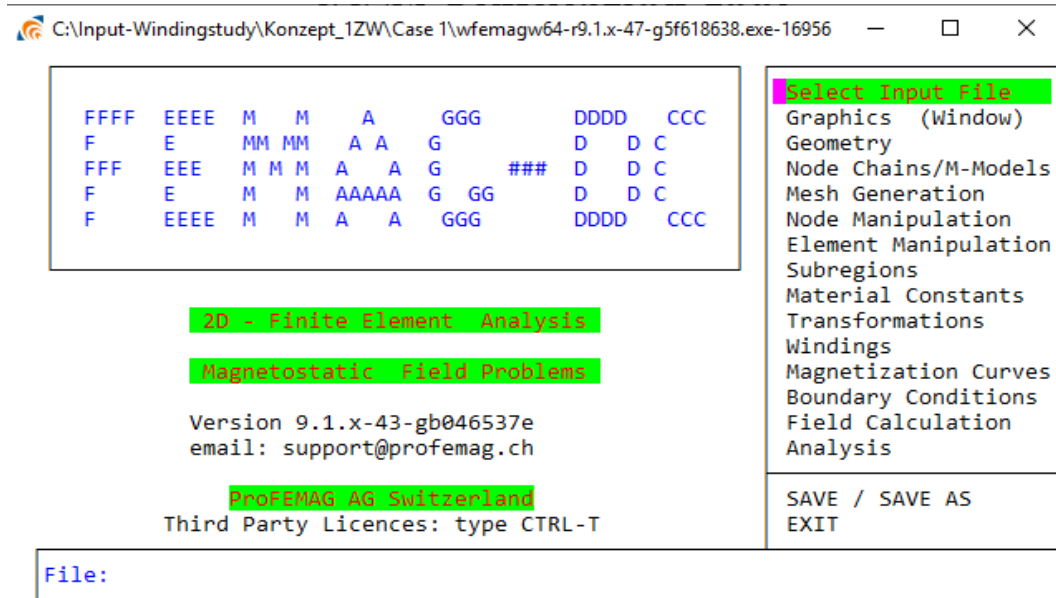
Figure 5 Control menu interface of FEMAG-DC

2. The window in blue colour is a graphic window where the geometry of an electrical machine, meshing, field lines, induction and other results are displayed.

Figure 6 Graphical interface of FEMAG-DC

Chapter 2 Theory of Superconductivity

2.1. Superconductivity

Heike Kamerlingh Onnes discovered superconductivity in 1911 when he noticed that when mercury was cooled in liquid helium boiling at T = 4.2 K, its electrical resistance vanished (-269 ° C). The disappearance of resistance (R = 0 Ω) led to the designation of this new material class as a superconductor, and the transition temperature was dubbed the critical temperature T_C [8]. The critical current (I_C) of a long straight wire is defined as the maximum current that a wire may carry with no resistance. In the case of superconducting materials, as temperature decreases resistance (R) decreases and critical current (T_C) increases. For superconducting materials, the resistance comes down to zero below the critical temperature. But in non-superconducting materials like copper, the resistance (R) reaches one particular value called residual resistance where there is no further reduction in resistance even when there is a decrease in temperature [17].

After numerous investigations, it was found that superconducting materials are divided into the following categories.
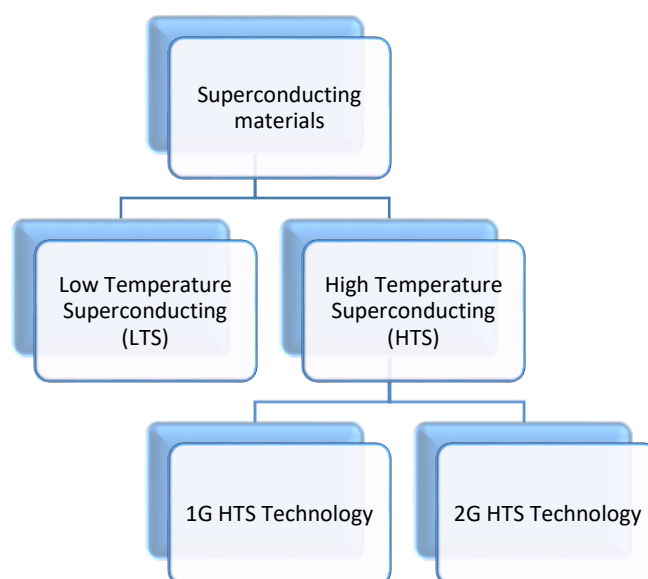
Figure 7 Classification of Superconducting materials

2.2. Low Temperature Superconducting (LTS) materials

In general, Low-Temperature Superconducting (LTS) materials operate at a critical temperature below 30 K (e.g., NbTi). These LTS materials are used in various designs even though the critical current is very low because it lowers the material cost. The major drawback of LTS materials is that it requires liquid helium or liquid hydrogen to cool down which makes the cryogenic system expensive [23]. The LTS materials are commonly used in Magneto Resonant Imaging (MRI) scanners, NMR Spectrometers, etc.

In 2001, the MgB_2 superconductor was discovered with a critical temperature of $T_C = 39$ K. The properties of the MgB_2 superconductor is similar to the first discovered LTS material NbTi but with a higher critical temperature. Usage of MgB_2 is considered as a replacement for other LTS materials with the operating temperature range between 10 K-30 K since it has proven that MgB_2 has comparably low AC losses because of its round wire structure [8].

2.3. High-Temperature Superconducting (HTS) materials

The High-Temperature Superconducting (HTS) materials were discovered in 1986 and are referred to as the materials which operate at very high critical temperatures ranging from 39 K-110 K [8]. This discovery of HTS superconductors makes the cryogenic system a little cheaper since the operating temperature is in the range of liquid nitrogen which is almost two times cheaper than the liquid helium. The HTS superconductors are preferred because of their high critical temperature, high critical current, and high critical magnetic field [23].

The availability of suitable high temperature superconducting wires for application in rotating machines with particular emphasis on wind power generators will be discussed below. In terms of various conductor classifications, the industry often distinguishes between:

- The first generation (1G) wire, which is a powder-in-tube conductor made of Bismuth (Bi), Strontium (Sr), Calcium (Ca), Copper (Cu), and Oxide (O), and
- The second generation (2G) wire, which is a coated conductor (CC) made of Yttrium (Y), Barium (Ba), Copper (Cu), and Oxide (O), with a buffer layer and an HTS layer coated on a flexible metal substrate.

Superconductivity can be achieved in the above metals through the pairing of electrons with extremely complex chemical compositions, such as:

- $YBa_2Cu_3O_{6+x}$ (YBCO),
- $Bi_2Sr_2CaCu_2O_{8+x}$ (Bi-222), and
- $Bi_2Sr_2Ca_2Cu_3O_{10+x}$ (Bi-2223).

In order to be successful commercially in the market of wind energy, the HTS wire production must be of large volume at a low cost. In technical terms, the cost of the HTS wire can be defined as the cost at which the HTS wire carries a specific amount of current over a specific distance and is measured in \$/kAm. Therefore, the HTS wind turbines can be cheaper only when the cost of HTS wire is low i.e., in the range of 10-20 \$/kAm [17]. In the past developments of HTS wires, the cost of the HTS wire was too high. The new developments are being made in HTS wires to become cost-effective. This early phase and ongoing phase of HTS wire developments are considered as 1G HTS technology and 2G HTS technology respectively.

2.3.1. 1G HTS Technology

1G HTS technology is referred to as first-generation wire technology which is completely based on BSCCO (BiSrCaCuO - Bismuth strontium calcium copper oxide) material [23]. The first commercially manufactured flat tape was Bi-2223 with a width of 4 mm and a thickness of 0.3 mm. The 1G HTS wires are manufactured using powder technologies known as the Powder in Tube method [17]. In this method, the ceramic HTS filaments are inserted into the silver matrix as shown in the below figure [8].
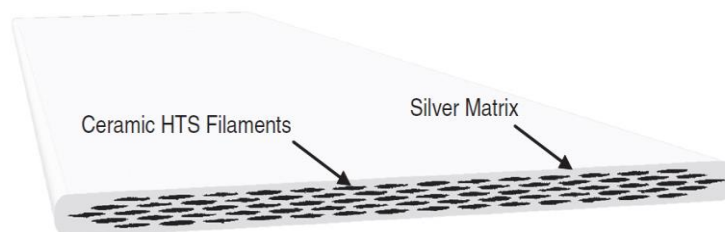
Figure 8 Structure of 1G HTS Technology [17]

2.3.2. 2G HTS Technology

The term 2G is referred to as second-generation HTS wire technology which is completely based on YBCO material. The superconducting material $YBa_2Cu_3O_x$, sometimes known as YBCO-123 or simply YBCO, is the foundation of the new 2G wires. 2G HTS wire has a considerably different structure and manufacturing process than 1G wire. On top of the substrate, the thin buffer layer is placed on which an YBCO superconductor of 1-5 µm thick is placed. The copper layer is placed on top of all layers to provide the stability as shown in the below figure [17].
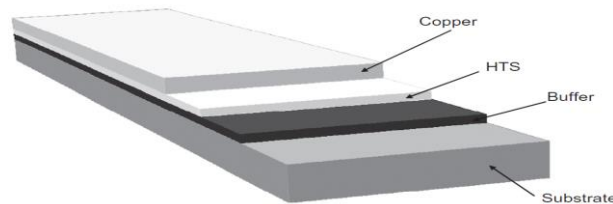
Figure 9 Structure of 2G HTS Technology [17]

2.4. SuperPower SCS4050

REBCO is another name for rare-earth barium copper oxide comes under the class of chemical compounds which exhibits high temperature superconductivity. A REBCO can be made of any rare-earth element, but common options include Yttrium (YBCO), Lanthanum (LBCO), Samarium (Sm123), Neodymium (Nd123 and Nd422), Gadolinium (Gd123), and Europium (Eu123). In the SuperGenSys project, the 2G HTS REBCO (Rare-earth barium copper oxide) tape named SCS4050 manufactured by SuperPower Inc. Company based in the USA specifications are considered. The tape has a thickness of 0.1 mm with different tape widths like 12 mm, 6 mm, 4 mm, 3 mm, and 2 mm [1]. The HTS tape specifications of stator coils considered for calculation purposes in this project are 2 mm wide and 0.1 mm thick. The architecture of SuperPower SCS4050 tape is clearly shown in the below figure.
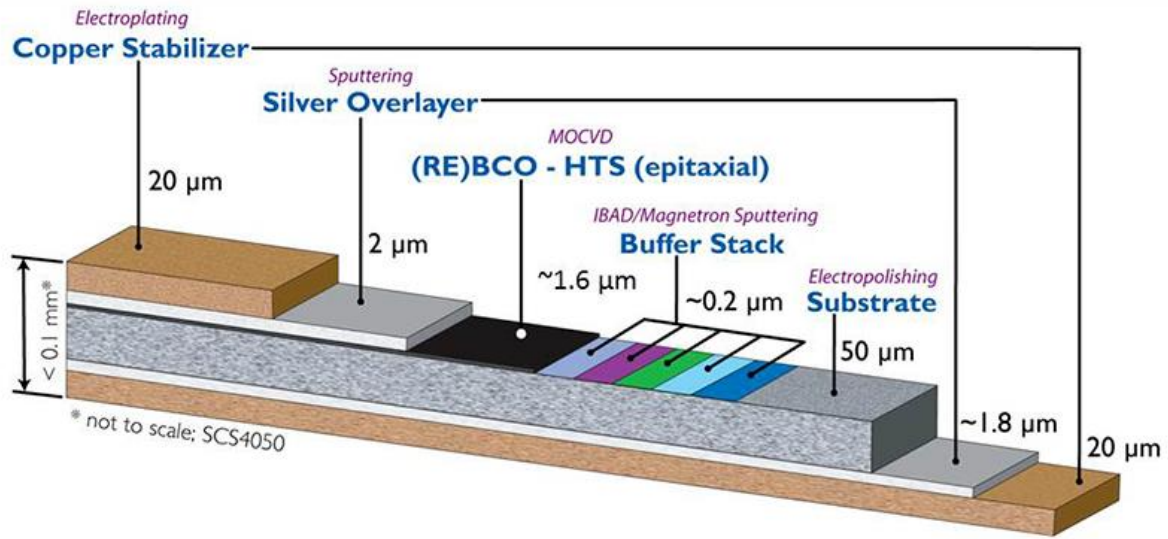
Figure 10 Architecture of SuperPower SCS4050 2G HTS tape [1]

The technical specifications of the product SCS4050 used in SuperGenSys project are shown in the below table.

Table 3 Specifications of SuperPower SCS4050 2G HTS tape

SuperPower SCS4050		
Parameter	**Value**	**Units**
Tape width	2	mm
Tape thickness	0.1	mm
HTS layer thickness	1.6	µm
Critical current I_C (77K, Self-field)	50	A
Critical bending diameter	11	mm

The critical current density J_c can be defined as the critical current I_c over the cross-sectional area A of the HTS tape.

$$J_c = \frac{I_c}{A} \qquad (1)$$

A is constant for all operating temperatures.

Therefore, from equation (1) and (2) the critical current I_c can be calculated since it depends on the operating temperature and magnetic flux density (self-field). In this study, the initial calculation for critical current $I_c(B, T)$ from the equation (2) was done at an operating temperature of 65 K using the critical current $I_c(77\,K, Self - field) = 50\,A$ from Table 3 and parameters mentioned in the Table 4 and.

$$L = \frac{J_c(B,T)}{J_c(77K)} = \frac{I_c(B,T)}{I_c(77K)} = \frac{L_0(T)}{\left(1 + \frac{\sqrt{k(T)^2 * B_x{}^2 + B_y{}^2}}{B_{c0}(T)}\right)^{b(T)}} \qquad (2)$$

In the above equation (2), $L_0(T)$, $k(T)$, $B_{c0}(T)$, and $b(T)$ are the constant parameters depending on the operating temperature T. B_x and B_y are the magnetic flux density's parallel and perpendicular components and assumed to be maximum of 0.8 T for each flux component.

Table 4 Parameters used to calculate Lift factor for different temperature levels [24]

T (K)	L_0	k	$B_{c0}(T)$	b
20	6.52	0.06	5.04	1.64
30	6.12	0.07	3.23	1.41
40	5.29	0.10	1.86	1.12
50	4.12	0.17	1.26	0.96
65	2.44	0.61	0.59	0.77

As discussed earlier in section 2.1, the critical current (initial approximation) decreases with the increase in temperature which is clearly shown in the below graph. This graph is plotted between critical current (approximation from equation (2) using the parameters in Table 4) and operating temperature.
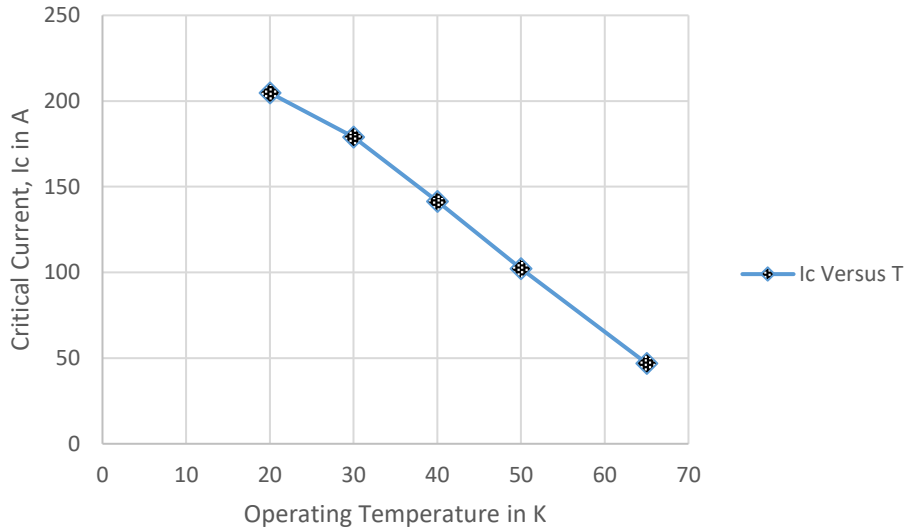
Figure 11 Critical current behaviour at different operating temperatures

2.5. AC Loss estimation

In type-II superconductors, energy dissipation is brought on by alternating magnetic fields and currents. The energy loss is referred to as AC loss. The energy is lost as heat in a low-temperature environment, so it is technically crucial to minimize AC loss. In general, the major classification of AC losses with respect to the superconductor are hysteresis losses and eddy current losses. The hysteresis losses are the ones used to describe the energy wasted as heat due to hysteresis. Eddy current losses are nothing but the ohmic dissipation caused by eddy currents. Eddy current loss cannot be produced since the superconductor has zero resistance. Therefore, approximate AC losses in this thesis are calculated using the below equation (3), which are considered as hysteresis losses with respect to the superconductor. Estimating the AC losses in the superconducting coils of the stator winding is a major challenge that directly affects the cryogenic system design which results in an expensive cooling system, and lowers the overall efficiency of the machine. [9].

$$P_{AC} = B_{avg} * f * I_c * d * l_{HTS} \qquad (3)$$

Where B_{avg} is the flux density of the average tangential magnetic field. The flux component is tangential to the surface of the HTS tape i.e., the perpendicular component. This can be obtained by doing flux distribution simulation using the 2D finite element analysis software FEMAG-DC.

The electrical frequency is denoted by f which can be calculated using the below equation.

$$f = n * p \qquad (4)$$

Where n is the speed of the machine and p is the number of pole pairs.

The critical current I_c of the HTS tape can be calculated from equation (2), d is the width of the tape and l_{HTS} is the length of the HTS tape. Therefore, the AC losses can be manipulated by increasing or decreasing any one of these parameters from the equation (3). In this study, critical current I_c is manipulated by decreasing the operating temperature where the I_c value is calculated using the equation (2).

In order to define the stator winding type, the ampere loading is an important design decision to be considered because as ampere loading (A) increases the AC losses in the machine also increase.

The ampere loading is described as the ampere turns over the slot pitch of the machine and is given by [9].

$$A_1 = \frac{\theta_{slot}}{\tau_{slot}} = \frac{W_{RT} * I_c}{\tau_{slot}} \qquad (5)$$

Where W_{RT} is the number of turns per slot and I_c is the critical current of the HTS tape.

Besides the AC losses in the superconductor, iron losses are also calculated in this thesis using the finite element analysis software FEMAG-DC. Since the superconducting material is present in both stator and rotor, there is no possibility of obtaining copper losses which is an advantage for this fully superconducting generator. Therefore, the generator total losses discussed in this thesis is the combination of AC losses and iron losses. The percentage values of iron losses and AC losses among total losses are clearly mentioned in each winding concept analysis in chapter 4. In the next chapter, an approach to optimize the stator using the AC loss and ampere loading equation is clearly discussed.

Chapter 3 Methodology

3.1. Geometry of the Generator

In the SuperGenSys project, the generator used is a 3-phase synchronous machine with a rated output power of 10 MW and rotational speed of 10 / min. It is referred to as a fully HTS wind turbine generator because both the armature and field windings are employed with superconducting material. The maximum flux density on the backside of the stator yoke is set to be 1.8 T and 2 T in rotor yoke.

The operating temperature of the stator was initially set to 65 K with the winding designed in star configuration for the following 4 different winding concepts.

1. Single Layer Concentrated Winding,
2. Double Layer Concentrated Winding,
3. Double Layer Distributed Air-gap Winding, and
4. Single Layer Distributed Winding

The main design variables are the operating temperature and ampere loading.

Stator core

Stator slots

Air-gap

Rotor slots

Rotor core
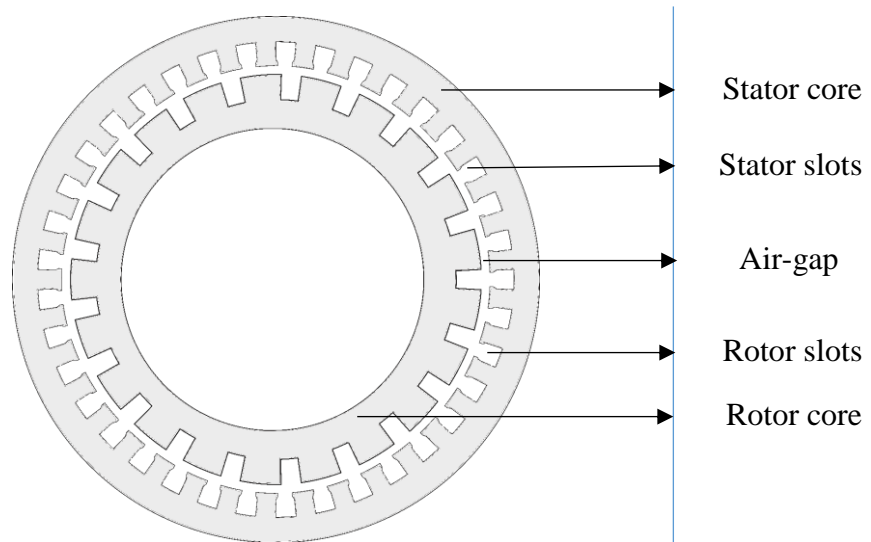
Figure 12 Cross-sectional view of Synchronous generator

The Air-gap in the generator is considered 10 mm. The HTS coils are placed in stator slots with 2mm width and have the critical current of 50 A at 77 K, 0 T. These HTS coils are surrounded by the cryogenic system with the thickness of 25 mm on all sides [13].
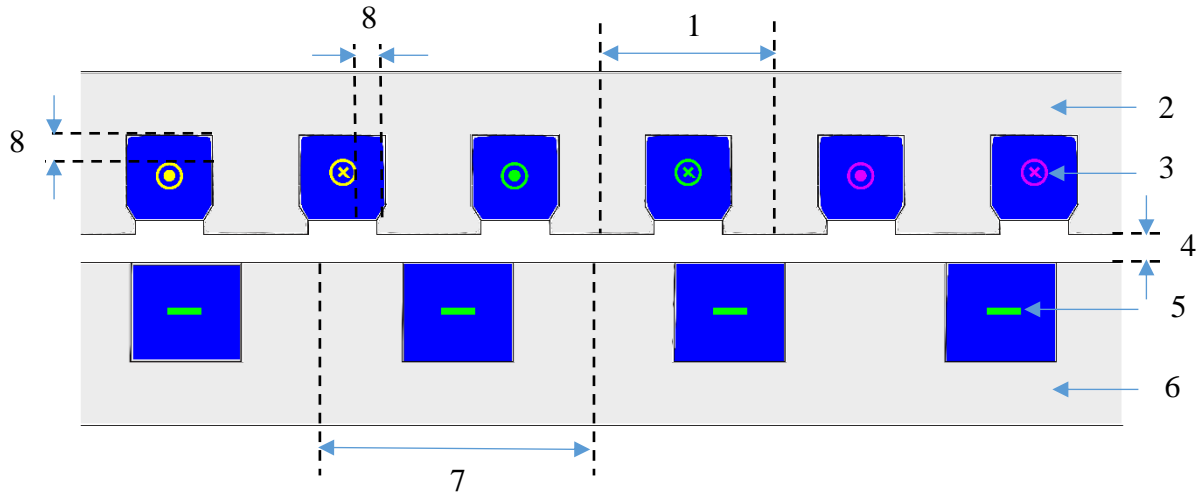
Figure 13 Detailed view of generator winding scheme

⊗ - W_in, ⊙ - W_out

(1) Slot pitch, (2) Stator yoke, (3) 3-phase Armature SC windings, (4) Air-gap, (5) Field SC windings, (6) Rotor yoke, (7) Pole pitch, (8) Cryostat (25 mm on all sides)

In this study, the total number of phases considered for the machine design are four (3 - stator and 1 - rotor). Therefore, the each phase is represented with different colour for easy identification. Throughout the study, the colours for each phase are represented as below.

Table 5 Phase colour and number representation

Phase number	Stator design	Rotor design
1	Yellow	
2	Magenta	
3	Cyan	
4		Green

3.2. Preliminary design of the 10 MW fully HTS generator

The major design decision to model the fully HTS generator is to define the armature winding in order to achieve cheaper and compact machine with high efficiency. The basic design was made for four different winding concepts as mentioned in the previous section at the operating temperature of 65 K. The winding configuration used in these designs in such a way to align the HTS tapes with the magnetic field which is called as star configuration helps in reducing the magnetic flux density's perpendicular component [19]. The reduction of perpendicular component is very important since it directly affects the reduction of AC losses in the machine. Therefore, the windings with star configuration is considered in these four basic designs. The maximum flux density in stator is set to be 1.8 T and 2 T in rotor.

The below figure shows the part of the single layer concentrated winding for 10 MW fully HTS generator. The part of the 1ZW shows six stator slots with two pole pairs.

(a)   (b)
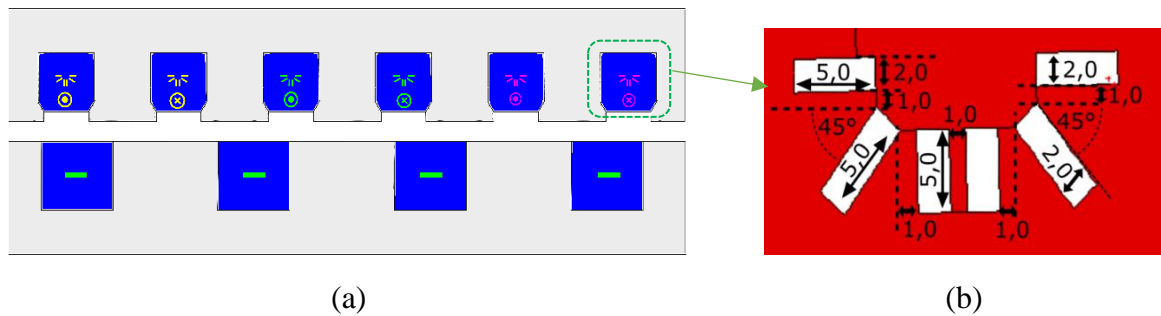
Figure 14 (a) Detailed geometry of single layer concentrated winding (b) zoom-in view of stator winding [13]

The winding arrangement is clearly shown in the enlarged view of the stator slot in figure 13. The six race track coils are placed in star configuration with the design parameters as mentioned in the table.

Table 6 Specifications of race track coil [13]

Parameter	Value
Height of the race track coil in mm	2
Width of the race track coil in mm	$0.1 * W_{RT}$
Distance between the race tracks in mm	1
Cryostat thickness in mm	25

The numerical calculation was performed for the four basic designs in FEMAG-DC for the field distribution to estimate the AC losses in the machine. In this study, analysis has been performed based on the single race track coil instead of star configuration which is described in the following sections.

3.3. Modelling approach

The initial modelling of the fully HTS generator with different winding concepts was done at an operating temperature of 65 K. In order to optimize the stator winding, the operating temperature is decreased from 65 K to 30 K by adjusting the critical current and number of winding turns according to the equation 5. In the process of reducing the operating temperature, the winding configuration is also changed from star configuration to a single race track coil since the critical current is higher at 30 K which results in less number of winding turns.

After simulating different ampere loading values at 30 K using finite element analysis software FEMAG-DC, one ampere loading optimum value is selected for each winding concept and the results are compared to make an important design decision as shown in the below figure.

Figure 15 Proceeding of the investigation in this Master thesis

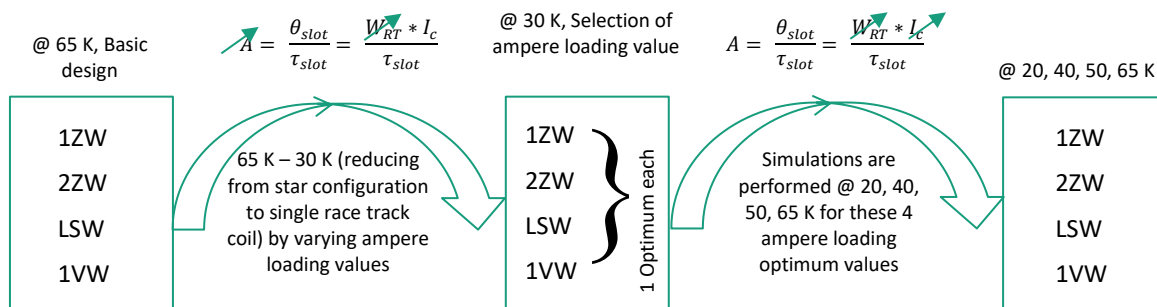Later, calculations are performed at 20 K, 40 K, 50 K, and 65 K for the selected ampere loading optimum values for each winding concept. Then the results are analyzed at all temperature levels for each winding concept which are clearly explained in the following sections.

3.4. Ampere loading calculation process

The simulation process for each winding concept in the finite element analysis software FEMAG-DC is clearly explained using the below process flow chart.

The process flow chart starts with initializing the value for ampere loading; it is denoted as n. In the below flow chart, single layer concentrated winding is considered to explain the simulation process clearly with the ampere loading values ranging from n = 20 A/mm to 110 A/mm. Initially, the value of ampere loading is defined as n = 20 A/mm. After defining the n value, the decision box checks for the condition n<=110 A/mm. If the condition is true, then the number of winding turns is adjusted in the script file in order to get the ampere loading value n = 20 A/mm, providing constant critical current I_c and slot pitch τ_{slot} according to equation (5).

Later, mechanical power and torque simulations are performed in the FEMAG-DC software and check for the maximum flux density in the stator and rotor, 1.8 T and 2 T, respectively. If the condition is not true, then the stator and rotor yoke heights are adjusted in such a way as to obtain the maximum flux density in the stator and rotor yoke as mentioned in the decision box.

Once the condition for the maximum flux density in stator and rotor becomes true, then the flux distribution calculations are performed using the script file in FEMAG-DC. This field calculation provides the field distribution at all points around the coil, which helps to calculate the average flux density of the tangential field, max flux density of the tangential magnetic field, and max flux density of the radial magnetic field.

The AC loss calculations are performed after the flux distribution calculation, which completes the simulation process for the ampere loading value of n = 20 A/mm. This calculation process continues in the loop till the condition n<=110 A/mm becomes false and comes out of the loop as shown in Figure 16.

Figure 17 shows the ampere loading simulation process of four winding concepts where the winding type is denoted by i and the ampere loading value is denoted by n. The calculation process continues in a loop until the condition becomes false for each winding concept, as explained before in Figure 16.
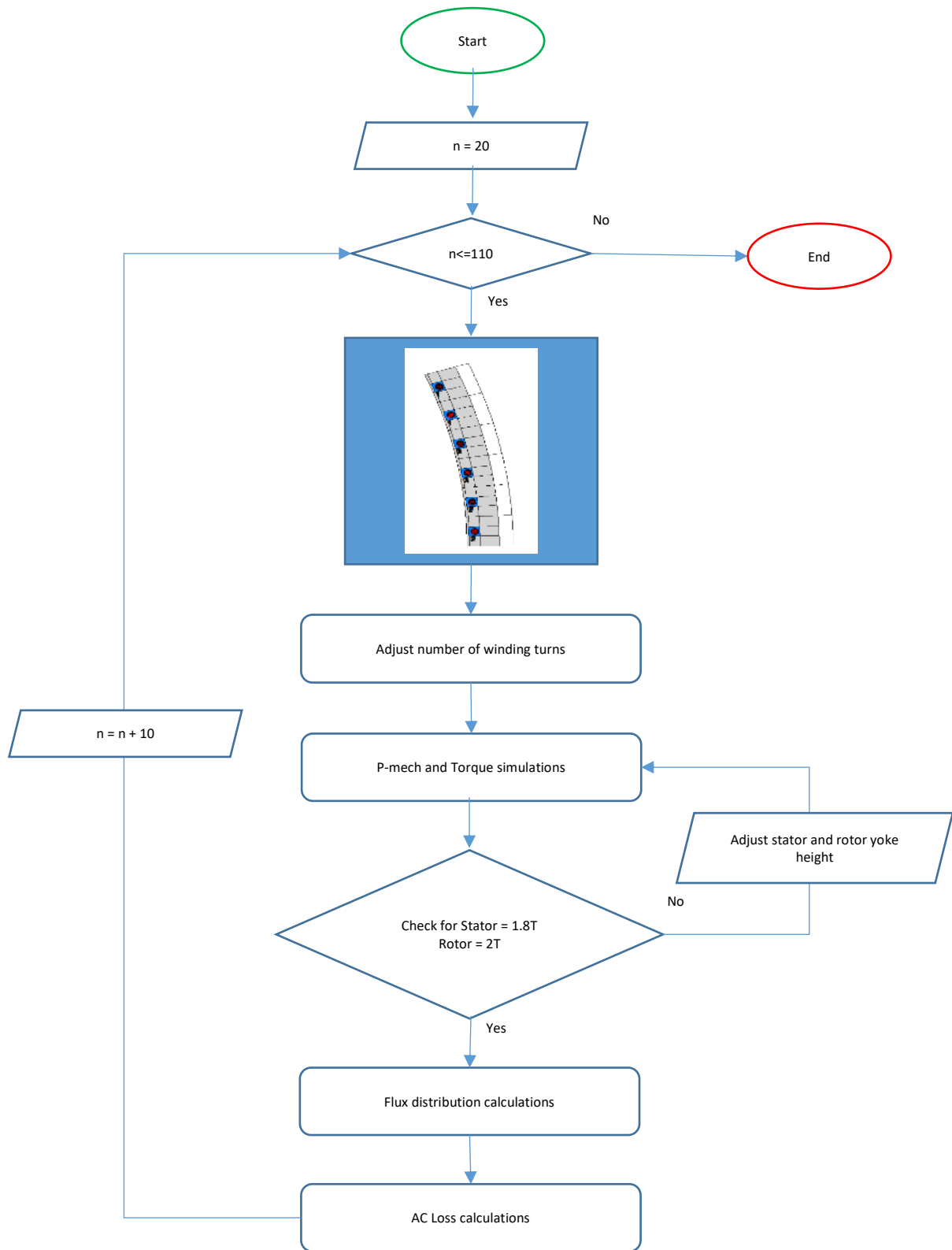
Figure 16 Process flow chart for the ampere loading calculation of 1ZW
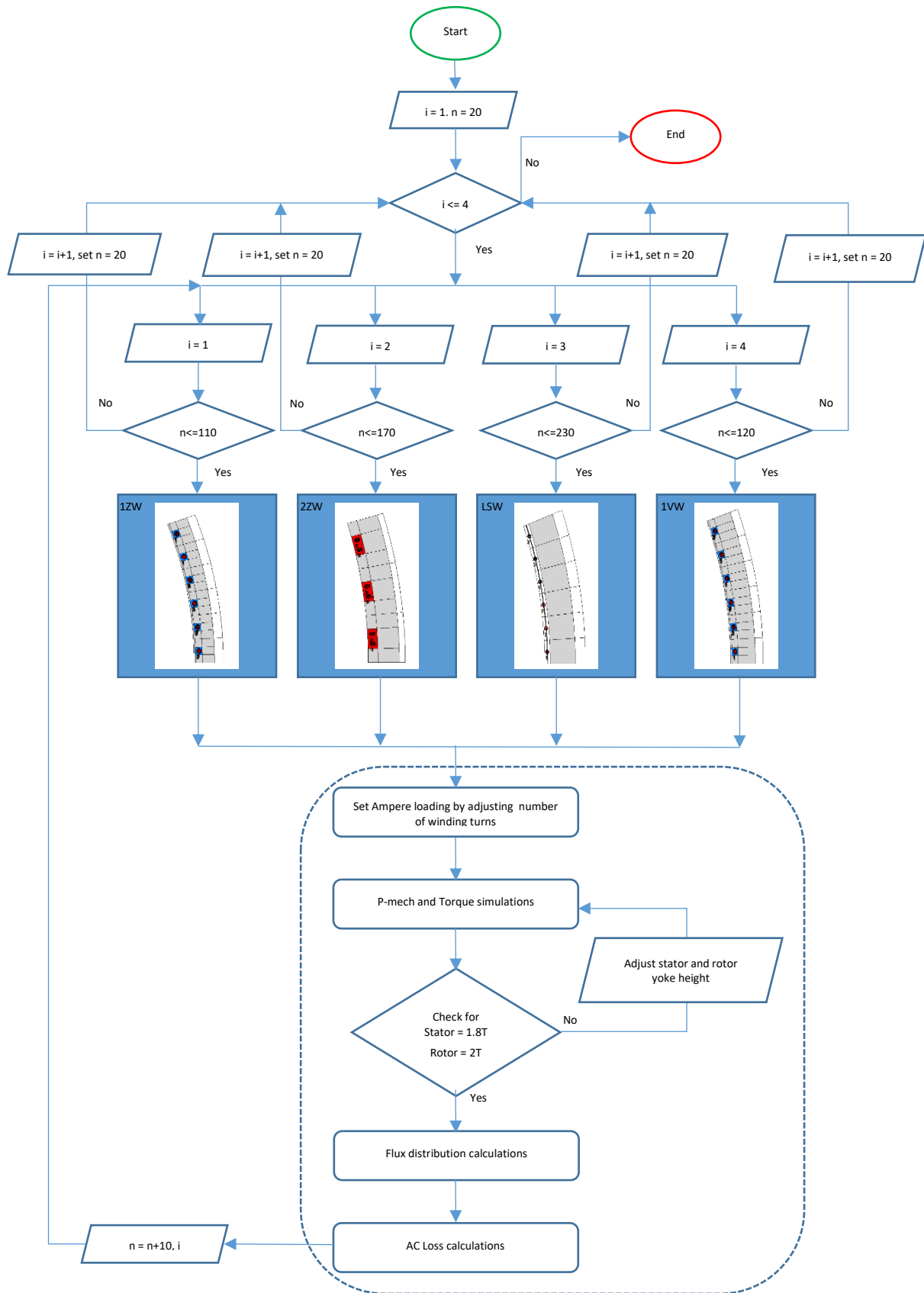
Figure 17 Process flow diagram for ampere loading calculation of four winding concepts

Chapter 4 Ampere Loading

Optimization

The stator winding of the 10 MW fully HTS generator is optimized by selecting an optimum ampere loading value for each winding concept at an operating temperature of 30 K. The winding configuration in these optimized designs is reduced from star configuration to single race track coil since the critical current is increased at 30 K results in the less number of winding turns. Therefore, the conventional single race track coil configuration is more suitable than the complex star configuration.

The Ampere loading can be varied for each winding concept based on the equation (5) as shown below.

$$A = \frac{\theta_{slot}}{\tau_{slot}} = \frac{W_{RT} * I_c}{\tau_{slot}}$$

Where,

$W_{RT} = Number\ of\ turns\ are\ varied$

$I_c = Set\ to\ 179.064\ A\ at\ 30\ K$

$\tau_{slot} = Constant(same\ as\ in\ basic\ design)$

Since the critical current (I_c = 179.064 A @ 30 K) and slot pitch are set to be constant, the ampere loading values can be varied by varying the number of winding turns of the coil. The detailed simulation process for ampere loading optimization is explained in section 3.4. The importance of optimizing the stator winding using different winding concepts is discussed in the following sections.

4.1. Armature windings

The armature winding in an electrical machine can be categorised in

1. Concentrated winding and Distributed winding
2. Single layer and Double layer winding
3. Fractional-slot and Integral-slot winding

4.1.1. Concentrated winding

This winding type takes only one stator tooth to wind the coil, which makes the winding heads less complex from a manufacturing point of view. The main advantage of concentrated winding is that it has high torque at low speed because of the trapezoidal waveform of the back EMF. At the same time, it has its own drawbacks that it has higher harmonics due to the distortions in the sine wave resulting in the increase of AC losses and the reduction in efficiency of the machine [16]. The schematics of concentrated winding are clearly shown in the below figure.
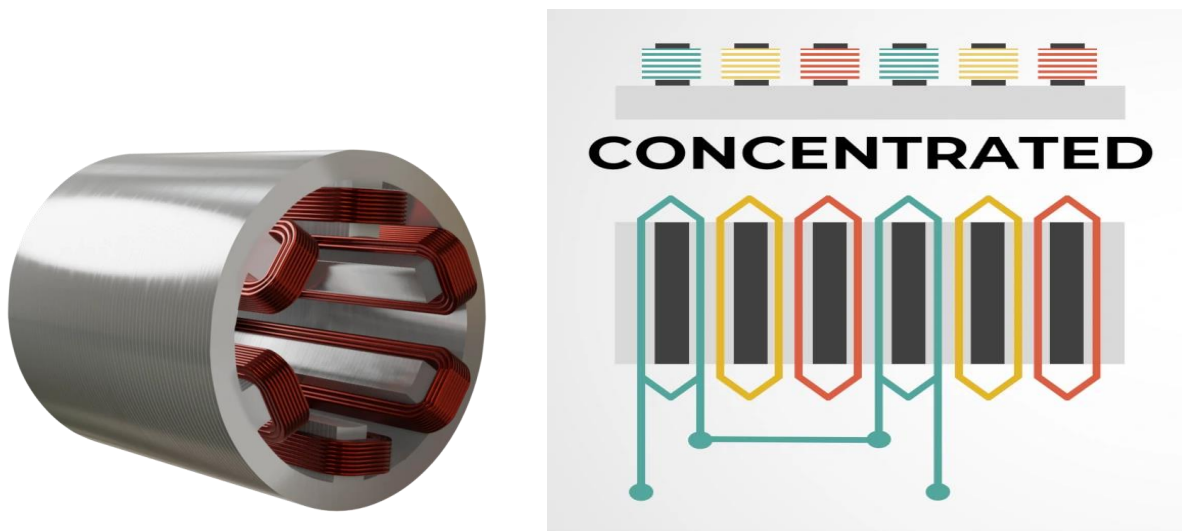
Figure 18 Schematic and winding diagram of concentrated winding [16]

4.1.2. Distributed winding

This winding type takes a minimum of two stator teeth to wind the coil, which makes the winding heads more complex from a manufacturing point of view. The main advantage of distributed winding is that it has higher performance because of the smooth sine waveform of the back EMF. At the same time, it has its own drawbacks that it has larger winding heads that result in ohmic losses in the machine, but they have very little influence on the total losses [16].

The schematics of distributed winding are clearly shown in the below figure.
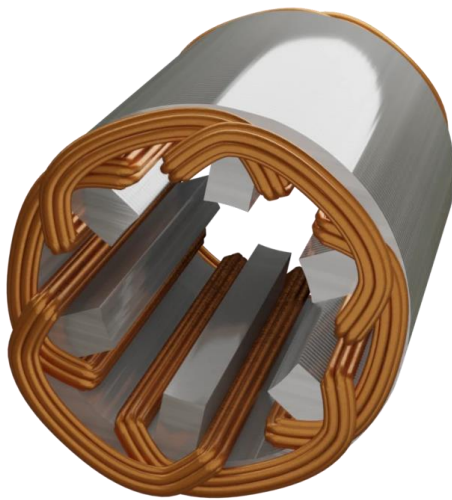
Figure 19 Schematic and winding diagram of distributed winding [16]

4.1.3. Single layer and Double layer winding

The winding is said to be single layer if it has only one coil side in the stator slot. If there are two coil sides in one stator slot then it is called as double layer winding as shown in the below figure [12].
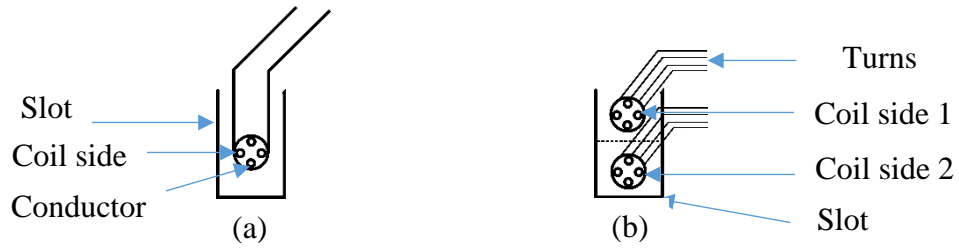
Figure 20 Single layer and double layer winding placement in the stator slots [12]

4.1.4. Fractional-slot and Integral-slot winding

This winding type is decided based on the number of slots per pole per phase given by,

$$q = \frac{Z_1}{2 * p * m} \qquad (6)$$

Where, Z_1 is the number of stator slots, p is number of pole pairs and m is the number of phases. If the value of number of slots per pole per phase (q) is a fraction then the winding type is said to be fractional-slot winding.

If the value of number of slots per pole per phase (q) is an integer then the winding type is said to be an integral-slot winding [12].

4.2. Single layer concentrated winding

Ampere loading calculations are performed for different ampere loading values ranging from 20 A/mm till 110 A/mm using FEMAG-DC. The calculations are done for each ampere loading value as mentioned in the Figure 16. This design contains the single layer concentrated winding with q = 0.5 from the equation (6) which involves two pole pairs.

The schematic and zone plan of a single layer concentrated winding is shown in the below figures.
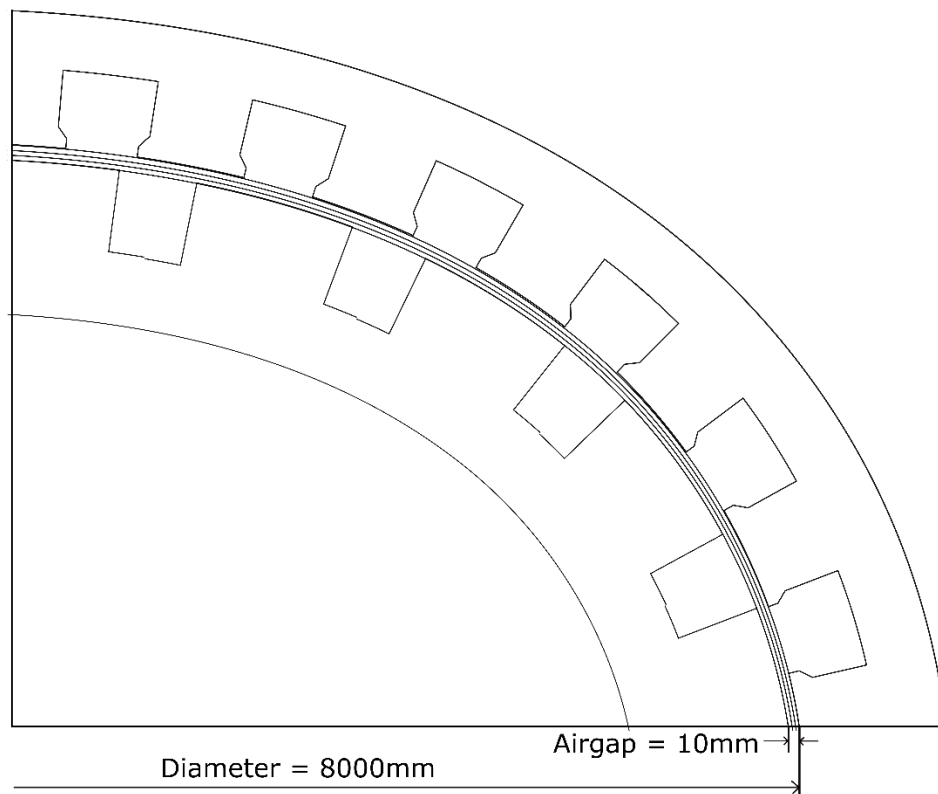
Figure 21 Technical drawing of single layer concentrated winding
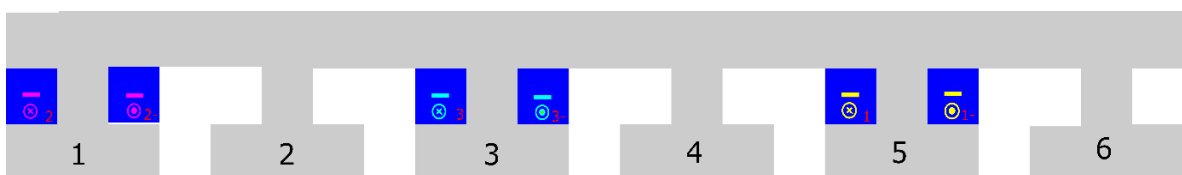
Figure 22 Zone plan of single layer concentrated winding

The below graphical analysis shows total costs, efficiency and active length curves for different ampere loading values. The optimum value for total costs is selected based on the cheaper machine concept. The total cost of the machine decreases gradually with the increase of ampere loading till 70 A/mm and remains constant till 100 A/mm and then the total cost curve starts increasing again. Therefore, at 70 A/mm the total costs of the machine is cheaper.
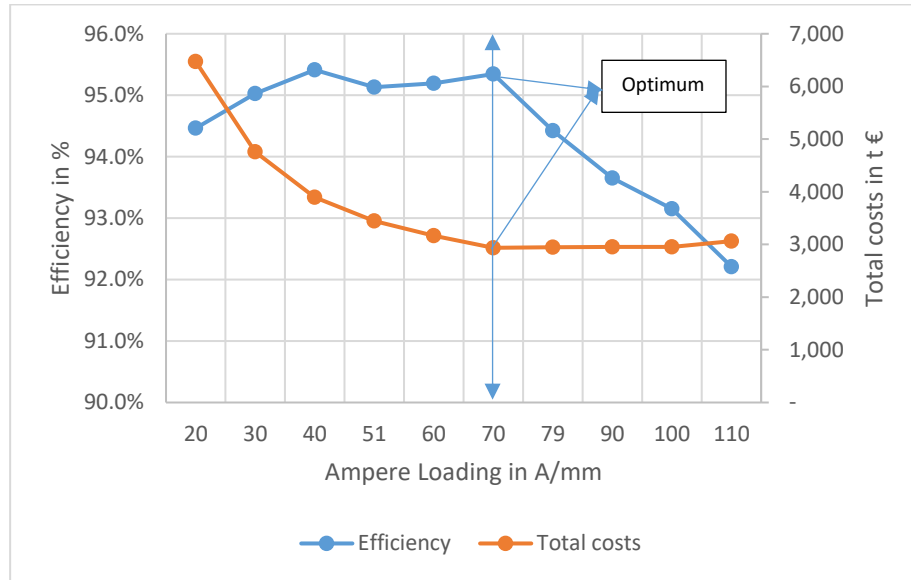
Figure 23 Graphical analysis of ampere loading vs. efficiency and total costs for concept 1ZW

Figure 24 Graphical analysis of ampere loading vs. active length for concept 1ZW

Later, an optimum is selected for the efficiency and active length to achieve the compact generator with high efficiency. There are two peak points in the efficiency curve but at the ampere loading value of 70 A/mm the active length is in the desired limit i.e., near to 1500 mm.

Whereas, at the ampere loading value of 40 A/mm the active length is more than the desired one. Therefore, the ampere loading value of 70 A/mm is selected as an optimum since the machine total cost is cheaper and the efficiency is high for the desired active length at this optimum to achieve the cheaper and compact machine with high efficiency.

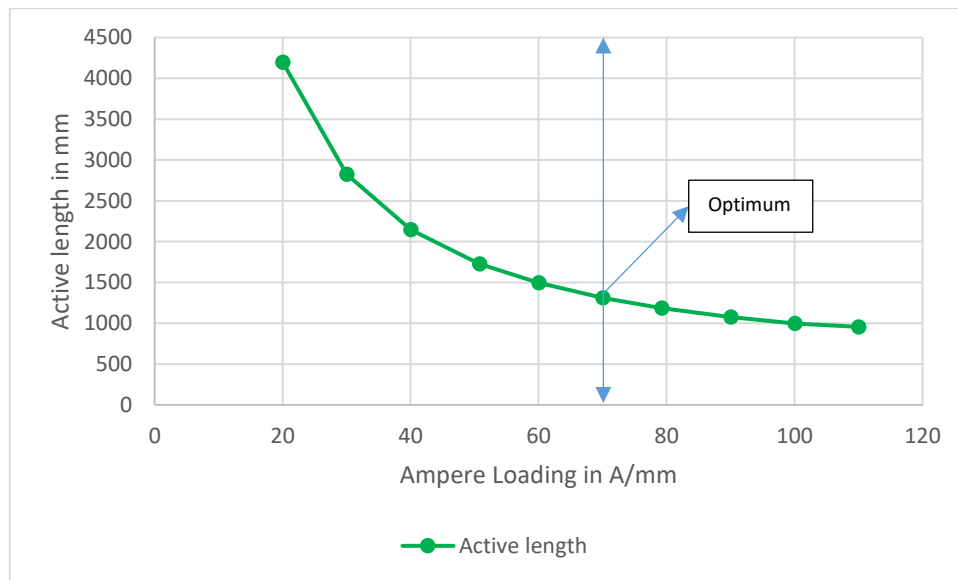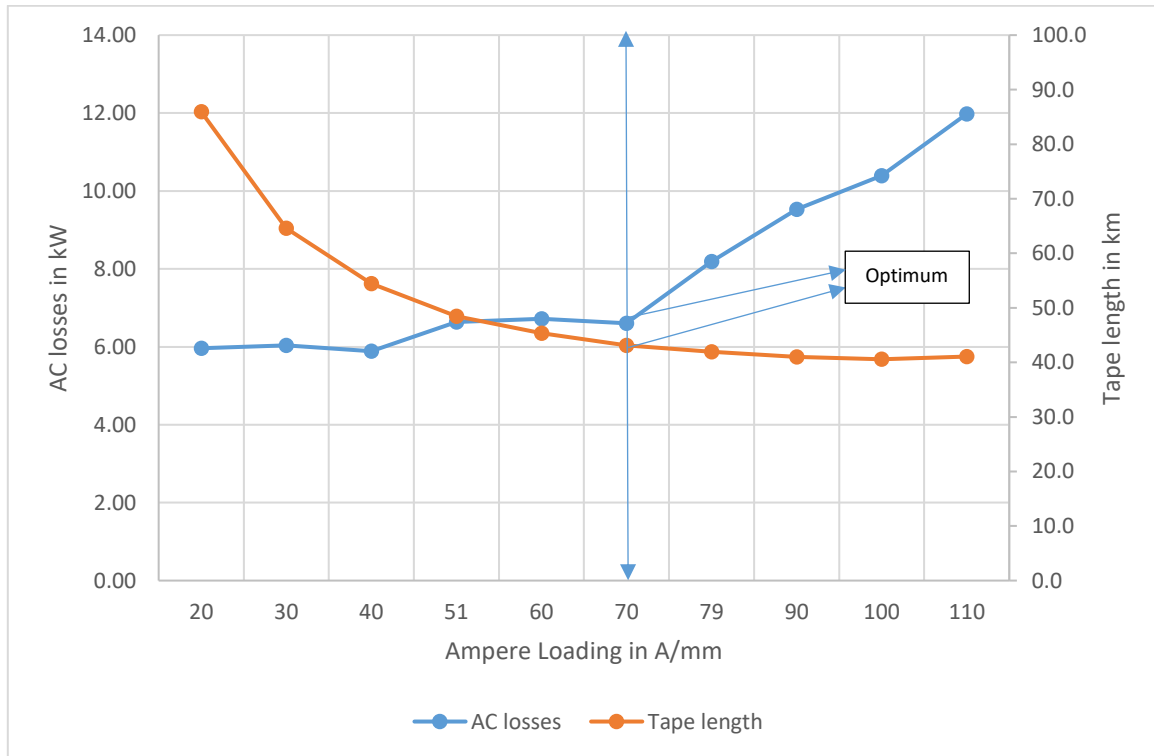*Figure 25 Graphical analysis of ampere loading vs. AC losses and tape length for concept 1ZW*

The above graphical analysis shows the behaviour of AC losses and tape length with different ampere loading values. The AC losses are on an increasing trend as the current loading increases. Whereas, the tape length keeps on decreasing gradually as the current loading increases since the torque is less which makes the machine bulk at low current loading value.

Therefore, at the selected optimum for ampere loading at 30 K, the machine has total losses of 65.91 kW, of which 89.97 % are iron losses and 10.02 % are AC losses, and the total HTS tape length of 43.1 km.

The important results obtained using FEMAG-DC are presented in the table below.

Table 7 Design parameters and results of the single layer concentrated winding

Parameter	Symbol	Value	Units
Diameter	D_i	8000	mm
Pole pairs	p	36	-
Number of slots	Z_1	108	-
Active length	l_i	1309	mm
Pole pitch	τ_p	349.1	mm
Active mass	m_{fe}	75.5	t
Total AC losses	P_{AC}	6.61	kW
Total Iron losses	P_{fe}	59.3	kW
Total losses	P_v	65.91	kW
Stator tape length	$l_{1,HTS}$	15.8	km
Rotor tape length	$l_{2,HTS}$	27.38	km
Total tape length	l_{HTS}	43.1	km
Efficiency	η	95.3	%
Total costs	C_t	2937	t €

At 70 A/mm, the flux distribution in the part of 10 MW fully HTS generator for single layer concentrated winding is shown in the Figure 26 where the stator and rotor yoke is designed to have maximum flux density as 1.8 T and 2 T respectively. The detailed results for the selected ampere loading optimum can be found in the appendix II.
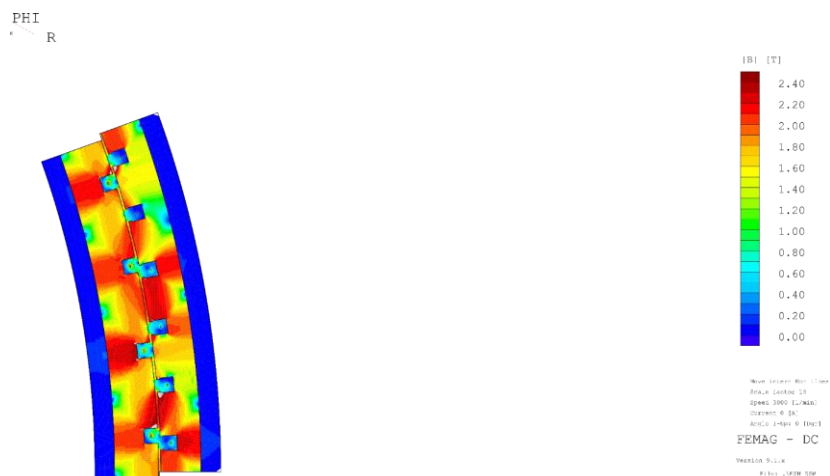
Figure 26 Magnetic flux density plot for single layer concentrated winding

4.3. Double layer concentrated winding

In this winding concept, FEMAG-DC is used to calculate different ampere loading values ranging from 20 A/mm to 170 A/mm to select an ampere loading optimum. As shown in Figure 58, simulations are run for each ampere loading value. The double layer concentrated winding with number of slots per pole per phase, q = 0.5 from equation (6) is used in this design, which involves one pole pair.

The schematic and zone plan of a double layer concentrated winding is shown in the below figures.
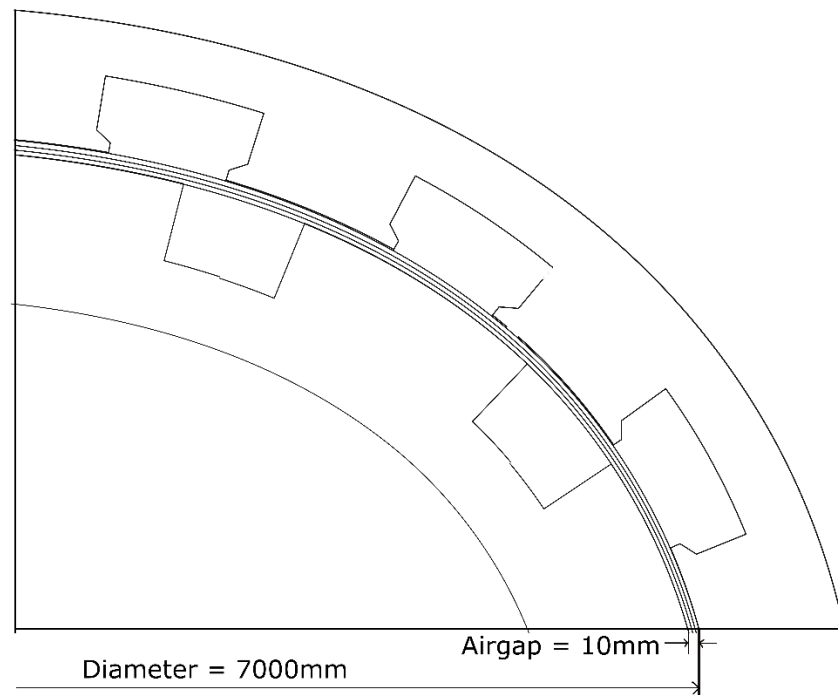
Figure 27 Technical drawing of double layer concentrated winding
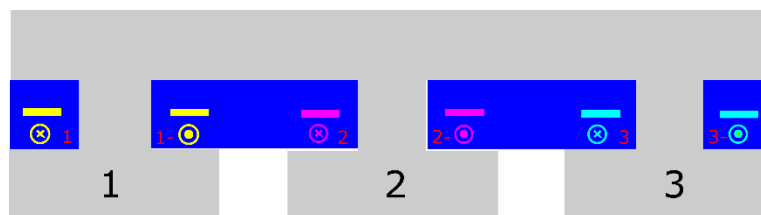
Figure 28 Zone plan of double layer concentrated winding

Total costs, efficiency, and active length curves for various ampere loading levels are shown in the graphs below. Based on the cheaper machine concept, the best overall cost value is chosen. The machine's total cost drops progressively as the ampere loading increases until it reaches 160 A/mm, at which point the total cost curve begins to rise again.
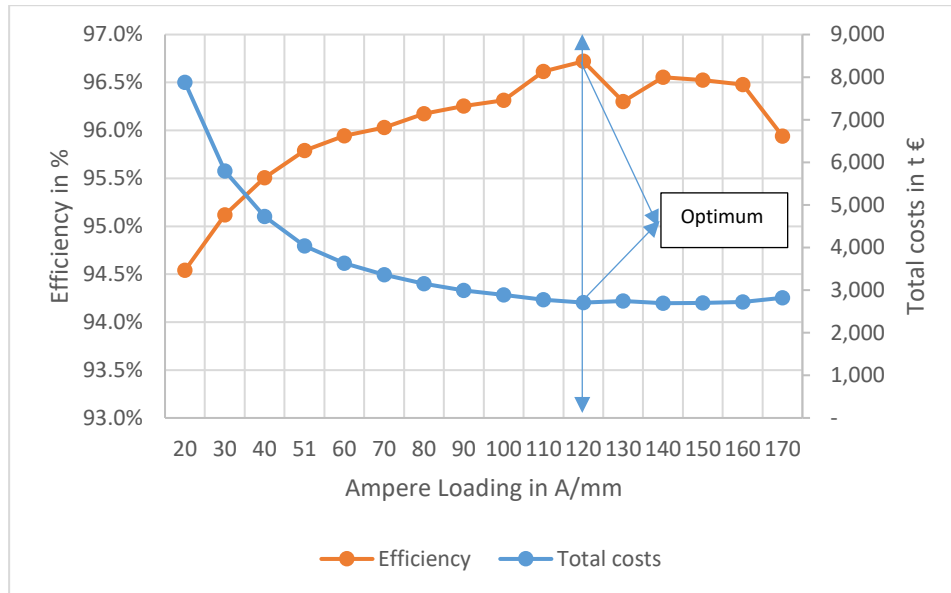
Figure 29 Graphical analysis of ampere loading vs. efficiency and total costs for concept 2ZW
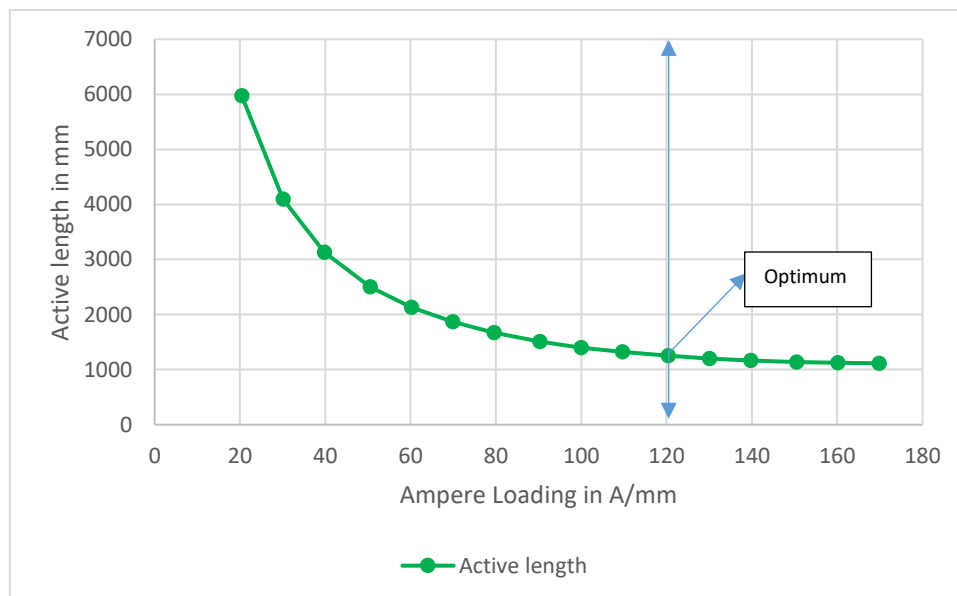
Figure 30 Graphical analysis of ampere loading vs. active length for concept 2ZW

After that, an optimum for efficiency and active length is chosen to provide a small generator with high efficiency. The graph clearly shows that the best efficiency is at 120 A/mm on the efficiency curve.

As a result, the ampere loading value of 120 A/mm is chosen as an optimum since the total cost of the machine is lower and the efficiency is higher for the desired active length at this optimum, resulting in a less expensive and compact machine with high efficiency.
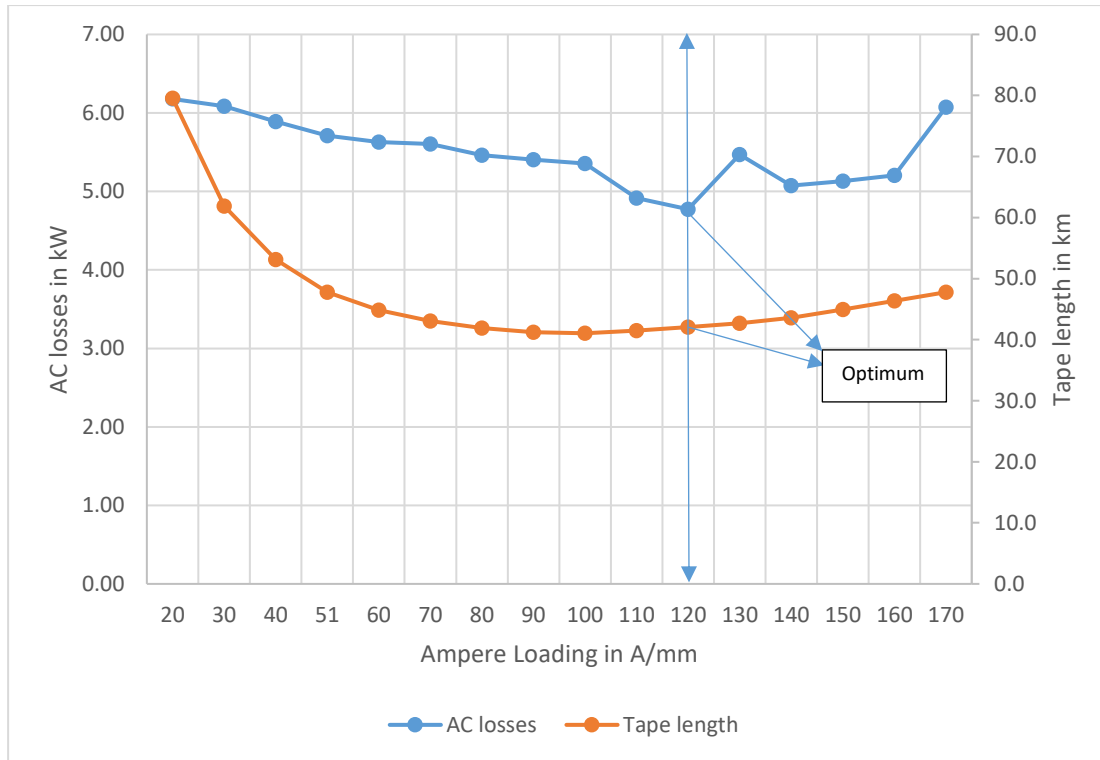
Figure 31 Graphical analysis of ampere loading vs. AC losses and tape length for concept 2ZW

The above graphical analysis shows the behaviour of AC losses and tape length with different ampere loading values. The AC losses are on a decreasing trend as the current loading increases. And the tape length keeps on decreasing gradually as the current loading increases because of the low torque which makes the machine bulk at low current loading value.

Therefore, at the selected optimum for ampere loading at 30 K, the machine has total losses of 38.87 kW, of which 87.72 % are iron losses and 12.27 % are AC losses, and the total HTS tape length of 42.1 km.

The important results obtained using FEMAG-DC are presented in the below table.

Table 8 Design parameters and results of the double layer concentrated winding

Parameter	Symbol	Value	Units
Diameter	D_i	7000	mm
Pole pairs	p	22	-
Number of slots	Z_1	66	-
Active length	l_i	1255	mm
Pole pitch	τ_p	499.8	mm
Active mass	m_{fe}	74.7	t
Total AC losses	P_{AC}	4.77	kW
Total Iron losses	P_{fe}	34.1	kW
Total losses	P_v	38.87	kW
Stator tape length	$l_{1,HTS}$	24.4	km
Rotor tape length	$l_{2,HTS}$	17.67	km
Total tape length	l_{HTS}	42.1	km
Efficiency	η	96.7	%
Total cost	C_t	2710	t €

At 120 A/mm, the flux distribution in the part of 10 MW fully HTS generator for double layer concentrated winding is shown in the Figure 32 where the stator and rotor yoke is designed to have maximum flux density as 1.8 T and 2 T respectively. The detailed results for the selected ampere loading optimum can be found in the appendix II.
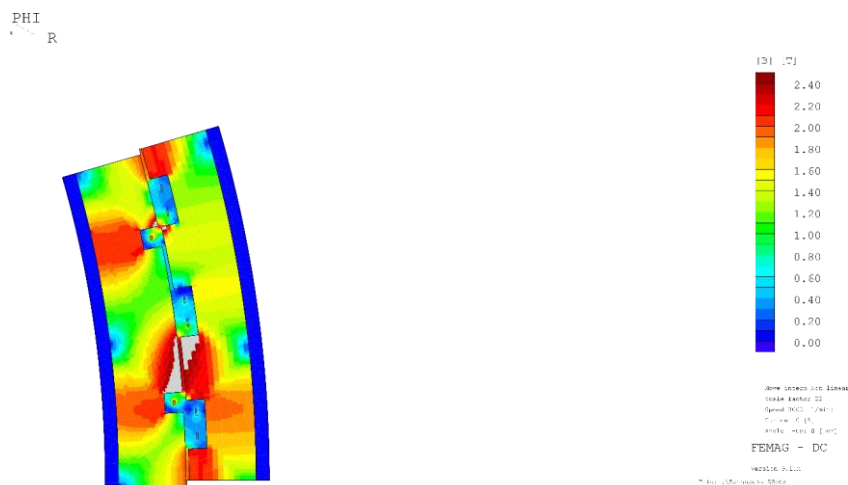
Figure 32 Magnetic flux density plot for double layer concentrated winding

4.4. Double layer distributed Air-gap winding

For various ampere loading values ranging from 15 A/mm to 230 A/mm, FEMAG-DC is utilized for performing ampere loading calculations. Simulations are done for each ampere loading value, as illustrated in Figure 59. This design employs a double layer distributed Air-gap winding with a number of slots per pole per phase of q = 1 from the equation (6).

The schematic and zone plan of a double layer distributed air-gap winding is shown in the below figures.
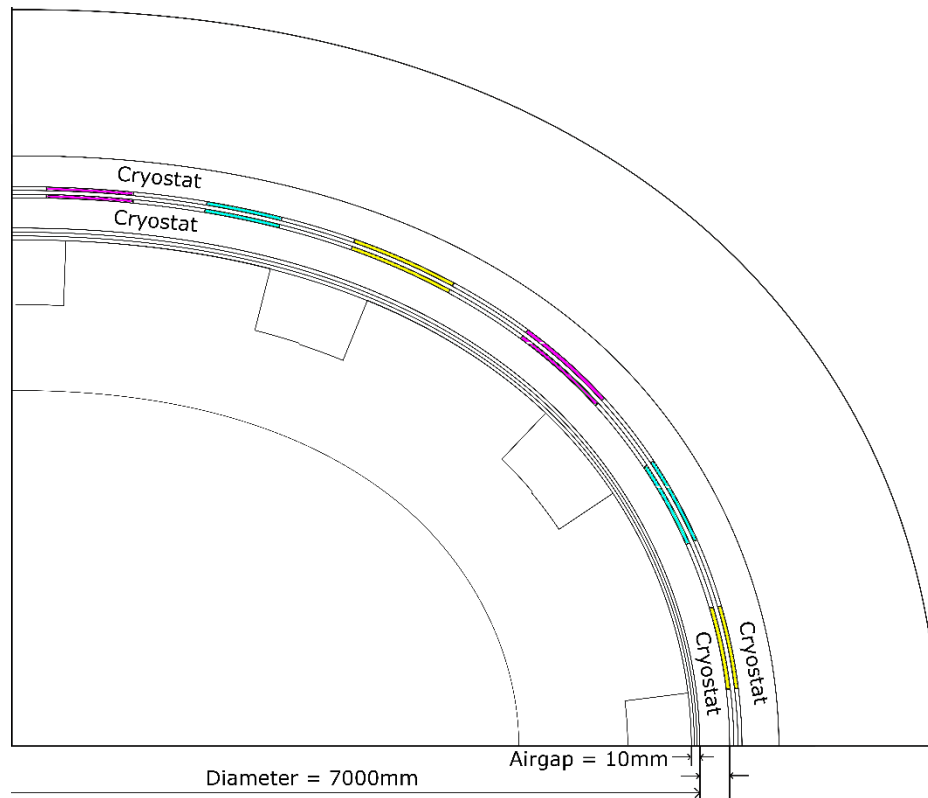
Figure 33 Technical drawing of double layer distributed Air-gap winding

Figure 34 Zone plan of double layer distributed Air-gap winding

The graph below shows total costs, efficiency, and active length curves for various ampere loading levels. The optimum total cost value is decided based on the less expensive machine concept. The total cost of the machine decreases as the ampere loading increases. Total expenses drop dramatically until 101 A/mm, after which they remain constant until 230 A/mm.

Figure 35 Graphical analysis of ampere loading vs. efficiency & total costs for concept LSW
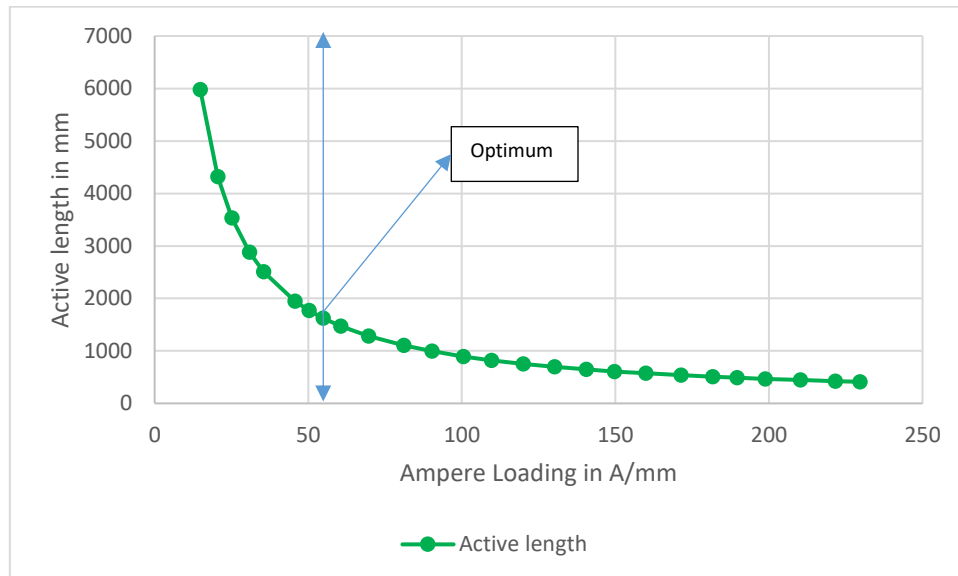
Figure 36 Graphical analysis of ampere loading vs. active length for concept LSW

Further, an optimum is selected for the efficiency and active length to achieve the compact generator with high efficiency. The efficiency curve increments till 25 A/mm and the efficiency has a declining trend till 230 A/mm.

Therefore, the ampere loading value of 55 A/mm is selected as an optimum since the machine total cost is cheaper and the efficiency is high for the desired active length at this optimum compared to other ampere loading values to achieve the cheaper and compact machine with high efficiency.
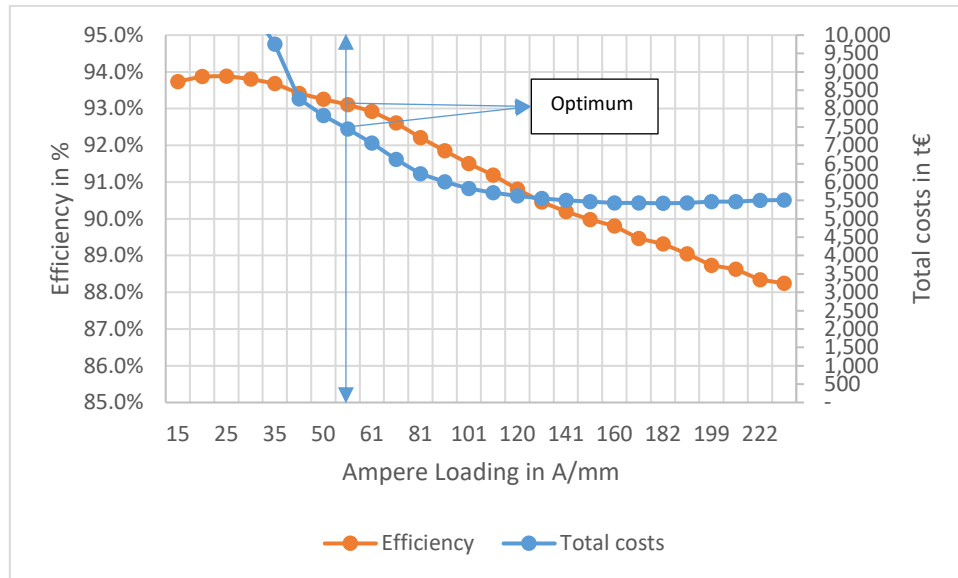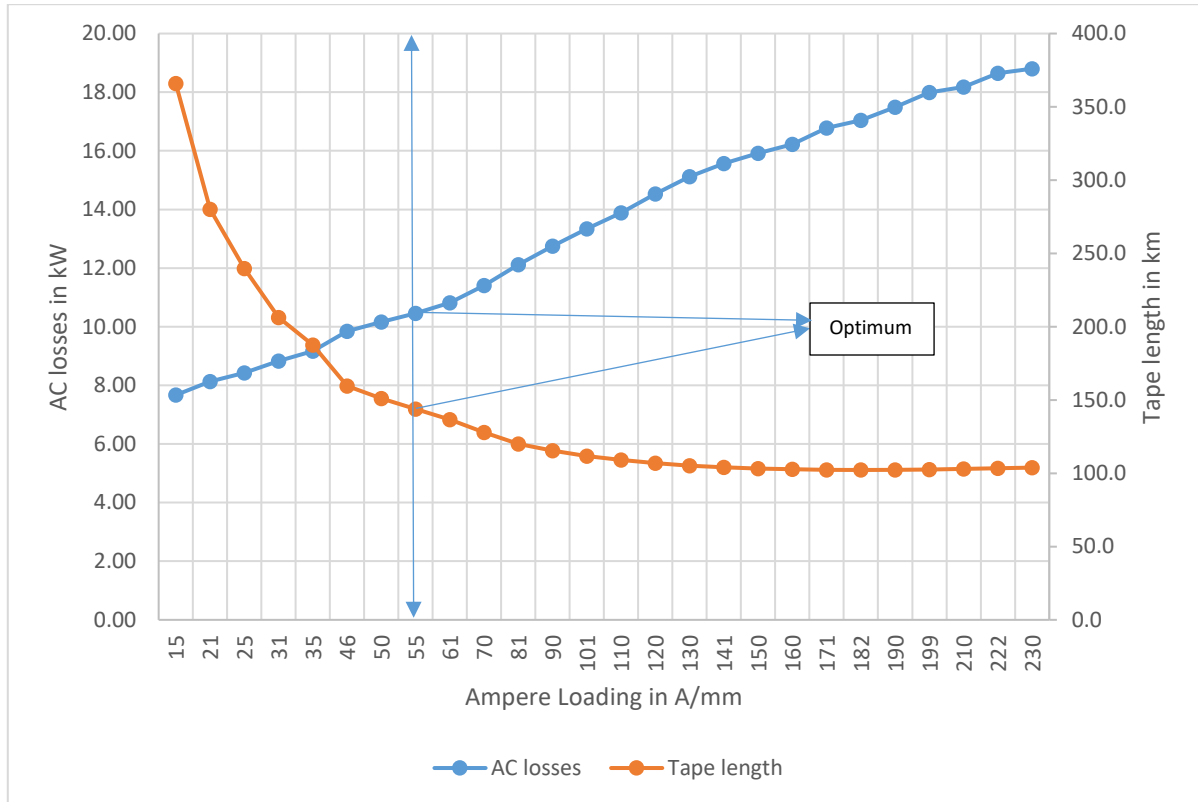

Figure 37 Graphical analysis of ampere loading vs. AC losses & tape length for concept LSW

The graph above depicts the relationship between AC losses and tape length for various ampere loading values. As the current loading increases, the AC losses are on the rise. The tape length, on the other hand, gradually decreases as the current loading increases since the torque is lower, causing the machine to become bulky at low current loading values.

Therefore, at the selected optimum for ampere loading at 30 K, the machine has total losses of 54.16 kW, of which 80.68 % are iron losses and 19.31 % are AC losses, and the total HTS tape length of 143.9 km.

The important results obtained using FEMAG-DC are presented in the below table.

Table 9 Design parameters and results of the double layer distributed Air-gap winding

| Parameter	Symbol	Value	Units
Diameter	D_i	7000	mm
Pole pairs	p	18	-
Number of slots	Z_1	108	-
Active length	l_i	1626	mm
Pole pitch	τ_p	610.9	mm
Active mass	m_{fe}	159.9	t
Total AC losses	P_{AC}	10.46	kW
Total Iron losses	P_{fe}	43.7	kW
Total losses	P_v	54.16	kW
Stator tape length	$l_{1,HTS}$	23.8	km
Rotor tape length	$l_{2,HTS}$	120.03	km
Total tape length	l_{HTS}	143.9	km
Efficiency	η	93.1	%
Total cost	C_t	7442	t €

At 55 A/mm, the flux distribution in the part of 10 MW fully HTS generator for double layer distributed air-gap winding is shown in the Figure 38 where the stator and rotor yoke is designed to have maximum flux density as 1.8 T and 2 T respectively. The red triangles in the rotor yoke represents the magnetic flux density between 2 T and 2.2 T and the grey part near the air-gap indicates the saturated region with magnetic flux density of above 2.4 T. The detailed results for the selected ampere loading optimum can be found in the appendix II.
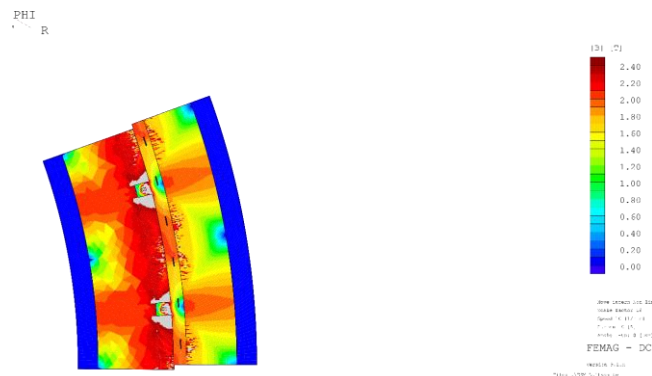
Figure 38 Magnetic flux density plot for double layer distributed Air-gap winding

4.5. Single layer distributed winding

Ampere loading calculations are performed for different ampere loading values ranging from 20 A/mm till 118 A/mm using FEMAG-DC. The simulations are done for each ampere loading value as mentioned in the Figure 60. This design contains the single layer distributed integral-slot winding with number of slots per pole per phase, q = 1 from the equation (6) with one pole pair involved.

The schematic and zone plan of a single layer distributed winding is shown in the below figures.
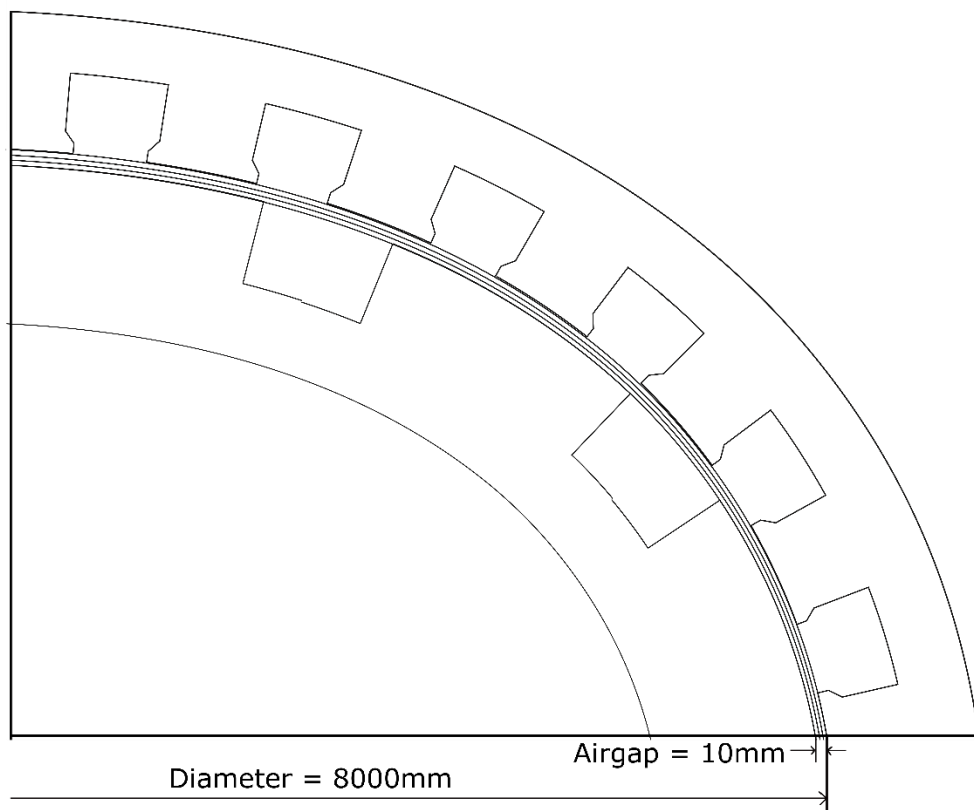
Figure 39 Technical drawing of single layer distributed winding
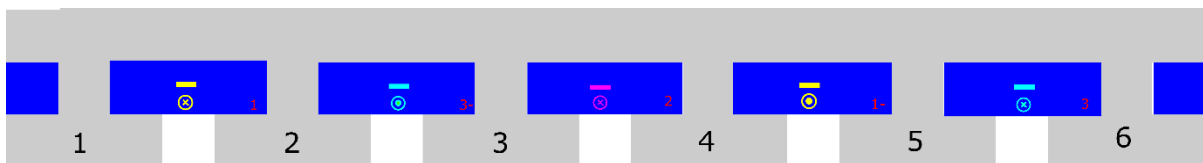
Figure 40 Zone plan of single layer distributed winding

The below graphical analysis shows total costs, efficiency and active length curves for different ampere loading values. The optimum value for total costs is selected based on the cheaper machine concept. The total cost of the machine decreases gradually with the increase of ampere loading till 79 A/mm and starts increasing again from 90 A/mm.

Figure 41 Graphical analysis of ampere loading vs. efficiency & total costs for concept 1VW

Figure 42 Graphical analysis of ampere loading vs. active length for concept 1VW

Later, an optimum is selected for the efficiency and active length to achieve the compact generator with high efficiency. The efficiency curve has a declining trend as ampere loading value increases.

Therefore, the ampere loading value of 49 A/mm is selected as an optimum since the machine total cost is cheaper and the efficiency is high for the desired active length at this optimum compared to the other ampere loading values to achieve the cheaper and compact machine with high efficiency.

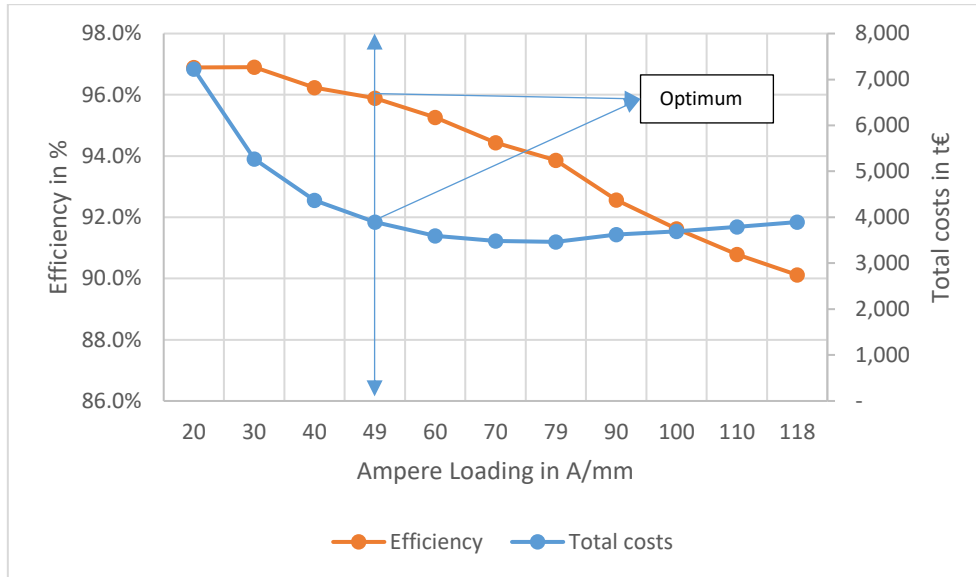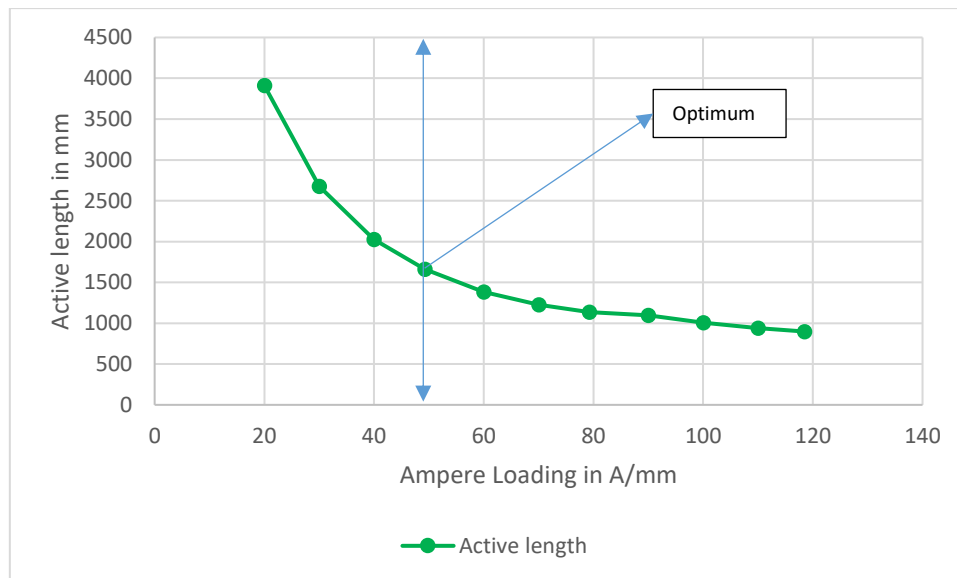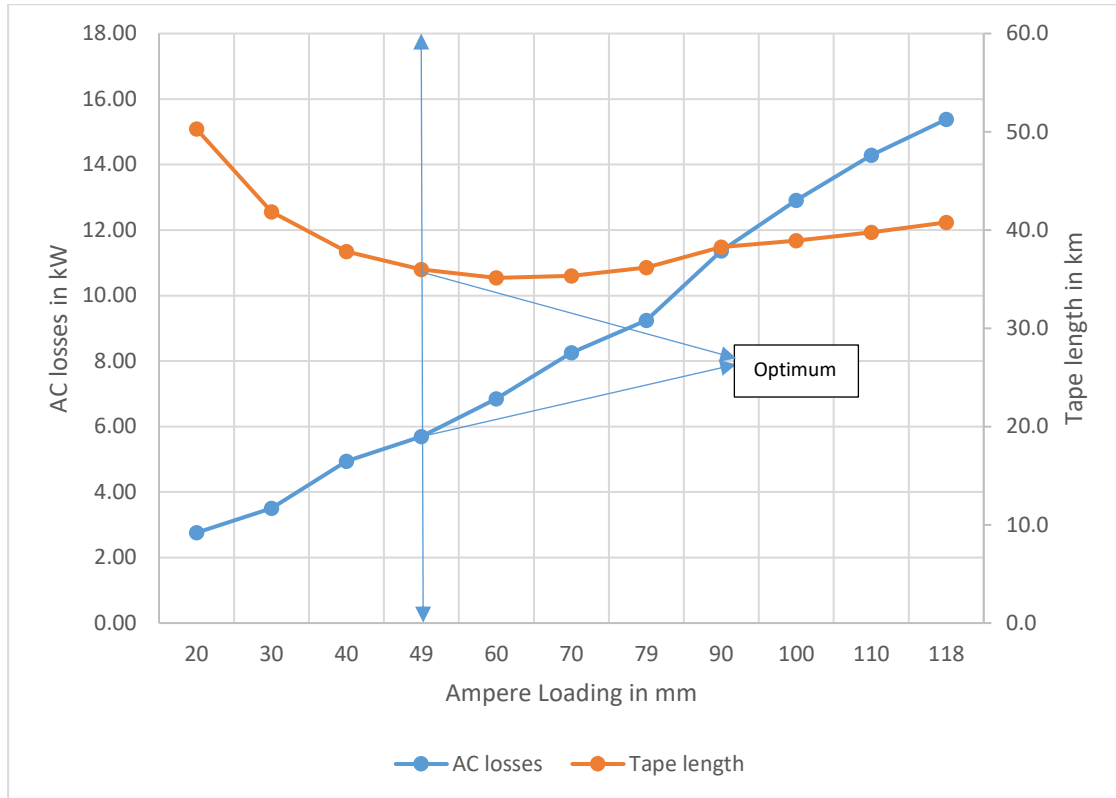*Figure 43 Graphical analysis of ampere loading vs. AC losses & tape length for concept 1VW*

The above graphical analysis shows the behaviour of AC losses and tape length with different ampere loading values. The AC losses are on an increasing trend as the current loading increases. Whereas, the tape length keeps on decreasing gradually as the current loading increases till 70 A/mm since the torque is less which makes the machine bulk at low current loading value. From 70 A/mm, the tape length increases as the current loading increases.

Therefore, at the selected optimum for ampere loading at 30 K, the machine has total losses of 67.1 kW, of which 91.50 % are iron losses and 8.49 % are AC losses, and the total HTS tape length of 36.0 km.

The important results obtained using FEMAG-DC are presented in the below table.

Table 10 Design parameters and results of the single layer distributed winding

| Parameter	Symbol	Value	Units
Inner diameter	D_i	8000	mm
Pole pairs	p	18	-
Number of slots	Z_1	108	-
Active length	l_i	1660	mm
Pole pitch	τ_p	698.1	mm
Active mass	m_{fe}	172.8	t
Total AC losses	P_{AC}	5.70	kW
Total Iron losses	P_{fe}	61.4	kW
Total losses	P_v	67.1	kW
Stator tape length	$l_{1,HTS}$	16.7	km
Rotor tape length	$l_{2,HTS}$	19.26	km
Total tape length	l_{HTS}	36.0	km
Efficiency	η	95.9	%
Total cost	C_t	3896	t €

At 49 A/mm, the flux distribution in the part of 10 MW fully HTS generator for single layer distributed winding is shown in the Figure 44 where the stator and rotor yoke is designed to have maximum flux density as 1.8 T and 2 T respectively. The detailed results for the selected ampere loading optimum can be found in the appendix II.
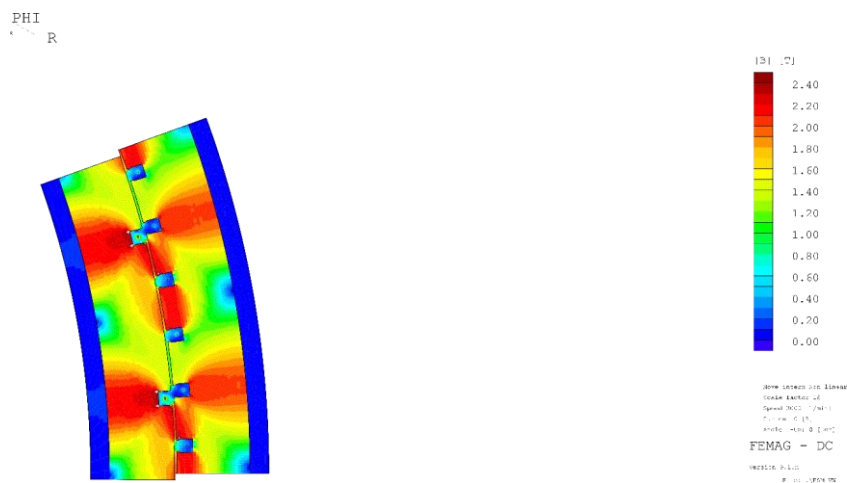
Figure 44 Magnetic flux density plot for single layer distributed winding
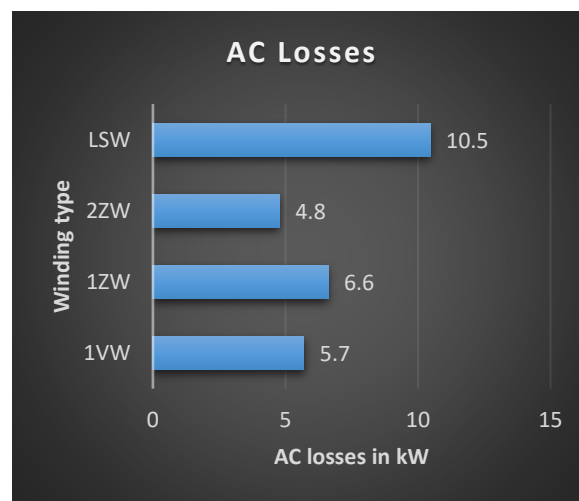
4.6. Comparison of the winding concepts

As discussed in the previous sections, the stator optimization is done by focusing on selecting a suitable winding type for the stator of the 10 MW fully HTS generator. Therefore, the above-mentioned four winding concepts are designed and simulated to calculate flux distribution and critical current at an operating temperature of 30 K using the finite element software FEMAG-DC. In this section, a detailed comparison of the four winding concepts is discussed for the selected ampere loading optimum values.

Table 11 Comparison of selected optimum values for four winding concepts

| Parameter	Symbol	1ZW	2ZW	LSW	1VW	Units
Rated power	P_N	10.5	10.5	10.5	10.5	MW
Diameter	D_i	8000	7000	7000	8000	mm
Pole pairs	p	36	22	18	18	-
Number of slots	Z_1	108	66	108	108	-
Number of winding turns	W_{RT}	91	112	48	64	-
Stator coil current	I_{SP}	179.064	179.064	116.3	179.064	A
Stator ampere loading	A_1	70	120	55	49	A/mm
Active length	l_i	1309	1255	1626	1660	mm
Pole pitch	τ_p	349.1	499.8	610.9	698.1	mm
Active mass	m_{fe}	75.5	74.7	159.9	172.8	t
Total AC losses	P_{AC}	6.61	4.77	10.46	5.70	kW
Total Iron losses	P_{fe}	59.3	34.1	43.7	61.4	kW
Total losses	P_v	65.91	38.87	54.16	67.1	kW
Stator tape length	$l_{1,HTS}$	15.8	24.4	23.8	16.7	km
Rotor tape length	$l_{2,HTS}$	27.38	17.67	120.03	19.26	km
Total tape length	l_{HTS}	43.18	42.1	143.9	36.0	km
Power density	P_D	139	141	66	61	W/kg
Efficiency	η	95.3	96.7	93.1	95.9	%
Total cost	C_t	2937	2710	7442	3896	t€

The important design parameters considered to select an optimum value for each winding concept are clearly shown in Table 11. Although many factors influence machine design, the appropriate winding type for the 10 MW fully HTS generator is chosen in this study based on the following factors.

1. The consideration of AC losses is very important in selecting an appropriate winding type in order to prevent the expensive cryogenic system, which also has an effect on the total cost of the generator. As a result, the 2ZW is the best choice in this case because its approximate AC losses are 4.77 kW, which are lower than those of other winding designs.


Figure 45 Comparison of AC losses for the winding concepts

2. The 2ZW electric efficiency of the generator is 96.7 percent, which is higher than the other winding designs since 2ZW has low total losses.
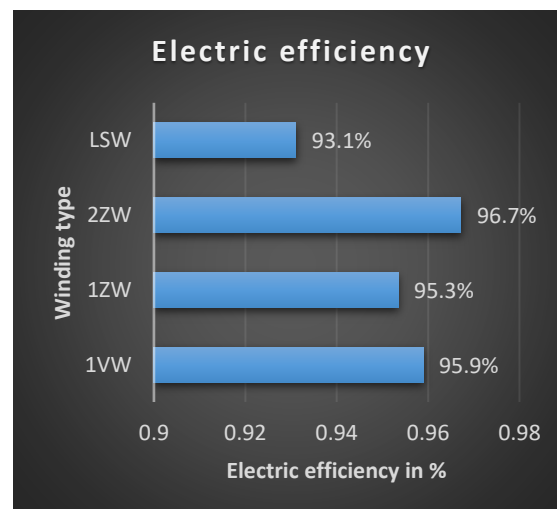
Figure 46 Comparison of electric efficiency for the winding concepts

3. Because of the decreased number of turns, the total HTS tape length required for 1VW is less than for the other winding concepts. Whereas the requirement for air-gap winding on HTS tape is larger due to the increased number of winding turns in field winding. Because air-gap winding lacks stator teeth and slots, the field winding must have a greater number of winding turns to magnetize the stator winding. Therefore, the HTS tape demand for air-gap winding is significantly high than other winding designs.

Tape length

| Winding type	Tape length in km
LSW	144
2ZW	42
1ZW	43
1VW	36
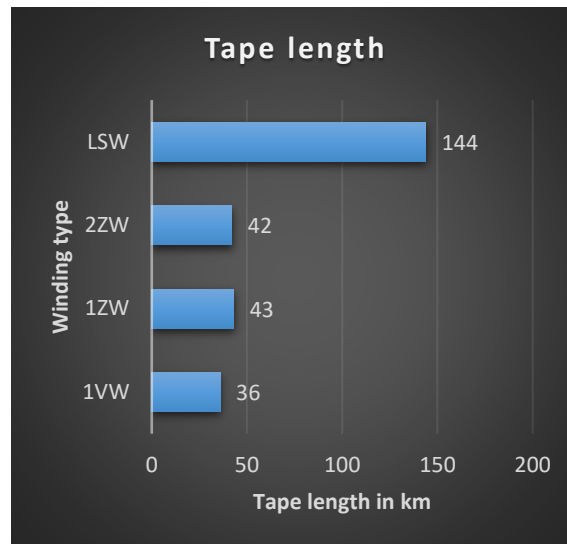
Figure 47 Comparison of tape length for the winding concepts

4. Estimating the generator's total cost is challenging due to the influence of several other design characteristics. The total cost of the generator is estimated in this study by adding the costs of the cryo-cooler, iron, and HTS tape. In this investigation, the 2ZW was found to be the most cost-effective machine when compared to other winding designs.

Total costs

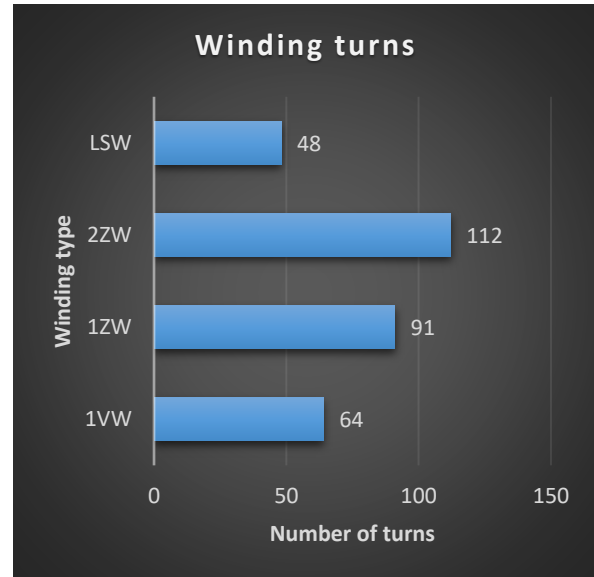| Winding type	Total costs in t €
LSW	7,442
2ZW	2,710
1ZW	2,937
1VW	3,896

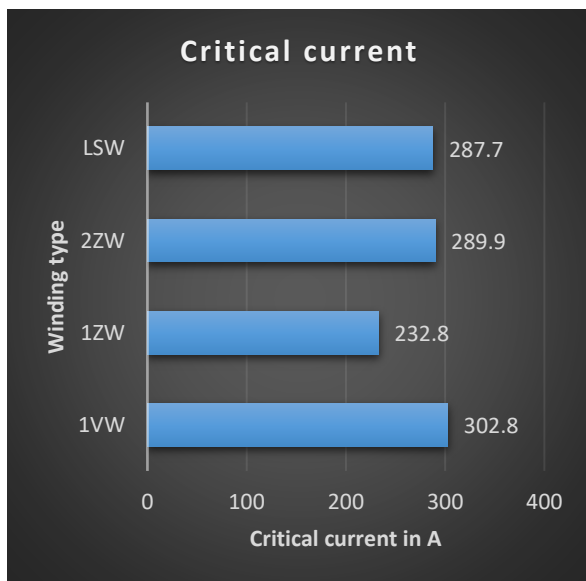*Figure 48 Comparison of total costs for the winding concepts*

The comparison of the winding concepts for other parameters like active length, winding turns, critical current, iron losses and power density can be found in the below table.
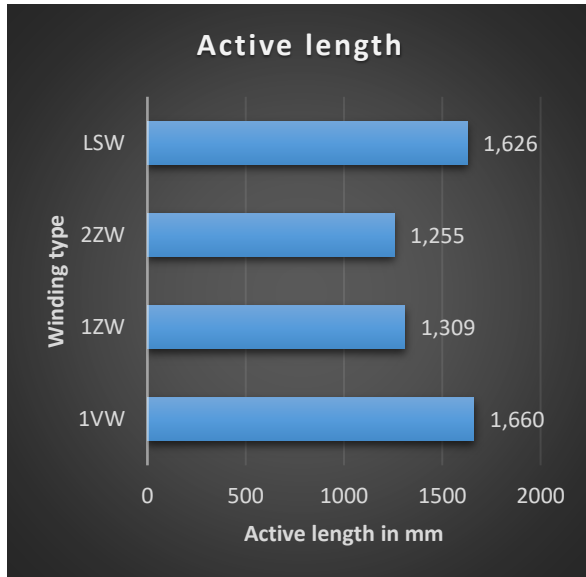
(a)

(b)

(c)
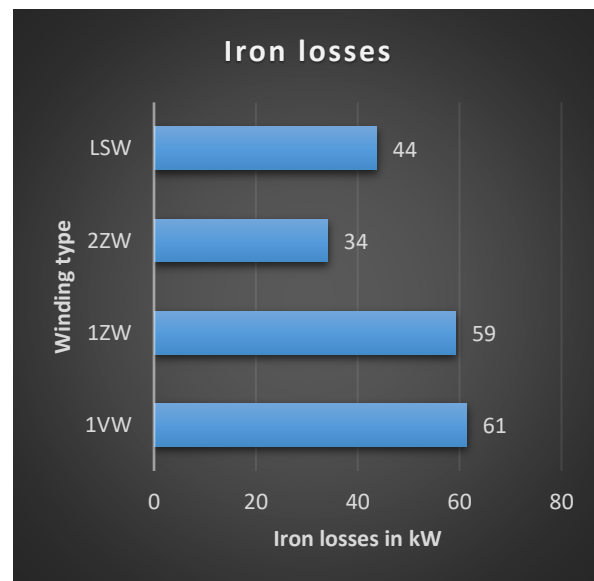
(d)

(e)

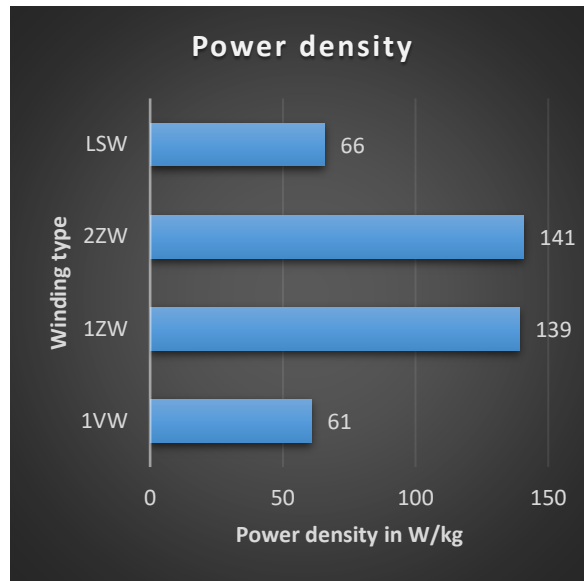*Figure 49 Comparison of (a) active length, (b) winding turns, (c) critical current, (d) iron losses, and (e) power density for the winding concepts*

From the above comparison, the two-layer concentrated winding (2ZW) can be considered a suitable winding type for the 10 MW fully HTS generator operating at 30 K, as it has a lower total cost, high efficiency, less tape length, low AC losses, and a high power density.

Chapter 5 Analysis of the winding concepts at different temperature levels

5.1. Introduction

An attempt was made in the previous chapter to identify a suitable winding type for the 10 MW fully HTS generator at an operating temperature of 30 K by analyzing the behaviour of the generator for various ampere loadings in the stator winding. Now in this chapter, the analysis has been carried out at various temperature levels (i.e., 20 K, 40 K, 50 K, and 65 K) to analyze the behaviour of the generator.

The operating temperature has a significant impact on the design parameters and performance of the generator. This investigation is focused on the parameters like critical current, power density, HTS tape length, AC losses, winding turns, and iron mass.

After running simulations at 30 K for various ampere loading levels, an optimum for each winding concept is chosen. As a result, additional simulations are run at various temperature levels for the selected ampere loading optimum for each winding design. Figure 50 depicts the simulation procedure for four winding concepts at an operating temperature of 20 K, where i represents the winding type and n represents the ampere loading value. As previously stated in section 3.4, the simulation procedure runs in a loop until the condition for each winding concept becomes false.
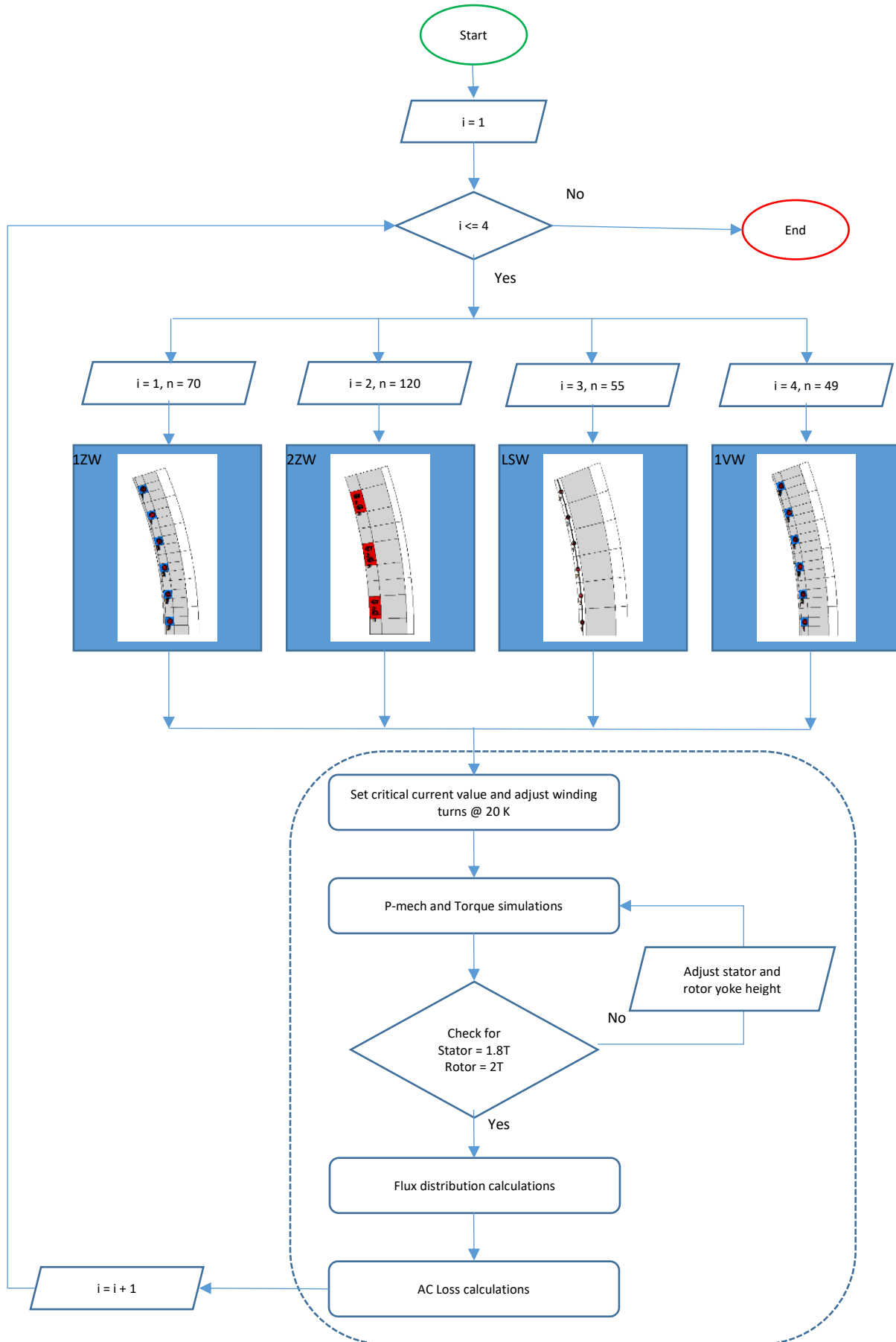
Figure 50 Process flow chart of the winding concepts at 20 K

5.2. Analysis

For the same 10 MW fully superconducting generator, analysis has been carried out at different intermediate temperature levels. Therefore, the operating temperature is a variable in this investigation i.e., operating temperature is varied from 20 K to 65 K. Although the operating temperature variation influences many parameters, some key parameters are analysed in this investigation as explained below.


(a)

(b)
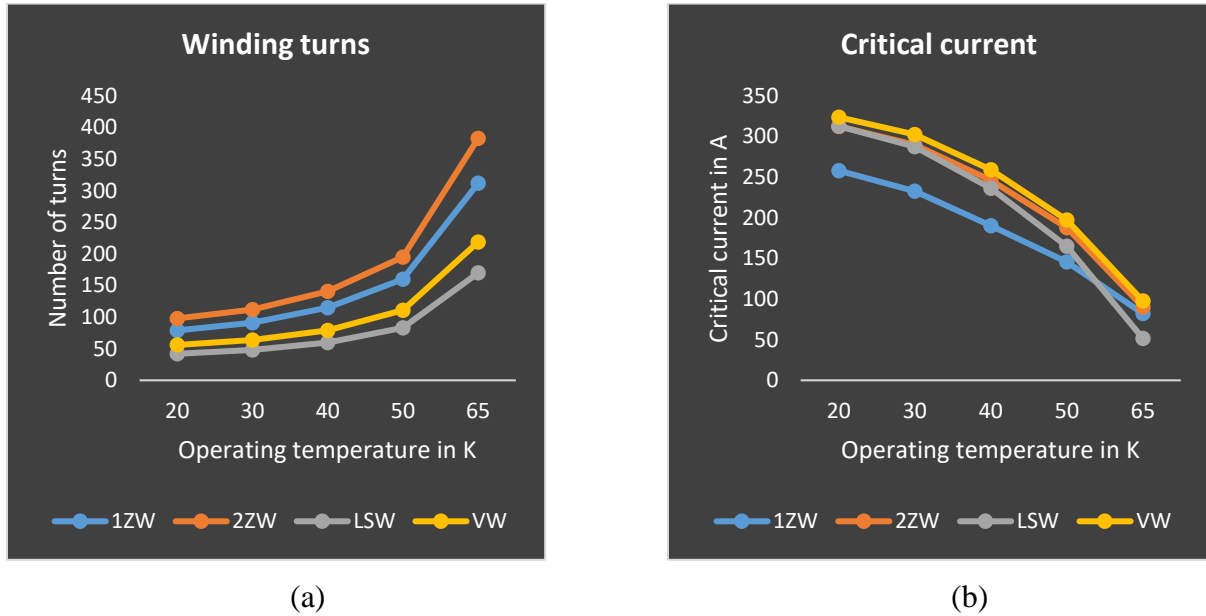
Figure 51 Graphical analysis of the winding concepts at different operating temperatures for (a) winding turns, and (b) critical current

The superconducting materials have the advantage that the critical current increases with the decrease in temperature since the resistance becomes zero as temperature decreases. Since an ampere loading optimum is selected for each winding concept at 30 K (in Chapter 4), the same ampere loading optimum values are considered in this investigation. Therefore, in order to maintain the constant ampere loading value, the number of turns must be varied with the calculated critical current (initial approximation) value at each temperature level. After the calculation, the above graphical analysis shows that the number of turns increases as the operating temperature increases because at a high critical current the required number of turns is less.

In Figure 52, it can be observed that the tape length increases as the operating temperature increases for four winding concepts. This is because of increase in number of turns in the stator winding since tape length is directly proportional to the number of turns.

However, air-gap winding needs more HTS tape because field winding has more winding turns. Since the air-gap winding lacks the stator teeth and slots, additional winding turns are required for the field winding in order to magnetize the stator winding. As a result, the air-gap winding requires substantially more HTS tape than other winding designs.
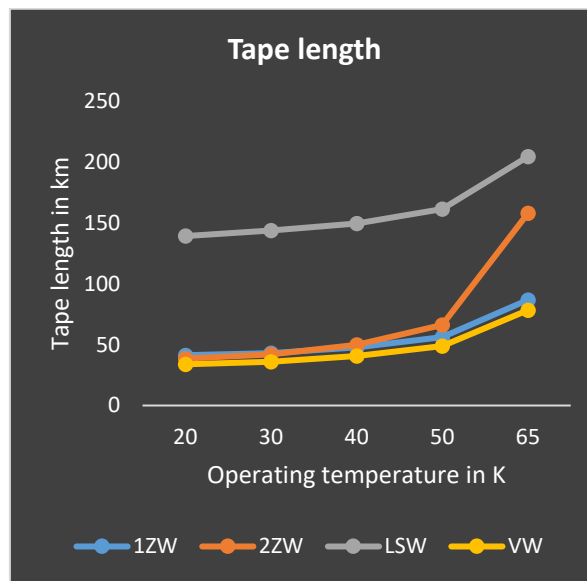
Figure 52 Graphical analysis of tape length for the winding concepts at different temperatures

The above analysis is restricted to a few parameters of the 10 MW fully HTS generator since there are some inconsistencies in the results of other parameters at different operating temperature levels. Therefore, further investigation is necessary to select the suitable operating temperature level like performing additional simulations to analyse the behaviour of AC losses, active length, efficiency and other relevant parameters.

Chapter 6 AC loss reduction method

Strong research on superconducting generators for wind turbine applications has been pushed by increasing global energy demand, where HTS could boost power density and lead to better multi-megawatt systems [18]. In comparison with conventional machines, HTS machines are predicted to be smaller and lighter because of higher current and magnetic fields. The HTS materials do not show losses when operating with DC current. But the losses are expected when HTS materials are exposed to alternating current and magnetic field even though there is zero resistance. Such losses are called AC losses. These AC losses must be investigated and reduced because they will increase the cooling system and, as a result, reduce the machine's overall efficiency [15].

Techniques to reduce AC losses in fully HTS generators have got a lot of attention. As a result, a number of researchers have come up with strategies for decreasing AC losses [4], [20], and [14]. This study focuses on one specific approach for minimizing AC losses, as stated in [4].

6.1. Motivation

The goal of this investigation [4] is to perform basic research on a method to reduce AC losses in HTS coils when they are used in the stator winding of AC rotating machines. They investigated a method for suppressing the perpendicular component of the magnetic flux density applied to the tape surface in the coil to reduce AC loss by inserting a magnetic substance in the region around the winding in the iron core slot. FEM is used to numerically examine the magnetic field distribution around the coil winding, as well as the effect of putting magnetic material around the coil winding to lower the magnetic flux density's perpendicular component.

The study was conducted on two racetrack coils wound by Bi2223 tape (coil 1) and YBCO tape (coil 2) to measure AC losses when a magnetic material is placed in the stator slots.

The magnetic material is inserted right below the HTS coil in the stator slot of the iron core, as indicated in the diagram below. The following three magnetic configurations are considered:

1. In arrangement A, the magnetic material is positioned below the HTS coil and covers the whole slot in the stator from the lower edge of the HTS coil

2. In arrangement B, the magnetic material is positioned beneath the HTS coil and covers half of the stator slot from the HTS coil's lower edge.

3. In arrangement C, there is no magnetic material placed below the HTS coil
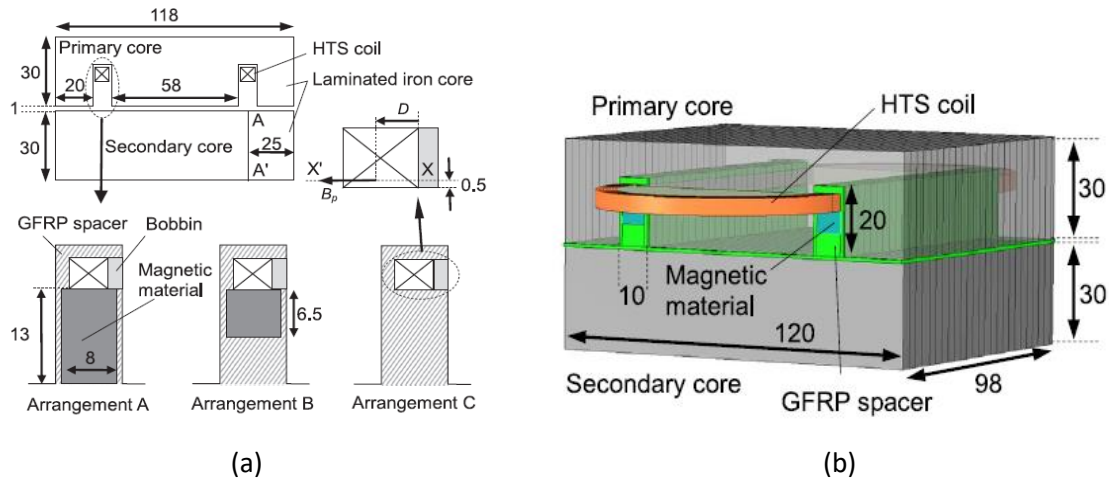

(a)   (b)

Figure 53 (a) Cross-sectional view of placing magnetic material in three different arrangements [4], (b) 3D view of the arrangement with magnets [4]

The plots of magnetic flux lines for coil 2 arrangements A, B, and C are shown in Figure 50. The magnetic field locally induced around the edge of the coil winding intersects the winding, as indicated in this diagram, and the HTS tapes are subjected to a perpendicular component of the magnetic flux density in arrangement C. The magnetic field surrounding the coil edge bypasses the magnetic material in arrangements A and B, on the other hand. These findings in Figure 54 imply that by strategically inserting magnetic material surrounding the coil winding, the AC loss can be decreased. The magnetic flux linked to the secondary core reduces as a portion of the magnetic flux produced by the HTS coil bypasses through the magnetic material inserted in the slot [4].
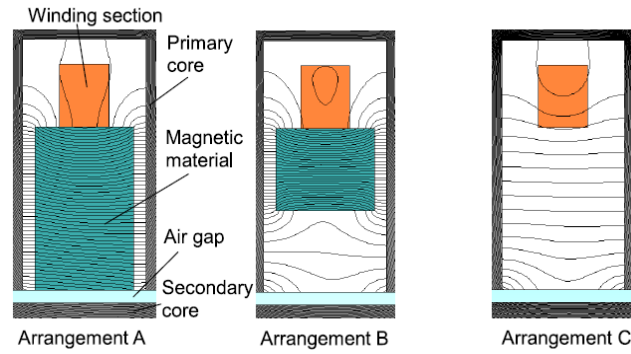
Figure 54 Magnetic field distribution for three different arrangements [4]

As a consequence of inserting a magnet below the HTS coil in the stator slot, they found that the coil wound with YBCO tape (coil 2) has reduced the perpendicular component of the magnetic flux density, resulting in a 50% reduction in AC loss [4].
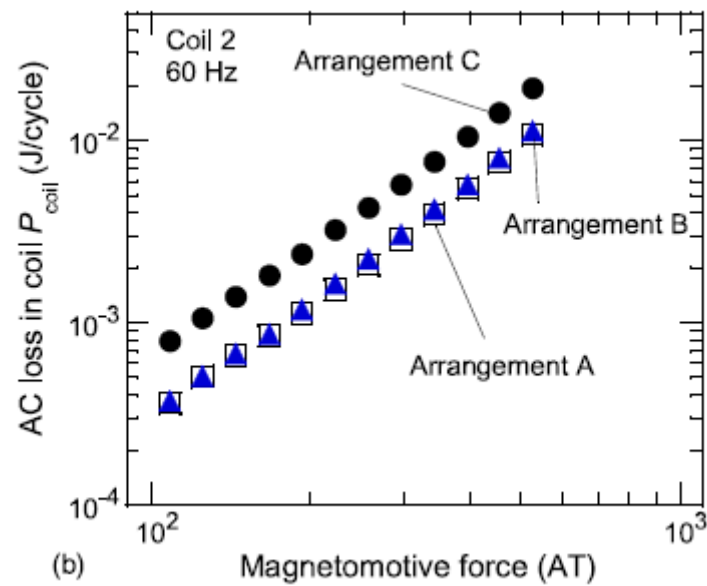

Figure 55 Graphical analysis for coil 2 arrangements A, B & C [4]

6.2. Design of the model with magnets

The investigation was carried out with the following four possible arrangements as shown in Figure 56 with magnets in the stator slots, based on the analysis of [4]. The major goal of this study is to see if there is a reduction in the magnetic flux density's perpendicular component when magnets are inserted in the stator slot of AC rotating machines (from a practical viewpoint).

The below designs are part of a single layer concentrated winding of 10 MW fully HTS generator at 30 K with single racetrack coil.
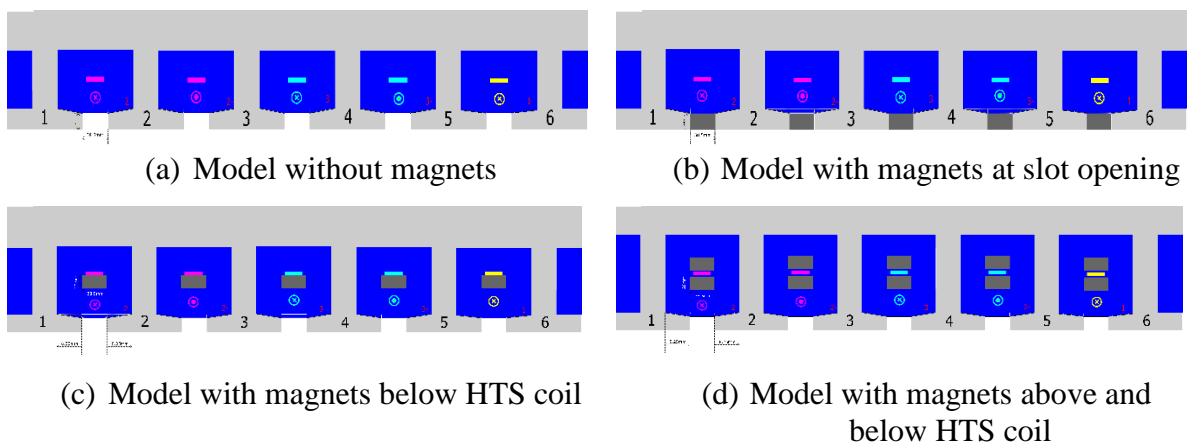

(a) Model without magnets

(b) Model with magnets at slot opening

(c) Model with magnets below HTS coil

(d) Model with magnets above and below HTS coil

Figure 56 Geometrical view of the models with magnets placed at different positions

The permanent magnet specifications used in this investigation are presented in Table 12.

Table 12 Permanent magnet specifications

| Parameter	Symbol	Value	Units
Height of permanent magnet	h_M	10, 20	mm
Remanence induction	B_r	1.5	T
Relative permeability	μ_r	1.0	-
Orientation of magnetization	$orient$	180	degree
Type of magnetization	$type$	radial	-
Relative axial length	$rlen$	100	%
Spacing between permanent magnet and HTS coil	-	1	mm
Width of the magnet	b_M	3 * 0.1 * wsp1	mm

6.3. Results and analysis

The numerical calculations are carried out to calculate flux distribution around the HTS coil using the finite element software FEMAG-DC. After the field calculation, average flux density of the tangential magnetic field, maximum flux density of the tangential magnetic field, and maximum flux density of the radial magnetic field are calculated and presented in the below table for the proposed arrangements with magnets as discussed in section 6.2.

Table 13 Comparison of the models with magnets placed at different positions

| Flux Diverter Type	Ic @ 30K(A)	Winding turns	Ampere Loading(A/mm)	B_tan_avg_eff(T)	B_tan_max(T)	B_rad_max(T)
Without Magnets	179.064	91	70	0.106	0.689	0.807
With Magnets at slot opening	179.064	91	70	0.106	0.689	0.807
With Magnets below HTS coil	179.064	91	70	0.115	0.753	0.624
With Magnets above and below HTS coil	179.064	91	70	0.109	0.695	0.158

The purpose of this study is to minimize the magnetic flux density's perpendicular component, but the graphical analysis below shows that when the magnets are installed in the stator slots, the flux density of the tangential (perpendicular) magnetic field increases.
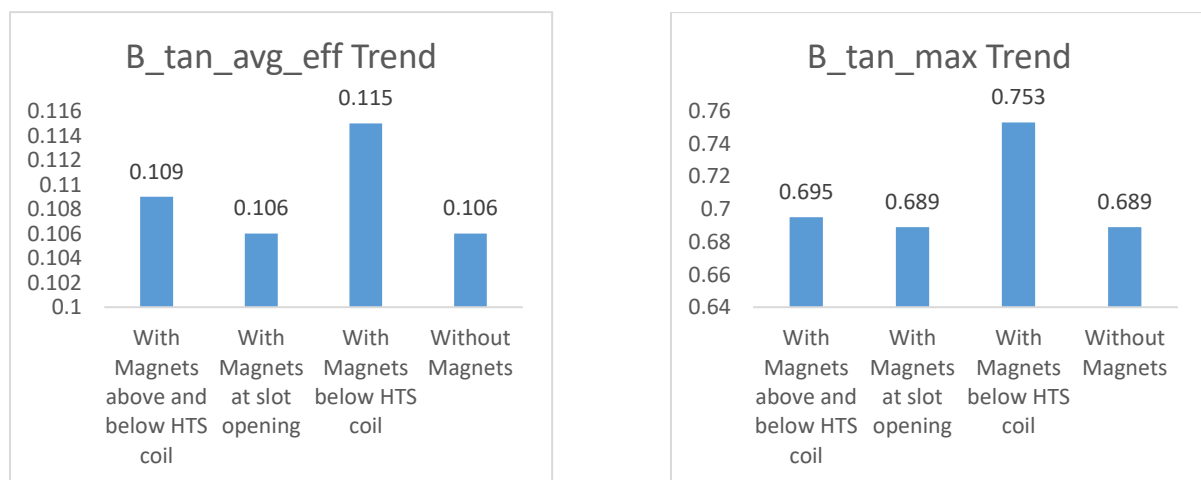
Figure 57 Graphical analysis of B_tan_avg_eff and B_tan_max

Whereas, the flux density of the radial (parallel) magnetic field in this study decreased significantly when the magnets are placed above and below HTS coil.
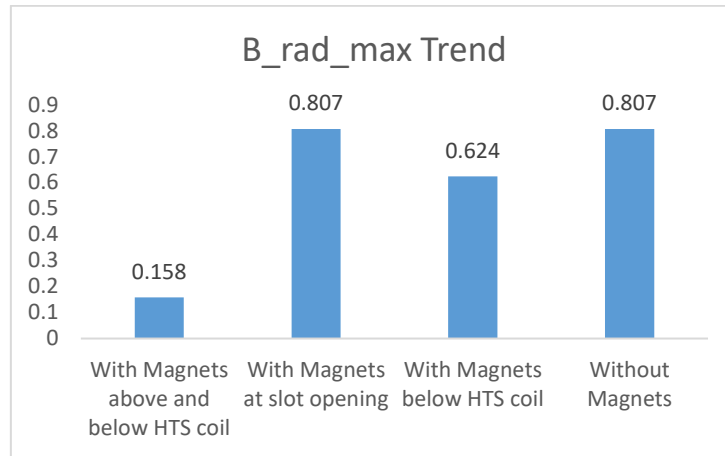
Figure 58 Graphical analysis of B_rad_max

As a result, the findings of this investigation contradict the findings of the research publication [4]. Further research is needed to see if the magnetic flux density's perpendicular component may be lowered by adding magnets into the stator slots. In the following steps, parameters such as magnetization orientation (180, 90, etc.), magnetization type (radial, axial, etc.), remanence, permanent magnet height, and armature winding type can be manipulated for a better understanding and analysis, as well as to match the results to the research paper [4].

Chapter 7 Conclusion and future recommendations

7.1. Conclusion

The main idea behind this thesis is to optimize and select the suitable stator winding type for the 10 MW fully HTS generator, which is a part of the SuperGenSys project at Fraunhofer IEE. As discussed in the previous chapters, one of the possible optimization processes includes reducing the operating temperature of the stator winding and analyzing the effects of reducing the operating temperature on the generator parameters. Furthermore, analysis has been done at different intermediate temperatures to analyze the behavior of the generator.

In chapter 4, a number of ampere loading calculations are performed at 30 K to determine the optimum value for the selected four winding concepts. The results from the discussions carried out in chapter 4 determine the appropriate winding type based on limited parameters. Therefore, it can be concluded that the 2ZW is the promising winding type for the 10 MW fully HTS generator since it satisfies to achieve a cheaper and compact machine with high efficiency.

To advance this investigation a little further, the analysis was carried out at various intermediate temperatures to analyze the effects of a few parameters on the generator's performance, which is explained in chapter 5. Due to the inconsistencies in the analysis, it is difficult to predict the appropriate operating temperature level. Therefore, in the next steps, the effects of other important parameters will be addressed in order to select the appropriate operating temperature level.

The major challenge in dealing with fully HTS generators is the AC losses. These AC losses must be reduced to prevent the expensive cooling system. Therefore, one way to reduce the AC losses is presented in chapter 6. Although further research is needed to gain a better understanding, the outcome of this investigation in the thesis proves that there is no significant reduction in the magnetic flux density's perpendicular component by inserting the magnets in the stator slots of the generator.

7.2. Future recommendations

The AC loss calculation plays a crucial role in determining the cryogenic system for the generator. Based on equation 3, approximate AC losses are determined in this thesis. As a result, a thorough investigation into the various methods for calculating accurate AC losses in the generator (eg: T-A formulation or H formulation) is required in order to acquire accurate AC losses.

There may be some discrepancies in the final results of this thesis because the comparison of the ampere loading optimum values for the four winding concepts at 30 K is restricted to a small number of parameters. Therefore, additional research is required to produce more accurate results. One strategy for conducting this research is to consider the same torque for all four selected optimum values by varying the diameter of the generator, which eventually results in a variation of number of pole pairs, and the results are again compared after this investigation.

Simultaneously, more research is needed to improve the results of the AC loss reduction approach outlined in Chapter 6 by manipulating the parameters such as magnetization orientation (180, 90, etc.), magnetization type (radial, axial, etc.), remanence, permanent magnet height, and armature winding type for a better understanding and analysis as well as to discover other alternative ways to reduce AC losses.

V Bibliography

[1]   2022. *2G HTS Wire Specification | SuperPower*. https://www.superpower-inc.com/specification.aspx. Accessed 21 April 2022.

[2]   Cao, W. 2011. High-Temperature Superconducting Wind Turbine Generators. In *Wind Turbines*, I. H. Al-Bahadly, Ed. InTech. DOI=10.5772/14660.

[3]   Fraunhofer IEE. Entwurf, Optimierung und Bewertung von energieeffizienten, supraleitenden Generatorsystemen, 4.

[4]   Fukui, S., Tsukamoto, S., Nohara, K., Ogawa, J., Sato, T., and Nakamura, T. 2016. Study on AC Loss Reduction in HTS Coil for Armature Winding of AC Rotating Machines. *IEEE Transactions on Applied Superconductivity* 26, 4, 1–5.

[5]   Henk Polinder, G. G. 1999. Feasibility Study of a 10 MW MgB2 Fully Superconducting Generator for Offshore Wind Turbines. In *Over The Rim*, W. B. Smart and D. T. Smart, Eds. Utah State University Press, 191–199. DOI=10.2307/j.ctt46nrzt.12.

[6]   J. Schellevis. Master Thesis: AC Loss Modeling of Superconducting Field Windings for a 10MW Wind Turbine Generator - mscThesis_jschellevis_rev_2.1FINAL.pdf.

[7]   Jannicke, M. 1981. *3 MW SUPERCONDUCTING WIND POWER GENERATOR – PROJECT ECOSWING SUCCESSFULLY COMPLETED*.

[8]   Jensen, B. B., Mijatovic, N., and Abrahamsen, A. B. 2012. Development of Superconducting Wind Turbine Generators. In Scientific Proceedings of EWEA 2012 - European Wind Energy Conference & Exhibition European Wind Energy Association (EWEA).

[9]   Lengsfeld, S., Grundmann, J., Oomen, M., Vargas-Llanos, C., Ponick, B., and Jung, M. 2022. Comparing Armature Windings for a 10 MW Fully Superconducting Synchronous Wind Turbine Generator. In *2022 12th International Conference on Power, Energy and Electrical Engineering (CPEEE)*. IEEE, 49–53. DOI=10.1109/CPEEE54404.2022.9738712.

[10]   ProFEMAG. 2022. *About ProFEMAG*. https://www.profemag.ch/en/about-femag. Accessed 21 April 2022.

[11]   ProFEMAG. 2022. *Electrical machine design based on 2D FE simulations*. https://www.profemag.ch/en/. Accessed 21 April 2022.

[12] Reddy, A. 2016. Armature Windings in Alternator & Types of Armature Windings. *Blogger* (Sep. 2016).

[13] S. Lengsfeld. SupraGenSys "Basisentwurf" des Voll-HTS 10 MW Generators.

[14] Simpson, N., North, D. J., Collins, S. M., and Mellor, P. H. 2020. Additive Manufacturing of Shaped Profile Windings for Minimal AC Loss in Electrical Machines. *IEEE Trans. on Ind. Applicat.* 56, 3, 2510–2519.

[15] Tara Benkel, Mayraluna Lao, Yingzhen Liu , Enric Pardo , Senior Member, IEEE, Simon Wolfstädter. 2020. T–A-Formulation to Model Electrical Machines With HTS Coated Conductor Coils. *IEEE Trans. Appl. Supercond.* 30, 6.

[16] tim. 2021. Motor windings. *OSWOS* (Dec. 2021).

[17] Tong, W. 2010. *Wind power generation and wind turbine design*. WIT Press, Southampton, Boston.

[18] Vargas-Llanos, C. R., Lengsfeld, S., and Grilli, F. 2020. T-A Formulation for the Design and AC Loss Calculation of a Superconducting Generator for a 10 MW Wind Turbine. *IEEE Access* 8, 208767–208778.

[19] Vargas-Llanos, C. R., Lengsfeld, S., Noe, M., Arndt, T., and Grilli, F. 2021. Influence of Coil Position on AC Losses of Stator Superconducting Windings of a Synchronous Machine for a 10 MW Wind Turbine. *IEEE Trans. Appl. Supercond.* 31, 7, 1–9.

[20] Wang, M., Zhang, M., Song, M., Li, Z., Dong, F., Hong, Z., and Jin, Z. 2019. An effective way to reduce AC loss of second-generation high temperature superconductors. *Supercond. Sci. Technol.* 32, 1, 01LT01.

[21] Winkler, T. 2019. The EcoSwing Project. *IOP Conf. Ser.: Mater. Sci. Eng.* 502, 12004.

[22] Xue, S., Thomas, A. S., Zhu, Z.-Q., Huang, L., Duke, A., Clark, R. E., and Azar, Z. 2021. Stator Optimization of Wind Power Generators With High-Temperature Superconducting Armature Windings and Permanent Magnet Rotor. *IEEE Trans. Appl. Supercond.* 31, 2, 1–10.

[23] Zhang, H., Wen, Z., Grilli, F., Gyftakis, K., and Mueller, M. 2021. Alternating Current Loss of Superconductors Applied to Superconducting Electrical Machines. *Energies* 14, 8, 2234.

[24] Zou, S., Zermeno, V. M. R., and Grilli, F. 2016. Simulation of Stacks of High-Temperature Superconducting Coated Conductors Magnetized by Pulsed Field Magnetization Using Controlled Magnetic Density Distribution Coils. *IEEE Trans. Appl. Supercond.* 26, 3, 1–5.
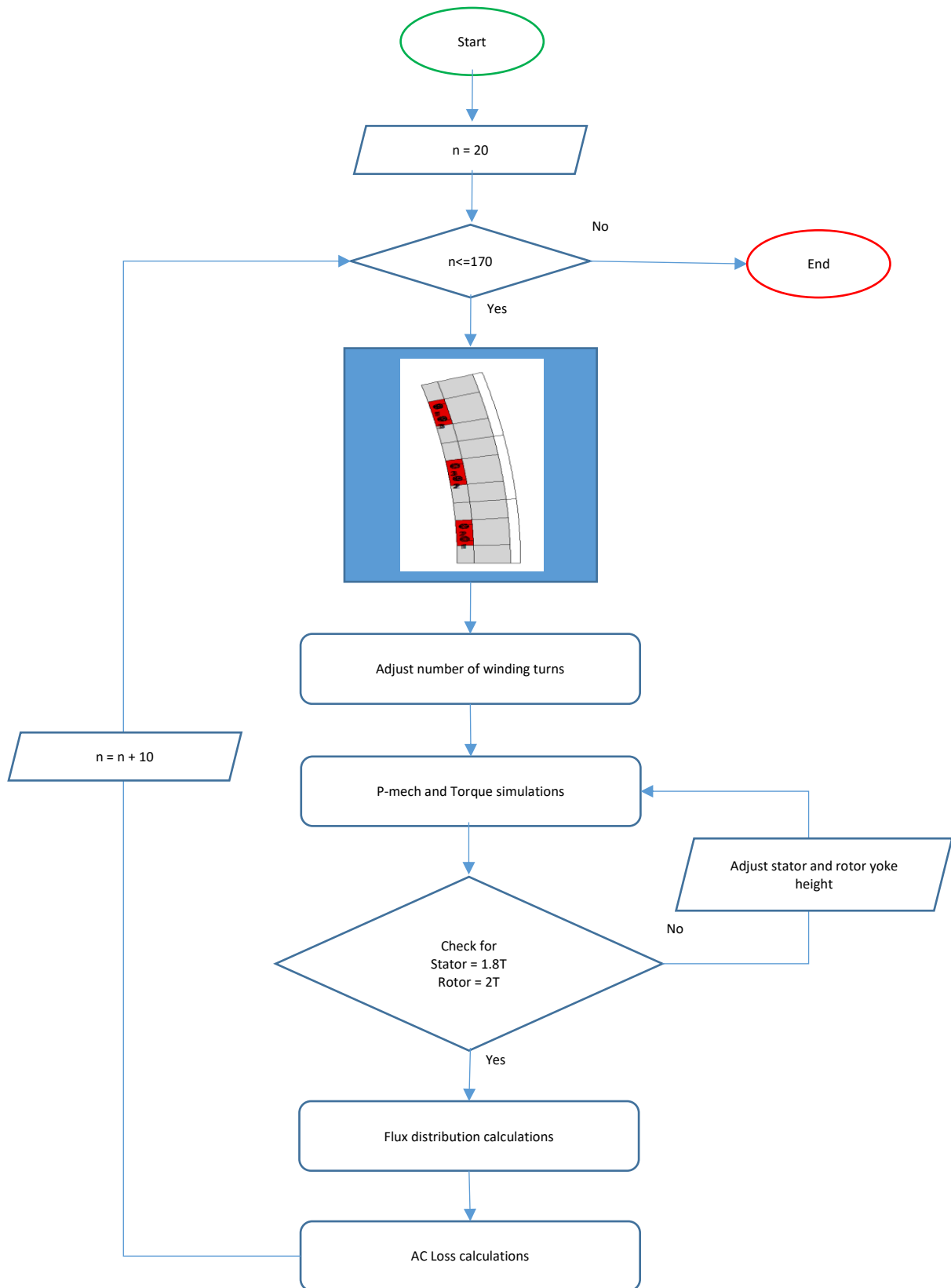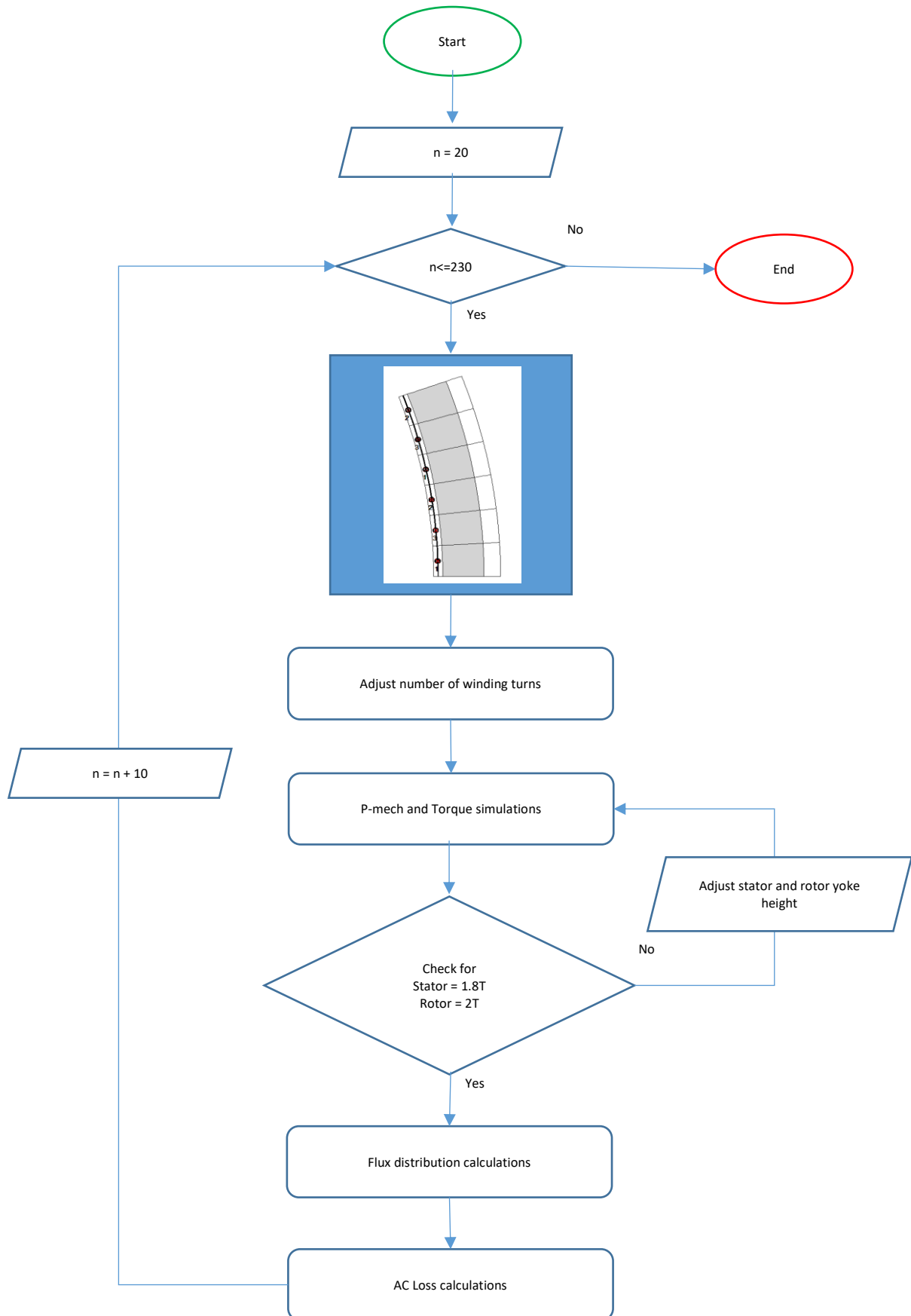
VI Appendix 1

Figure 59 Process flow chart for the ampere loading simulation of 2ZW

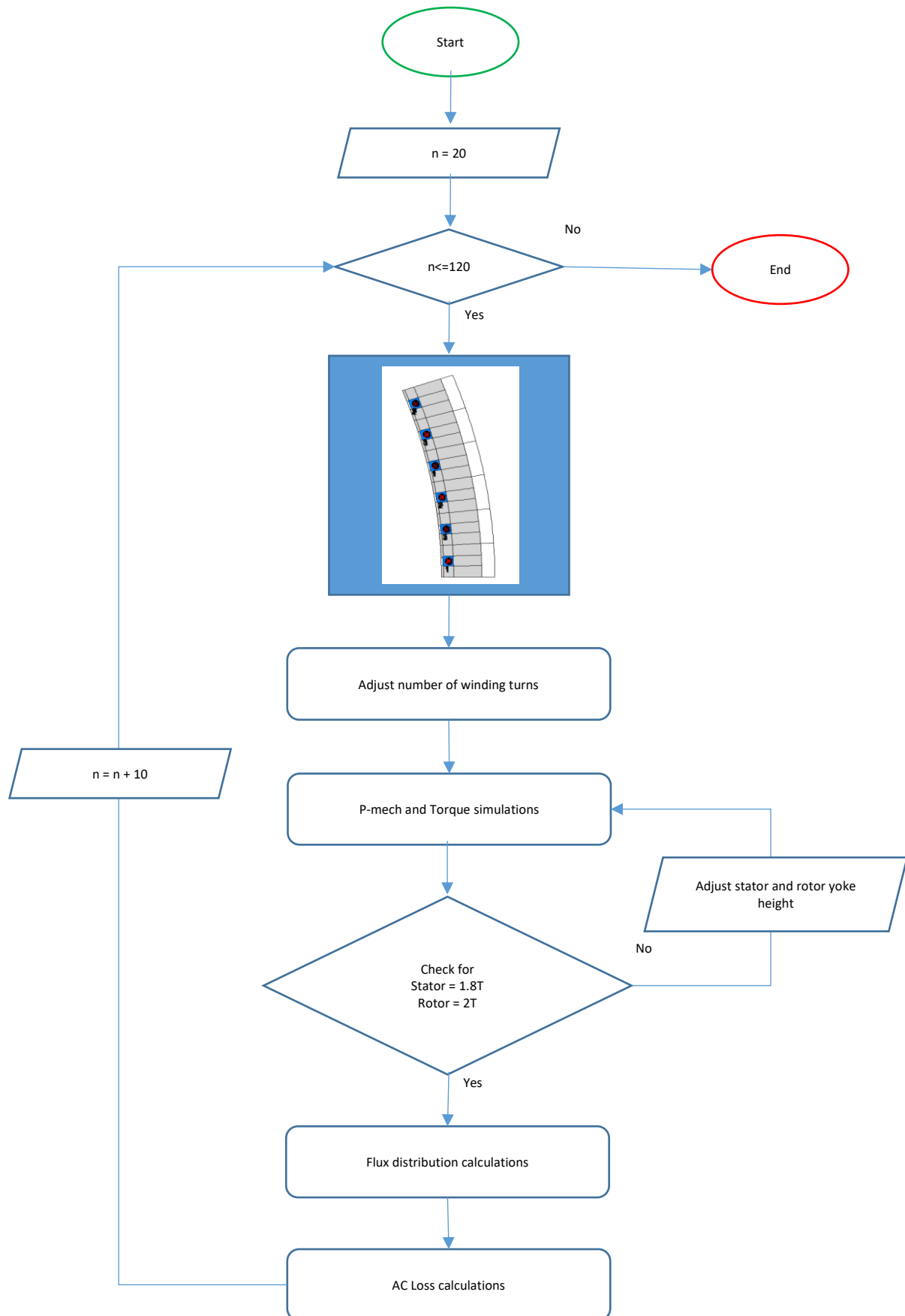*Figure 60 Process flow chart for the ampere loading simulation of LSW*

Figure 61 Process flow chart for the ampere loading simulation of 1VW
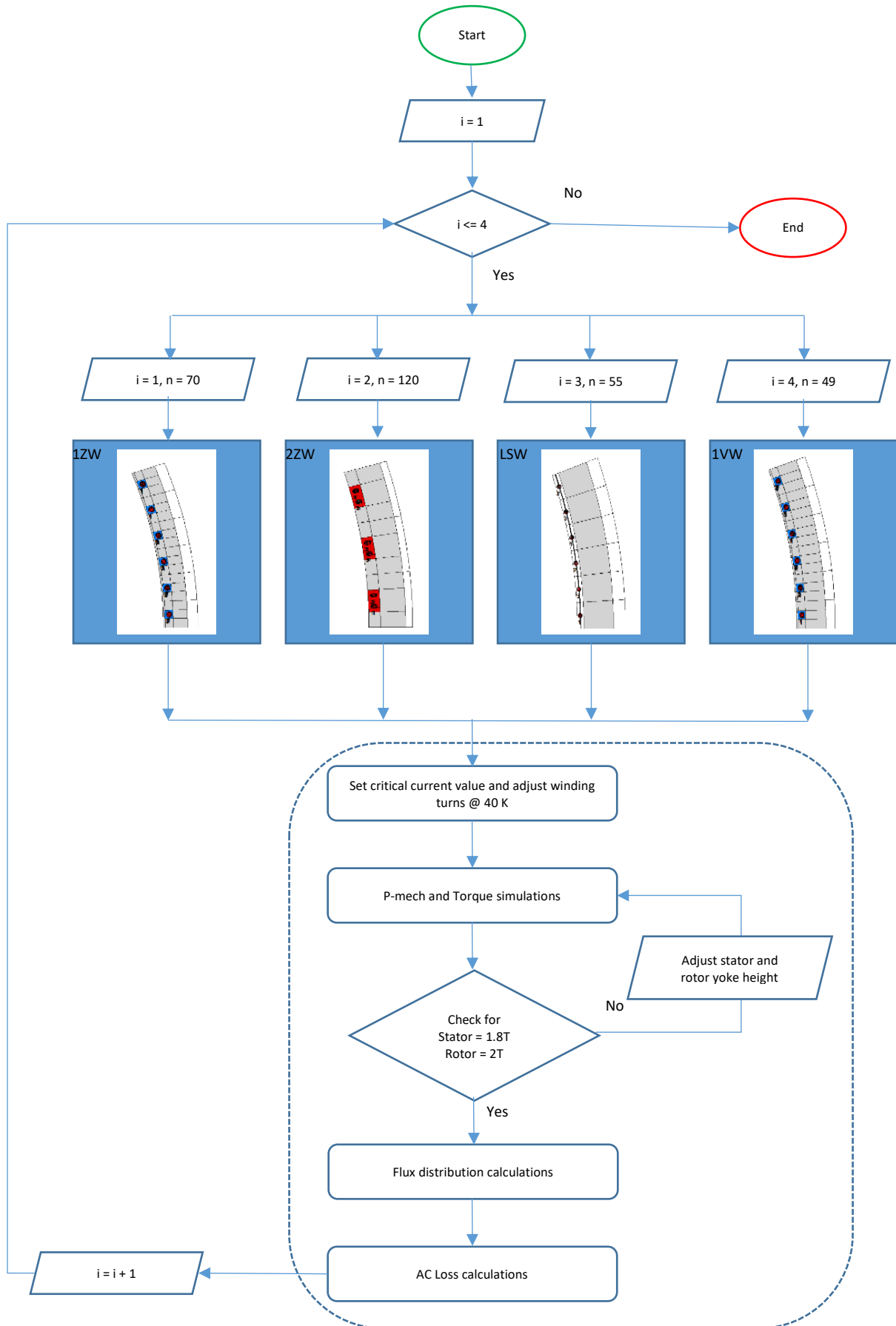
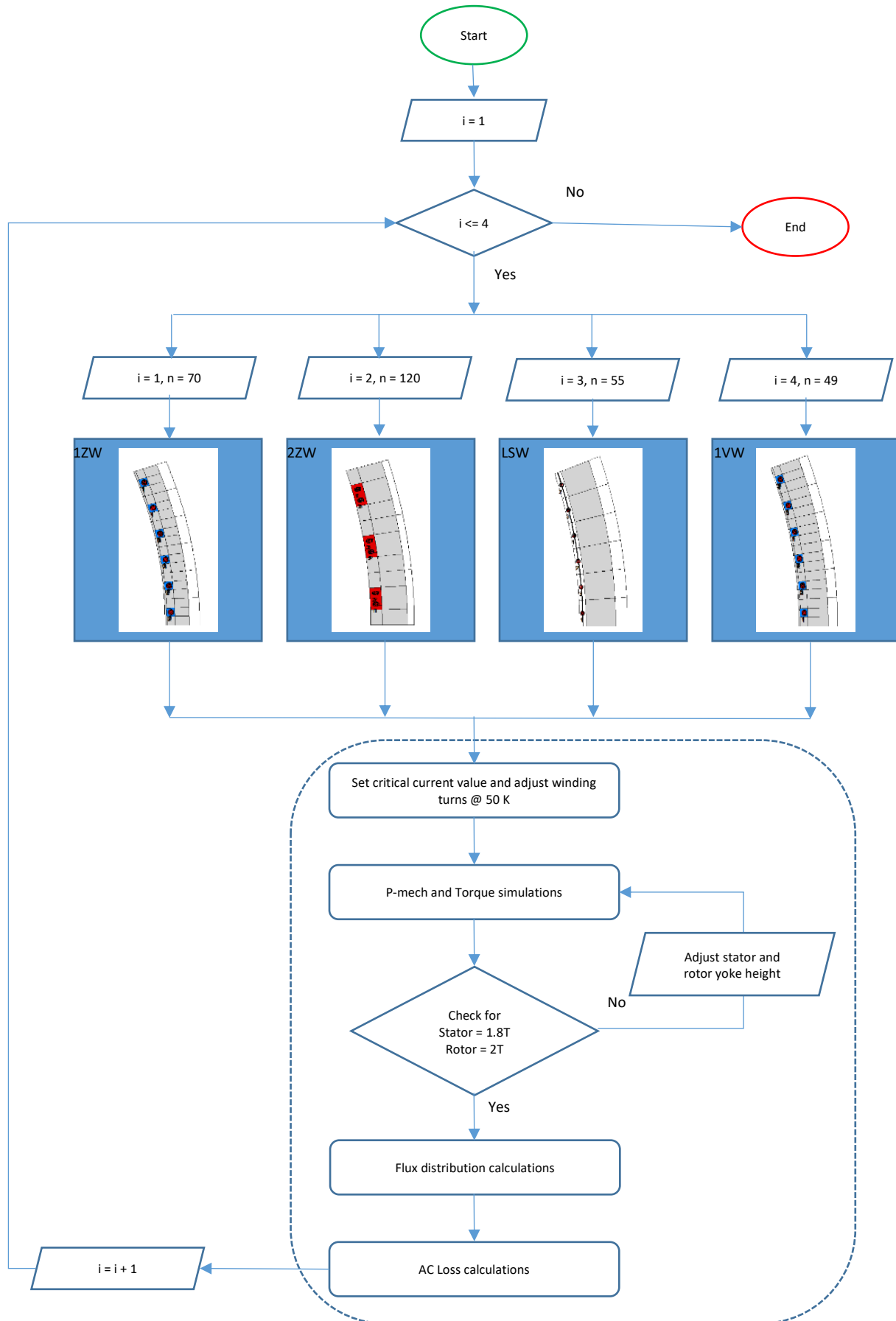*Figure 62 Process flow chart of the winding concepts at 40 K*

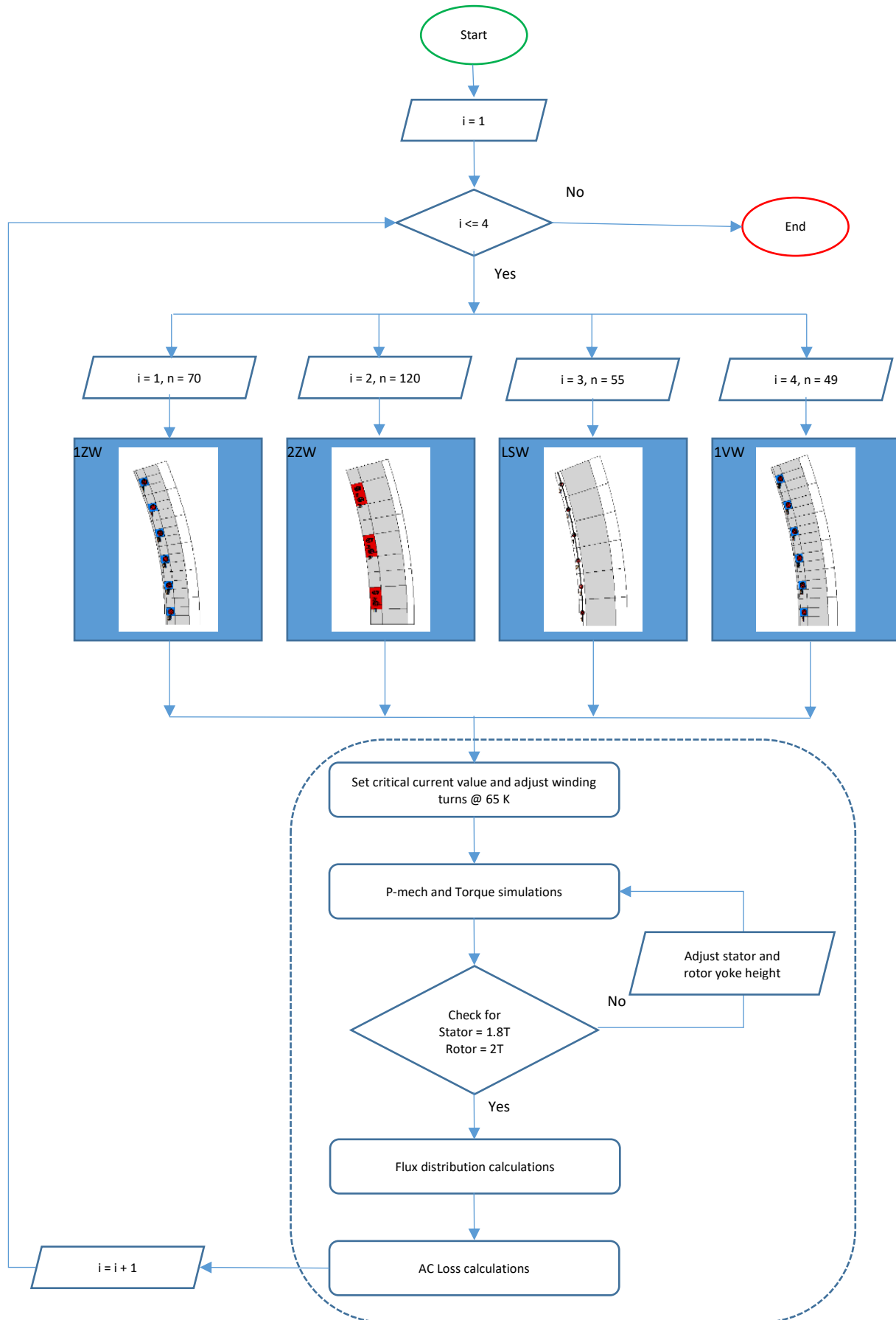*Figure 63 Process flow chart of the winding concepts at 50 K*

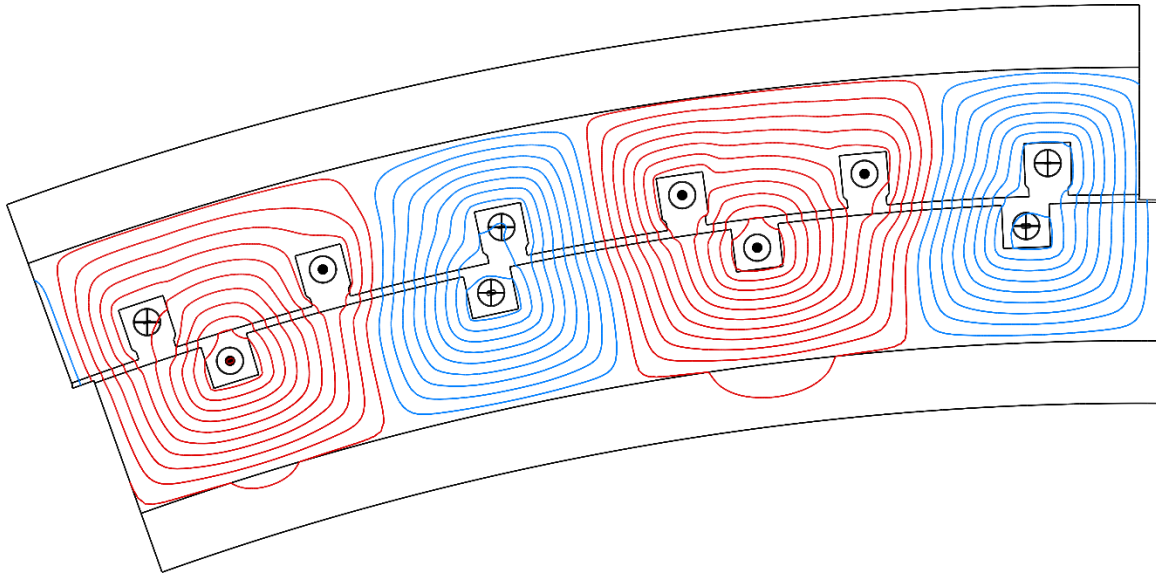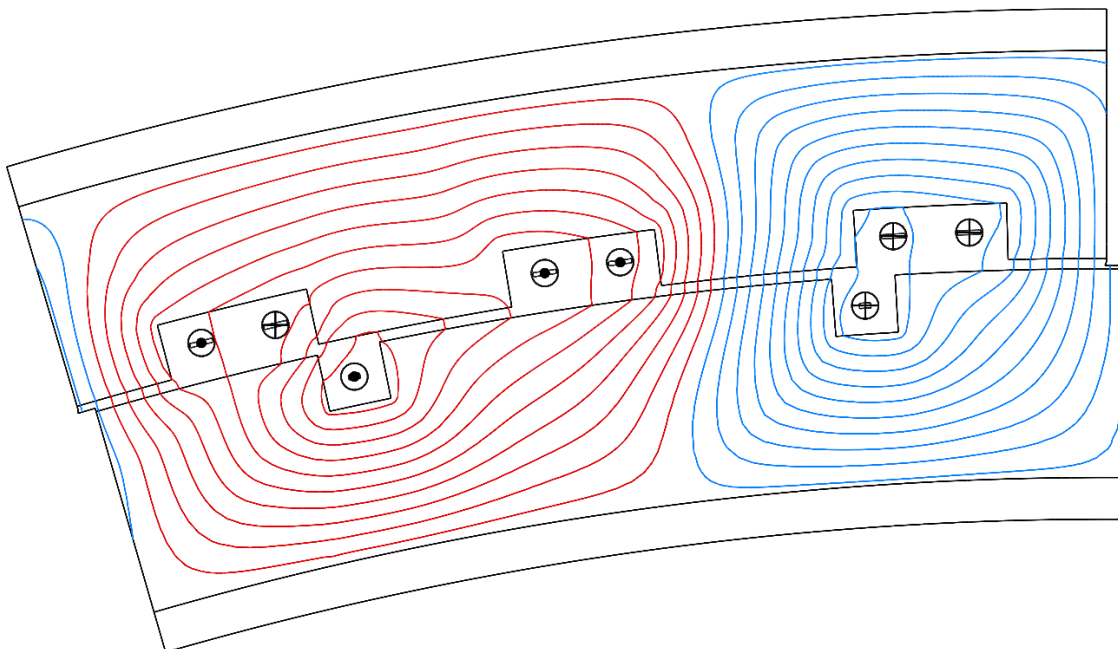*Figure 64 Process flow chart of the winding concepts at 65 K*

Figure 65 Field lines plot for concept 1ZW at 30 K

Figure 66 Field lines plot for concept 2ZW at 30 K
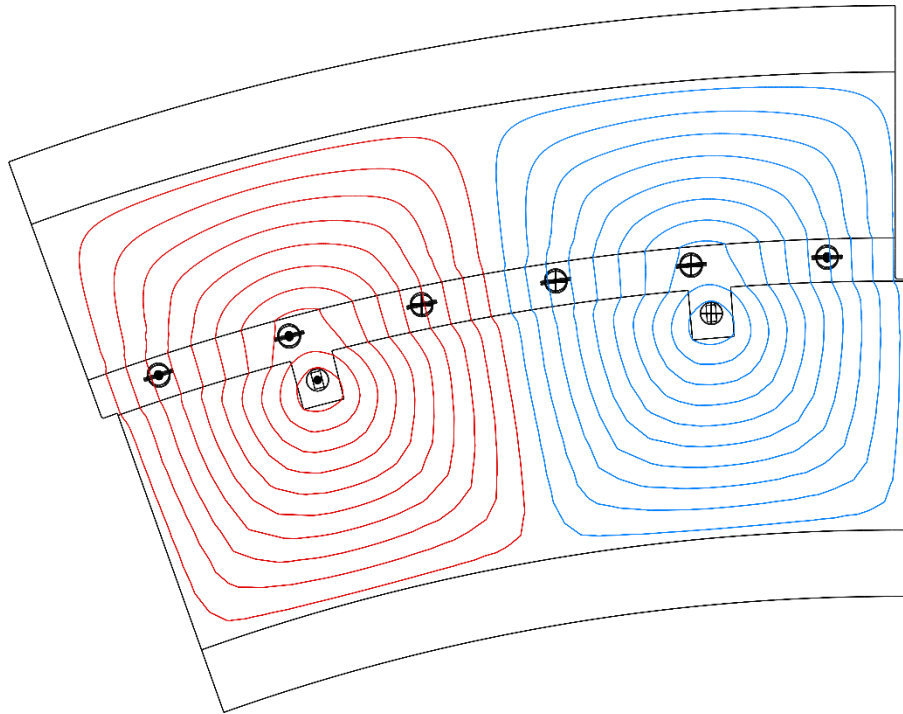
Figure 67 Field lines plot for concept LSW at 30 K
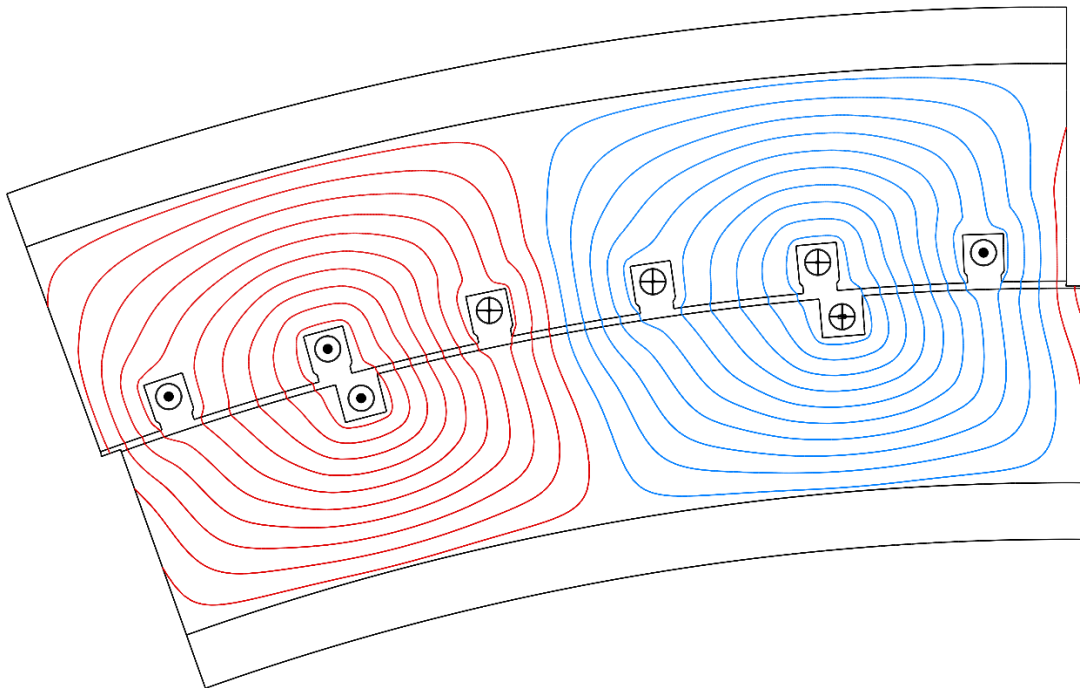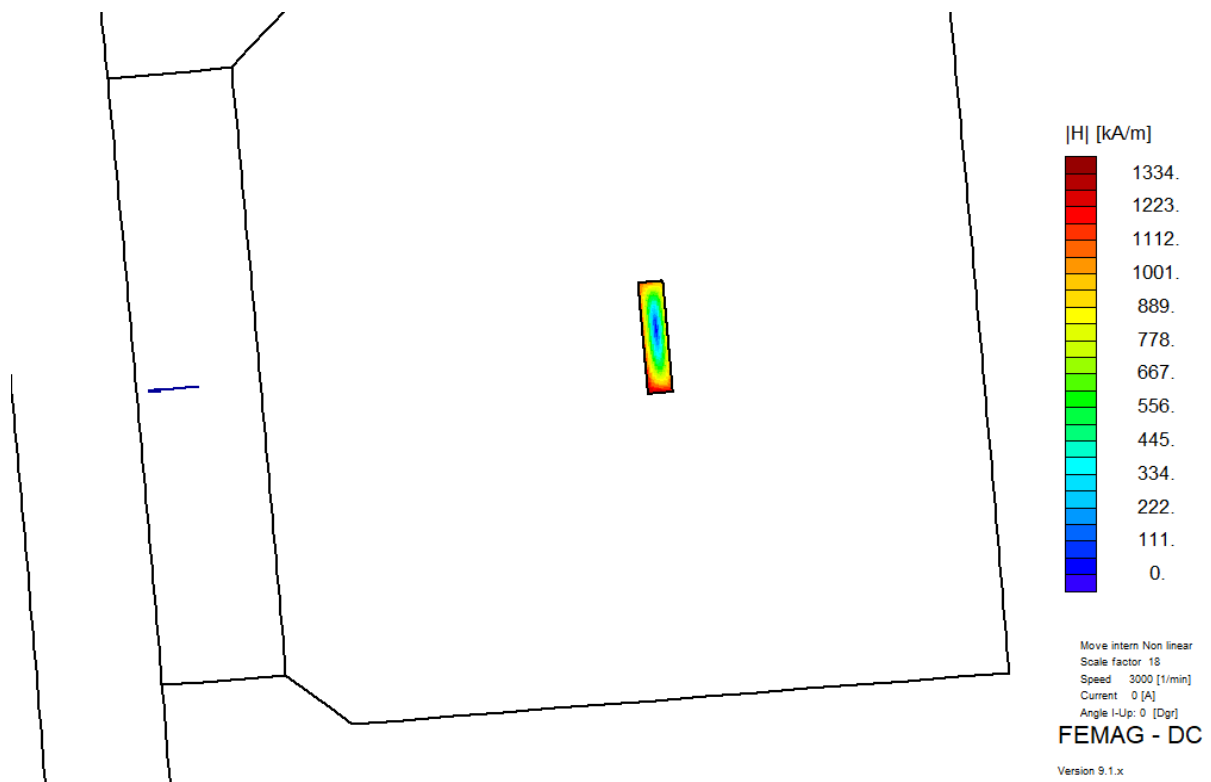

Figure 68 Field lines plot for concept 1VW at 30 K
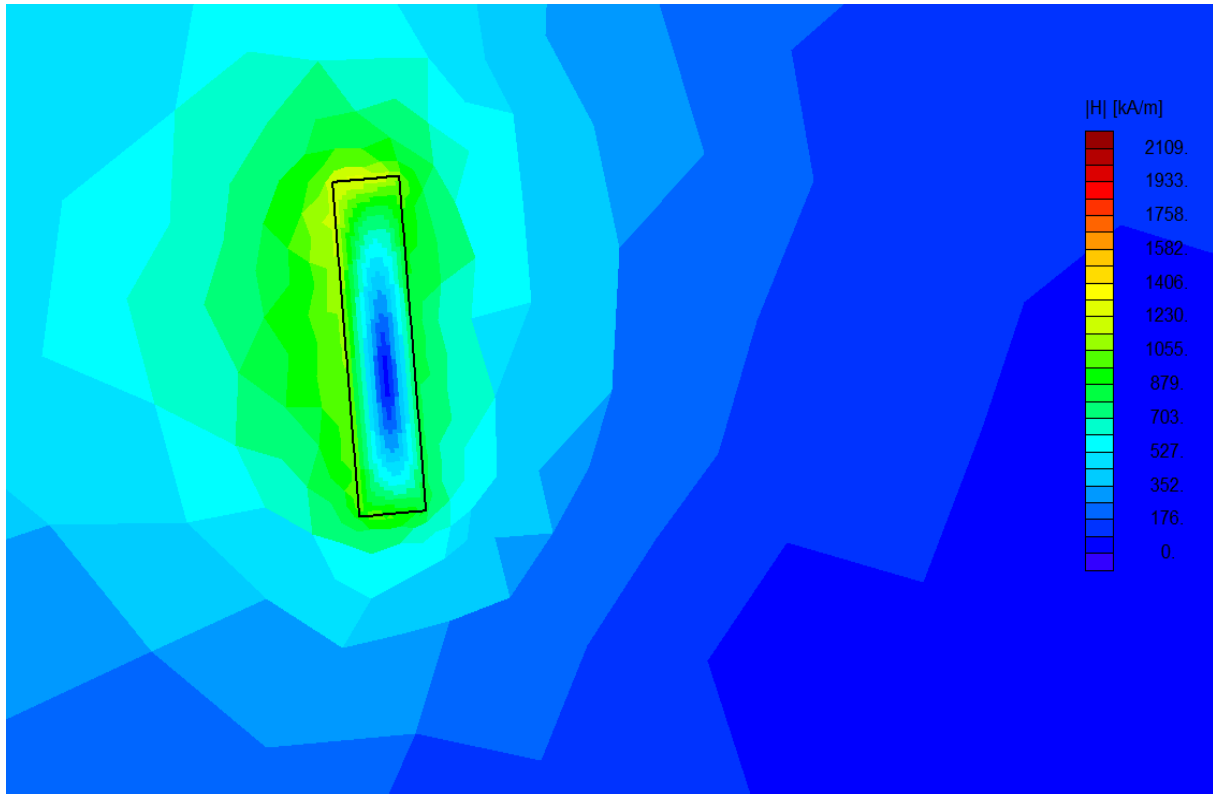
Figure 69 Absolute field strength of the 1ZW model without magnets (Total)
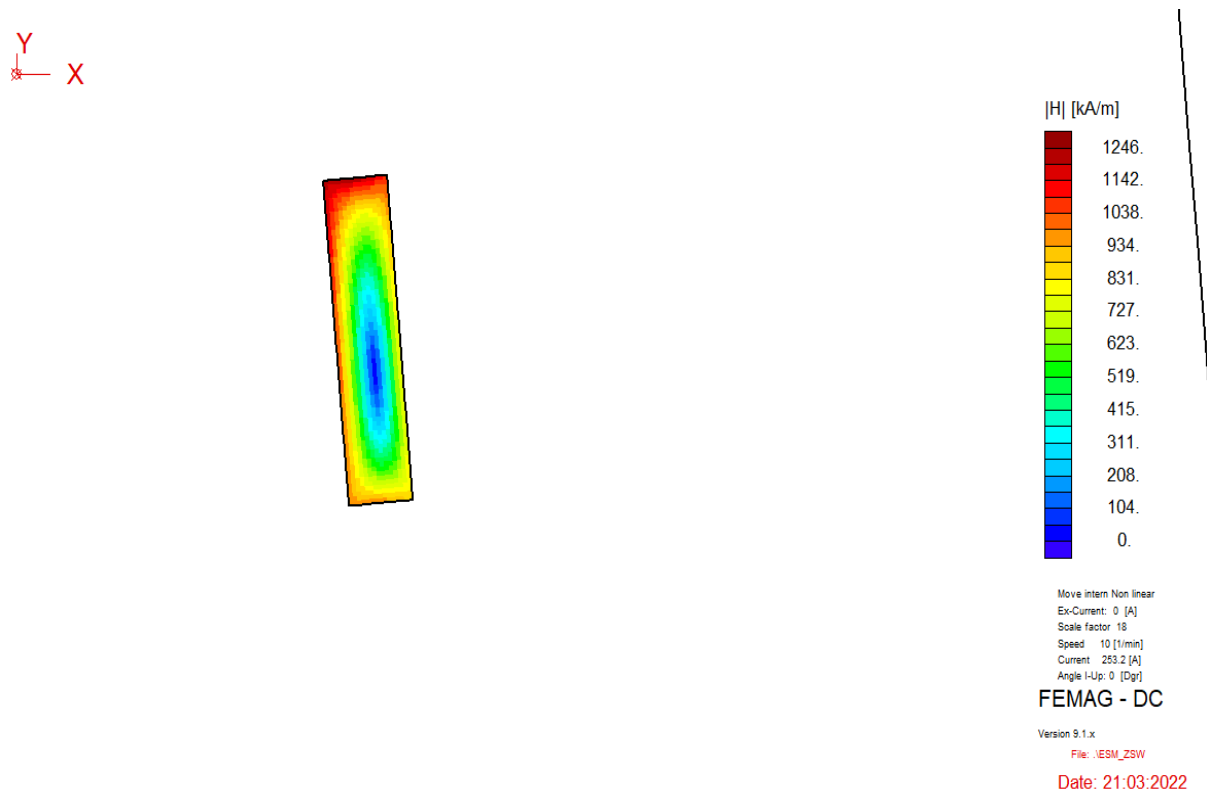
Figure 70 Absolute field strength of the 1ZW model without magnets (Winding coil)
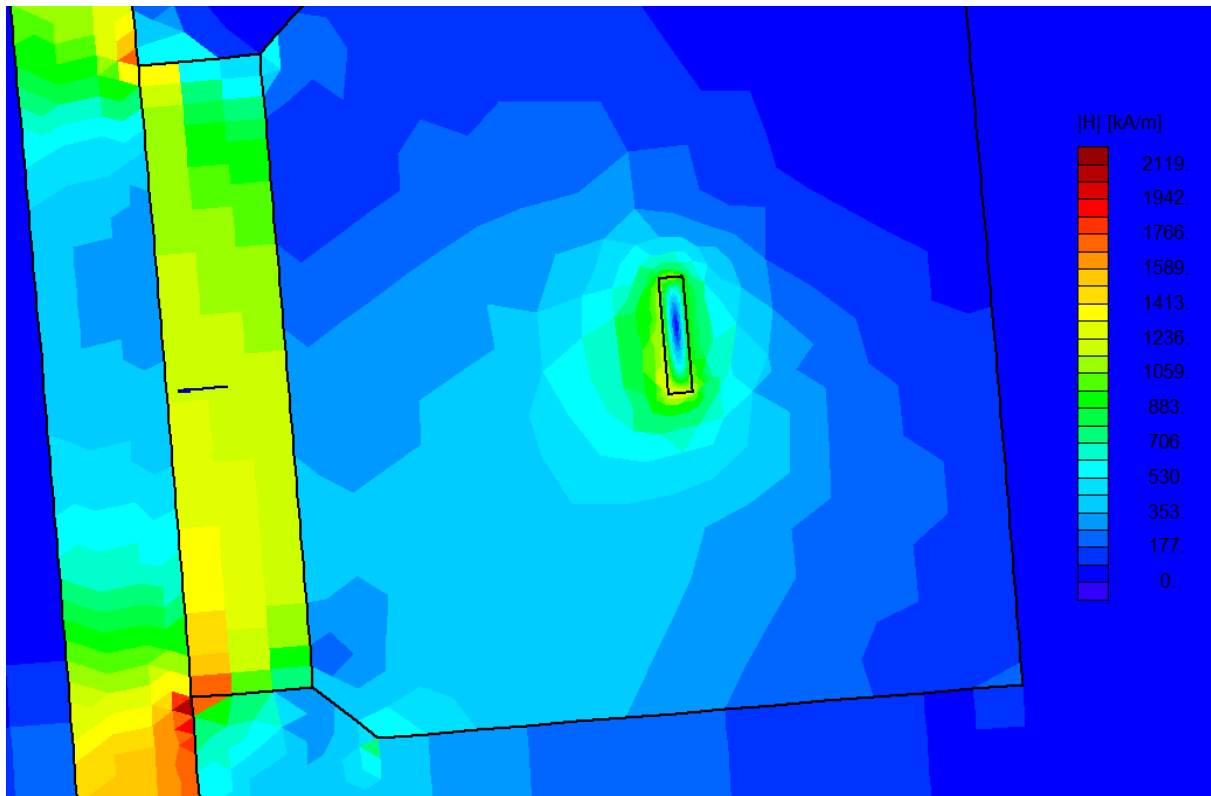
Figure 71 Absolute field strength of the 1ZW model with magnets at slot opening (Total)

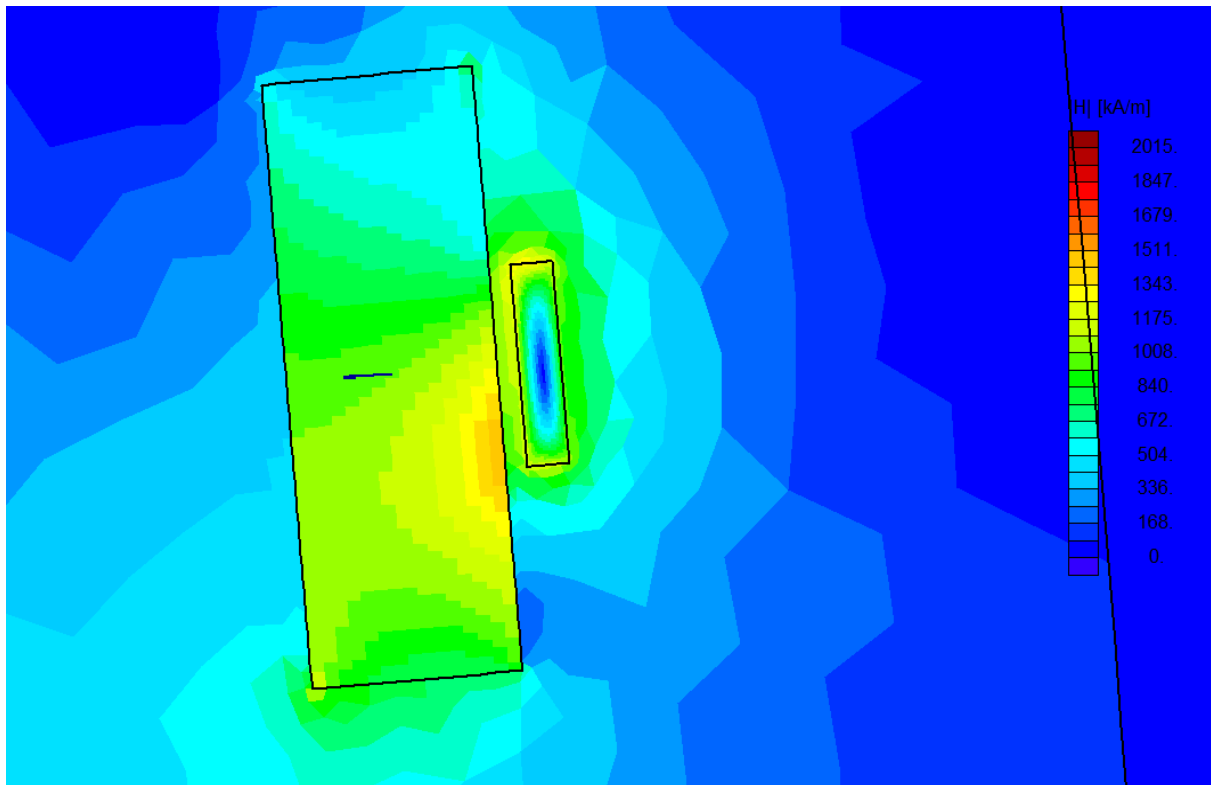*Figure 72 Absolute field strength of the 1ZW model with magnets at slot opening (Winding coil)*

Figure 73 Absolute field strength of the 1ZW model with magnets below HTS coil (Total)
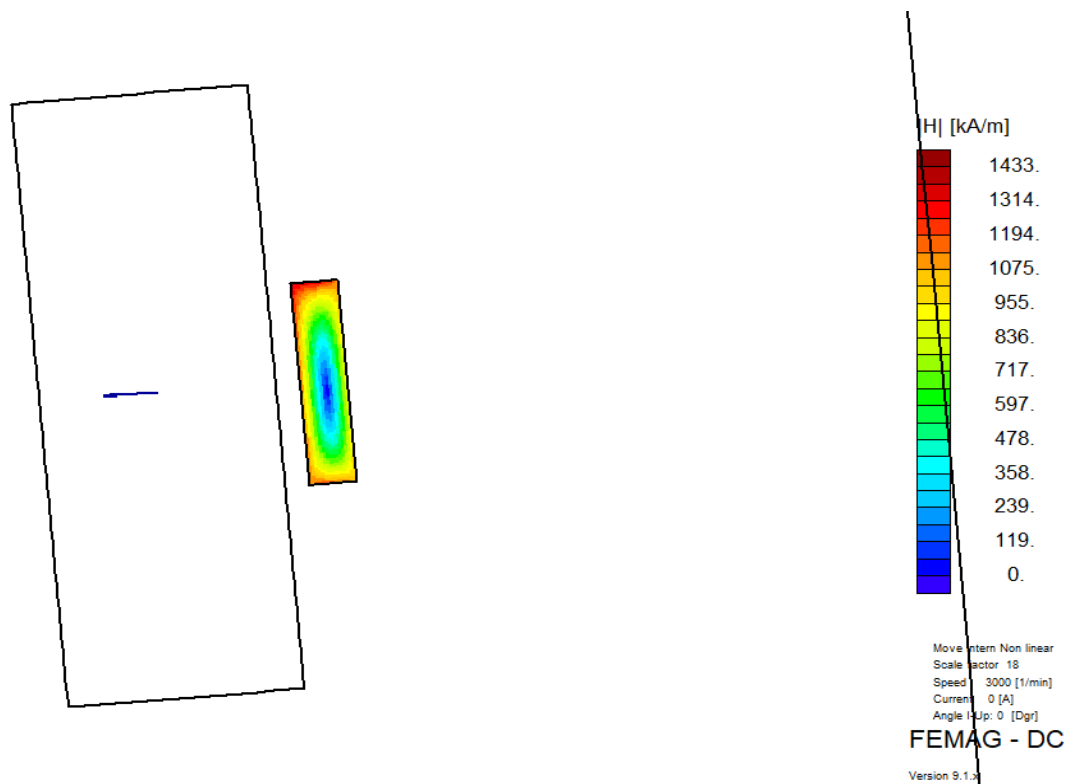

Figure 74 Absolute field strength of the 1ZW model with magnets below HTS coil (Winding coil)
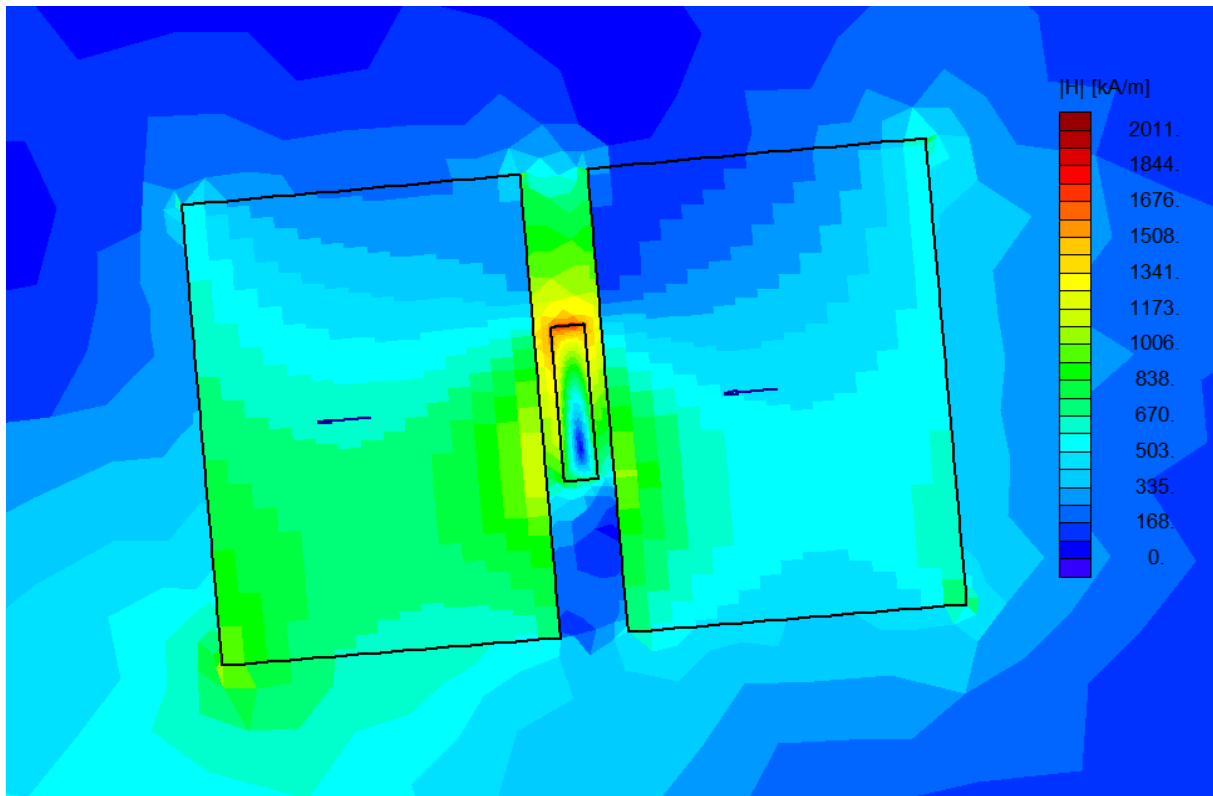
Figure 75 Absolute field strength of the 1ZW model with magnets above and below HTS coil (Total)
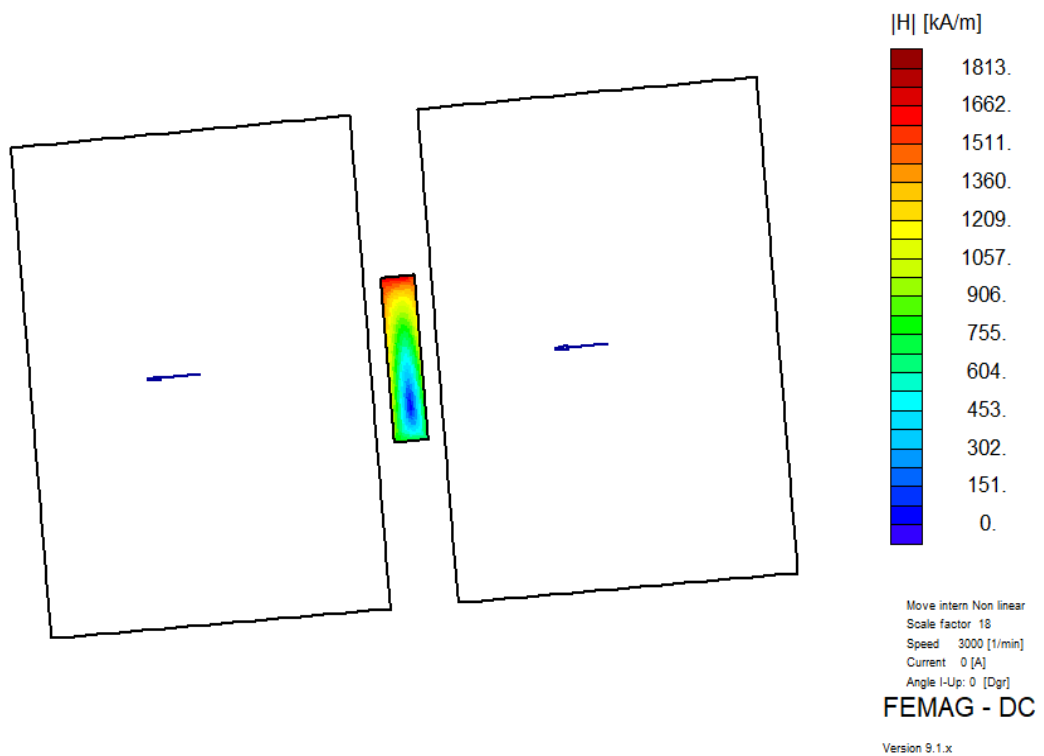

Figure 76 Absolute field strength of the 1ZW model with magnets above and below HTS coil (Winding coil)